UC Riverside
UC Riverside Electronic Theses and Dissertations

Title

Physical and Chemical Factors Influencing the Transport and Fate of Microorganisms in Soils With Preferential Flow

Permalink

https://escholarship.org/uc/item/3qc5m1g2

Author

Wang, Yusong

Publication Date

2013

Peer reviewed|Thesis/dissertation

UNIVERSITY OF CALIFORNIA
RIVERSIDE

Physical and Chemical Factors Influencing the Transport and Fate of Microorganisms in
Soils With Preferential Flow

A Dissertation submitted in partial satisfaction
of the requirements for the degree of

Doctor of Philosophy

in

Environmental Sciences

by

Yusong Wang

August 2013

Dissertation Committee:
        Dr. Jiří Šimůnek, Chairperson
        Dr. Scott A. Bradford
        Dr. David E. Crowley

The Dissertation of Yusong Wang is approved:

_____

_____

_____

Committee Chairperson

University of California, Riverside

Acknowledgements

ABSTRACT OF THE DISSERTATION

Physical and Chemical Factors Influencing the Transport and Fate of Microorganisms in
Soils With Preferential Flow

by

Yusong Wang

Doctor of Philosophy, Graduate Program in Environmental Sciences
University of California, Riverside, August 2013
Dr. Jiří Šimůnek, Chairperson

An understanding of the processes that influence the transport and fate of microorganisms in porous media is needed to protect water resources from pathogenic microorganisms and contaminants associated with the colloidal phase, and to optimize bioremediation strategies. As the physical and chemical factors influencing the transport of microorganisms have been well understood in homogeneous systems, accurate description of microorganism transport in field scale is hampered by the existence of preferential flow.

The objective of this research was to better understand and quantify physical and chemical factors that influence microorganism transport and fate in soils that exhibit preferential flow. *E. coli* D21g and coliphage phiX174 were selected in this study as the representative bacterial pathogen and the surrogate for human viruses, respectively. The transport of microorganisms was examined in well defined and controlled soil columns

containing artificial macropores (sand lenses) of different length and configuration under different solution ionic strength (IS).

Transport experiments demonstrated that retention of *E. coli* D21g and φX174 increased with IS in both homogeneous and heterogeneous systems. The importance of preferential flow on microbe transport was found to be enhanced at higher IS, even though the overall transport decreased. Deposition profiles revealed significant cell retention at the interface of the coarse sand lens and fine sand matrix as a result of mass transfer. The length and configuration of the artificial macropore proved to have a great impact on the transport of *E.coli* D21g, especially under high ionic strength conditions. At low ionic strength, more extensive transport in the preferential path and earlier arrival time were observed for *E.coli* D21g compared to bromide as a result of size exclusion. Cell release from the preferential flow system with a reduction of solution IS exhibited multi-pulse breakthrough behavior that was strongly dependent on the initial amount of cell retention, especially at the lens-matrix interface, and the lens configuration. Simulations in 2D models were capable to describe the transport and deposition, and the release process during transients in chemistry in preferential flow systems. Dual-permeability models were also successfully applied to simulate microorganism transport in preferential flow systems with different configuration and length of preferential path, and correlations found between the parameters of dual-permeability model and preferential path characters could promote the upcaling from local to field scale for microorganism transport in preferential flow systems.

Table of Contents

List of Tables

Chapter 1

Introduction

1.1 Motivation and Background

Waterborne disease outbreaks associated with drinking water in the United States during 1971–2002 are known to have resulted in 575,457 cases of illness and 79 deaths, with 14% caused by bacteria, 19% by protozoa, 8% by viral pathogens, and 47% by unknown acute gastrointestinal illness [*Reynolds et al.*, 2008]. Wastes from humans, domesticated and wild animals, birds, and insects frequently contain high concentrations of pathogenic microorganisms [*USDA*, 1992; *USEPA*, 1998; *Gerba and Smith*, 2005] that serve as pathogen sources in agricultural settings. Pathogenic microorganisms can be transported to streams by surface water runoff and to ground water by recharge through the vadose zone. These contaminated surface and ground water supplies may eventually serve as drinking water and/or irrigation water for fresh produce. If these contaminated water supplies are not adequately treated before use, ground water typically receives minimal or no treatment, then they can put the public's health at risk.

The problem is not limited to these pathogens. Mobile colloids and bacteria can also facilitate the transport of a wide variety of inorganic and organic contaminants that can adsorb onto these high surface area particles [*Šimůnek et al.*, 2006]. This colloid-facilitated transport has been illustrated in the literature for numerous contaminants,

including heavy metals [*Grolimund et al.*, 1996], radionuclides [*Noell et al.*, 1998],

pesticides [*Kan and Tomson*, 1990; *Lindqvist and Enfield*, 1992; *Vinten et al.*, 1983],

pharmaceuticals [*Tolls*, 2001], hormones [*Hanselman et al.*, 2003], and other

contaminants [*Magee et al.*, 1991]. On the other hand, bioremediation and/or bio-

augmentation strategies to clean up recalcitrant chemicals in subsurface environments

could be greatly enhanced by the efficient delivery of specialized bacteria to targeted

locations in the subsurface [*Gargiulo et al.*, 2007]. An ability to accurately predict the

fate and transport of pathogenic microorganisms and other colloids in subsurface is

therefore necessary for a wide variety of purposes.

Much research has examined physical (size of the microbe and the porous

medium, microbe concentration, water velocity, water content, and surface roughness)

and chemical (surface chemistry of the microbe and soil, and aqueous solution pH, ionic

strength, and chemical composition) factors that influence the retention of

microorganisms in homogeneous porous media under relatively uniform flow [*Mills et al.*,

1994; *Mccaulou et al.*, 1995; *Hendry et al.*, 1999; *Yee et al.*, 2000; *Dong et al.*, 2002;

Bradford et al., 2006; *Chen and Walker* 2007]. Mechanisms of microbe retention have

been inferred from repacked column breakthrough curves (BTCs) and retention profiles

3

(RPs), batch experiments, and complimentary micromodel studies that allowed for direct

microscopic observation [*Ochiai et al.*, 2006]. The mechanisms governing transport and

retention of microbes in porous media have been described by several review articles

[*Stevik et al.*, 2004; *Sen and Khilar*, 2006; *Bradford and Torkzaban*, 2008]. In brief,

attachment is the removal of microbes from solution via collision with and fixation to the

solid-water interface (SWI) [*Topol et al.*, 1998] and/or air-water interface (AWI).

Microbe attachment under saturated conditions has traditional been described using

colloid filtration theory [*Yao et al.*, 1971]. This theory assumes that the attachment rate is

dependent on the mass transfer of microbes to the SWI and subsequent microbe-surface

interactions. Pore scale water flow and colloid transport simulations in simple geometries

have been used to develop correlation equations to predict the rate of microbe mass

transfer as a function of velocity, grain size, and microbe size and density [*Tufenkji and

Elimelech*, 2004]. Filtration theory originally assumed that all microbes that collide with

the SWI will be irreversibly attached in the primary minimum of the Derjaguin-Landau-

Verwey-Overbeek (DLVO) interaction energy as result of favorable chemical

interactions. However, most microbes, soils, and the AWI are negatively charged under

ambient conditions that are unfavorable for attachment. In this case, only a fraction of the

microbes that collide with the SWI and AWI will result in attachment. This fraction is

dependent on the balance of adhesive and hydrodynamic forces and torques that act at a

particular location [*Torkzaban et al.*, 2007], and can vary spatially and temporally.

Attachment will tend to increase with increasing chemical forces and decreasing

hydrodynamic forces [*Bradford and Torkzaban*, 2008].

Field, lysimeter, and undisturbed soil column experiments have frequently

revealed that microorganisms, colloids, and other contaminants can travel much deeper

and faster than would be predicted based on results from laboratory studies in

homogeneous porous media [*Bales et al.*, 1989; *Abu-Ashour et al*., 1994; *Pivets and

Sttenhuis*, 1995; *Pivetz et al.,* 1996; *Jiang et al*., 2010]. This phenomenon has been

ascribed to transport in preferential flow pathways created by plant roots, burrowing

earthworms [*Beven and Germann*, 1982; *Madsen and Alexander*, 1982; *Unc and Goss*,

2003; *Cey et al.*, 2009] and/or natural structural heterogeneities [*Wollum, and Cassel*,

1978]. Preferential flow can also occur in soils and aquifers with strong contrasts in

hydraulic conductivity between sediment layers [*Harvey et al*., 1993]. Considerable

research has indicated that colloids and microorganisms can be transported in preferential

flow pathways [*McGechan and Lewis*, 2002; *Jarvis*, 2007; *Pang et al.*, 2008; *Cey et al.*,

2009; *Cey and Rudolph*, 2009; *Passmore et al.*, 2010]. Preferential flow has also been

implicated in the rapid transport of bacteria to field tile drains [*Evans and Owens*, 1972;

Dean and Foran, 1992; *Guzman et al.*, 2009]. However, most of this research is

qualitative in nature because of difficulty in quantifying the physical and chemical

complexities of the soil matrix and macropore system with regard to microbe transport.

This gap in information currently presents a great obstacle to predicting the fate of

microbes in natural environments [*McCarthy and McKay*, 2004].

The exchange rate of water between the macropore and the matrix, or between

layers with contrasting hydraulic conductivities, will likely be a critical factor in

determining the rate of microbe migration in preferential flow systems [*Harvey et al.*,

1993; *Morley et al.*,1998; *Allaire-Leung et al.*, 2000a, 2000b; *Allaire et al.*, 2002a, 2002b]

because of the potential for greater retention of microbes in the matrix as a result of

enhanced chemical interactions, lower hydrodynamic forces, and smaller pore spaces. It

is also possible that microbes may be physically excluded from the matrix, and in this

case transport of microbes would exclusively occur in macropores. Optimum conditions

for microbe transport in preferential flow systems will therefore likely depend on a wide

variety of chemical and physical factors of both the matrix and macropore domains, but

6

little quantitative research has addressed this issue and the relative importance of these factors has not yet been fully determined [*Fontes et al.*, 1991].

It is important to be able to describe water flow in the preferential flow domain in order to quantitatively simulate the transport of microorganisms in the field. Various conceptual models of preferential flow exist that are dependent on a great number of parameters (e.g., macropore hydraulic properties, mass transfer terms, and macropore geometry) [*Šimůnek and van Genuchten*, 2008]. It is difficult, if not impossible, to independently determine all of the required model parameters under natural conditions [*Šimůnek et al.*, 2003]. Thus, some assumptions have to be made to simplify the preferential flow path for simulation purposes. Artifical macropores can be systematically created by leaving small cylindrical openings in repacked columns [*Pivetz and Steenhuis*, 1995; *Castiglione et al.*, 2003], or by packing different sized sands to generate layers and/or lens with contrasting hydraulic conductivities [*Fontes et al.*, 1991; *Saiers et al.*, 1994; *Morley et al.*, 1998; *Bradford et al.*, 2004]. The study of preferential flow and transport through artificial macropores provides an opportunity to overcome many modeling challenges because the macropore geometry and hydraulic properties can be well defined and controlled in a repeatable manner [*Pivetz and Steenhuis*, 1995;

Castiglione et al., 2003; *Guzman et al.*, 2009; *Arora et al.*, 2011; *Arora et al.*, 2012].

Hence, it is possible to isolate and identify factors that have the greatest influence on

preferential flow and transport in such systems. Furthermore, controlled preferential flow

and transport studies provide valuable information on parameterization that is needed to

help adapt numerical models to complex natural systems.

Solution chemistry (pH, ionic strength and composition) has proven to be an

important factor that influences the transport and retention of microorganisms in porous

media [*Mills et al.*, 1994; *Yee et al.*, 2000; *Dong et al.*, 2002; *Chen and Walker*, 2007] and

in systems with preferential flow [*Fontes et al.*, 1991; *Wang et al.*, 2013]. The solution

chemistry may change dramatically in the vadose zone during infiltration and drainage

events as a result of differences in water quality at the soil surface (rain, irrigation, and

runoff), evapotranspiration, and the mineral composition of the soil and groundwater.

Such transients in solution chemistry are well-known to induce the release of colloids and

microbes in homogeneous porous media [*Bales et al.*, 1989; *McDowell-Boyer*, 1992;

Ryan and Gschwend, 1994; *Nocito-Gobel and Tobiason*, 1996; *Roy and Dzombak*, 1996;

Grolimund et al., 2001; *Lenhart and Saiers*, 2003; *Cheng and Saiers*, 2009; *Tosco et al.*,

2009; *Bradford and Kim*, 2010; *Bradford et al.*, 2012]. Consequently, transients in

solution chemistry may jeopardize the purification capability of the vadose zone by

inducing microbial release. There is presently a great need to understand processes that

influence microbial remobilization, especially in soils with preferential flow. *Wang et al.*

[2013] demonstrated that transients in solution chemistry can remobilize retained

microbes and rapidly transport them in a preferential flow system. However, numerical

modeling of this microbe release and transport still has not yet been reported.

1.2 Objectives

The objective of this dissertation work was to better understand and quantify physical

and chemical factors that influence microorganism transport and fate in soils that exhibit

preferential flow. To achieve the overall objective of this dissertation work, specific

objectives were set and these are presented below:

1) To investigate the role of solution chemistry on the transport of two different sized

microorganisms in preferential flow systems (Chapter 2). For this purpose, transport

experiments were conducted for *E. coli* D21g and coliphage φX174 in packed columns

with an artificial macropore at various IS conditions (1, 5, 20, and 100 mM);

2) To systematically investigate the role of lens length and configuration on the

transport of *E. coli* D21g at low and high IS (1 and 20 mM, respectively), and the release

of retained cells after transport experiments at high IS (Chapter 3). In order to achieve

this purpose, transport experiments of *E. coli* D21g was carried in columns with artificial

macropores of selected configuration and length at low and high IS. After the transport

experiments at high IS, the inlet solution was switched to deionized water in order to

release the retained cells;

3) To simulated the laboratory experiments of preferential transport under constant and transient chemistry conditions with numerical models in 2D systems (Chapter 2 and 3), and then relate the parameters and geometry information in 2D systems to parameters of preferential flow model (1D dual-permeability model) (Chapter 4).

1.3 References

Abu-Ashour, J., D. M. Joy, H. LEE, H. R. Whiteley, and S. Zelin, Transport of microorganisms through soil, *Water Air Soil Pollut.*, *75*, 141-158, 1994.

Allaire-Leung, S. E., S. C. Gupta, and J. F. Moncrief (2000a), Water and solute movement in soil as influenced by macropore characteristics - 1. Macropore continuity, *J. Contam. Hydrol.*, 41(3-4), 283-301.

Allaire-Leung, S. E., S. C. Gupta, and J. F. Moncrief (2000b), Water and solute movement in soil as influenced by macropore characteristics - 2. Macropore tortuosity, *J. Contam. Hydrol.*, 41(3-4), 303-315.

Allaire, S. E., S. C. Gupta, J. Nieber, and J. F. Moncrief (2002a), Role of macropore continuity and tortuosity on solute transport in soils: 2. Interactions with model assumptions for macropore description, *J. Contam. Hydrol.*, 58(3-4), 283-298.

Allaire, S. E., S. C. Gupta, J. Nieber, and J. F. Moncrief (2002b), Role of macropore continuity and tortuosity on solute transport in soils: 1. Effects of initial and boundary conditions, *J. Contam. Hydrol.*, 58(3-4), 299-321.

Arora, B., B. P. Mohanty, and J. T. McGuire (2011), Inverse estimation of parameters for multidomain flow models in soil columns with different macropore densities, *Water Resour. Res.*, 47(4), W04512, doi:10.1029/2010wr009451.

Arora, B., B. P. Mohanty, and J. T. McGuire (2012), Uncertainty in dual permeability model parameters for structured soils, *Water Resour. Res.*, 48(1), W01524, doi:10.1029/2011wr010500.

Bales, R. C., C. P. Gerba, G. H. Grondin, and S. L. Jensen, Bacteriophage transport in sandy soil and fractured tuff, *Appl. Environ. Microbiol.*, 55(8), 2061-2067,1989.

Beven, K., and P. Germann (1982), Macropores and Water-Flow in Soils, *Water Resour. Res.*, 18(5), 1311-1325.

Bradford, S. A., and H. Kim (2010), Implications of Cation Exchange on Clay Release and Colloid-Facilitated Transport in Porous Media, *J. Environ. Qual.*, 39(6), 2040-2046. doi:10.2134/Jeq2010.0156.

Bradford, S. A., J. Šimůnek, and S. L. Walker (2006), Transport and straining of E-coli O157 : H7 in saturated porous media, *Water Resour. Res.*, 42(12), doi:10.1029/2005WR004805.

Bradford, S. A., and S. Torkzaban (2008), Colloid transport and retention in unsaturated porous media: A review of interface-, collector-, and pore-scale processes and models, *Vadose Zone J.*, 7(2), 667-681.

Bradford, S. A., M. Bettehar, J. Šimůnek, and M. Th. van Genuchten (2004), Straining and attachment of colloids in physically heterogeneous porous media, *Vadose Zone Journal*, *3*(2), 384-394.

Bradford, S. A., S. Torkzaban, H. Kim, and J. Šimůnek (2012), Modeling colloid and microorganism transport and release with transients in solution ionic strength, *Water Resour. Res.*, 48(9), W09509.

Castiglione, P., B. P. Mohanty, P. J. Shouse, J. Šimůnek, M. T. van Genuchten, and A. Santini (2003), Lateral Water Diffusion in an Artificial Macroporous System, *Vadose Zone J.*, 2(2), 212-221. doi:10.2113/2.2.212.

Cey, E. E., and D. L. Rudolph (2009), Field study of macropore flow processes using tension infiltration of a dye tracer in partially saturated soils, *Hydrol. Processes*, 23(12), 1768-1779.

Cey, E. E., D. L. Rudolph, and J. Passmore (2009), Influence of macroporosity on preferential solute and colloid transport in unsaturated field soils, *J. Contam. Hydrol*, 107(1-2), 45-57.

Chen, G. X., and S. L. Walker (2007), Role of solution chemistry and ion valence on the adhesion kinetics of groundwater and marine bacteria, *Langmuir*, 23(13), 7162-7169.

Cheng, T., and J. E. Saiers (2009), Mobilization and transport of in situ colloids during drainage and imbibition of partially saturated sediments, *Water Resour. Res.*, 45(8), W08414.

Dean, D. M., and M. E. Foran (1992), The Effect of Farm Liquid Waste Application on Tile Drainage, *J. Soil Water Conserv.*, 47(5), 368-369.

Dong, H. L., T. C. Onstott, M. F. Deflaun, M. E. Fuller, T. D. Scheibe, S. H. Streger, R. K. Rothmel, and B. J. Mailloux (2002), Relative dominance of physical versus chemical effects on the transport of adhesion-deficient bacteria in intact cores from South Oyster, Virginia, *Environ. Sci. Technol.*, 36(5), 891-900.

Evans, M. R., and J. D. Owens (1972), Factors Affecting the Concentration of Faecal Bacteria in Land-drainage Water, *J. Gen. Microbiol.*, 71(3), 477-485. doi:10.1099/00221287-71-3-477.

Fontes, D. E., A. L. Mills, G. M. Hornberger and J. S. Herman (1991), Physical and chemical factors influencing transport of microorganisms through porous media, *Appl. Environ. Microbiol.* 57(9):2473-2481.

Gargiulo, G., S. A. Bradford, J. Šimunek, H. Vereecken, and E. Klumpp. (2006). Transport and deposition of metabolically active and stationary phase Deinococcus Radiodurans in unsaturated porous media. *Environ. Sci. Technol.* 41, 1265-1271.

Gerba, C.P. and J.E. Smith. (2005), Sources of Pathogenic Microorganisms and Their Fate during Land Application of Wastes. *J. Environ. Qual.* 34: 42-48. doi:10.2134/jeq2005.0042.

Grolimund, D., M. Borkovec, K. Barmettler, and H. Sticher (1996), Colloid-facilitated transport of strongly sorbing contaminants in natural porous media: A laboratory column study, *Environ. Sci. Technol.*, 30(10), 3118-3123.

Grolimund, D., K. Barmettler, and M. Borkovec (2001), Release and transport of colloidal particles in natural porous media: 2. Experimental results and effects of ligands, *Water Resour. Res.*, 37(3), 571-582.

Guzman, J. A., G. A. Fox, R. W. Malone, and R. S. Kanwar (2009), Transport from Surface-Applied Manure to Subsurface Drains through Artificial Biopores, *J. Environ. Qual.*, 38(6), 2412-2421.

Hanselman, T. A., D. A. Graetz, and A. C. Wilkie (2003), Manure-Borne Estrogens as Potential Environmental Contaminants: A Review, *Environ. Sci. Technol.*, 37(24), 5471-5478.

Harvey, R. W., N. E. Kinner, D. MacDonald, D. W. Metge, and A. Bunn (1993), Role of physical heterogeneity in the interpretation of small-scale laboratory and field observations of bacteria, microbial-sized microsphere, and bromide transport through aquifer sediments, *Water Resour. Res.*, 29(8), 2713-2721.

Hendry, M. J., J. R. Lawrence, and P. Maloszewski (1999), Effects of velocity on the transport of two bacteria through saturated sand, *Ground Water*, 37(1), 103-112.

Jarvis, N. J. (2007), A review of non-equilibrium water flow and solute transport in soil macropores: principles, controlling factors and consequences for water quality, *Eur J Soil Sci*, 58(3), 523-546.

Jiang, S., L. Pang, G. D. Buchan, J. Šimůnek, M. J. Noonan, and M. E. Close, Modeling water flow and bacterial transport in undisturbed lysimeters under irrigations of dairy shed effluent and water using HYDRUS-1D, *Water Research*, special issue, doi:10.1016/j.watres.2009.08.039, *44*, 1050-1061, 2010.

Kan, A. T., and M. B. Tomson (1990), Ground-Water Transport of Hydrophobic Organic-Compounds in the Presence of Dissolved Organic-Matter, *Environ. Toxicol. Chem.*, 9(3), 253-263.

Lenhart, J. J., and J. E. Saiers (2003), Colloid mobilization in water-saturated porous media under transient chemical conditions, *Environ. Sci. Technol.*, 37(12), 2780-2787.

Lindqvist, R., and C. G. Enfield (1992), Biosorption of Dichlorodiphenyltrichloroethane and Hexachlorobenzene in Groundwater and Its Implications for Facilitated Transport, *Appl. Environ. Microbiol.*, 58(7), 2211-2218.

Madsen, E. L., and M. Alexander (1982), Transport of Rhizobium and Pseudomonas through Soil1, *Soil Sci. Soc. Am. J.*, 46(3), 557-560.

Magee, B. R., L. W. Lion, and A. T. Lemley (1991), Transport of Dissolved Organic Macromolecules and Their Effect on the Transport of Phenanthrene in Porous-Media, *Environ. Sci. Technol.*, 25(2), 323-331.

McCarthy, J. F., and L. D. McKay (2004), Colloid transport in the subsurface: Past, present, and future challenges, *Vadose Zone J.*, 3, 326–337.

Mccaulou, D. R., R. C. Bales, and R. G. Arnold (1995), Effect of Temperature-Controlled Motility on Transport of Bacteria and Microspheres through Saturated Sediment, *Water Resour. Res.*, 31(2), 271-280.

McDowell-Boyer, L. M. (1992), Chemical mobilization of micron-sized particles in saturated porous media under steady flow conditions, *Environ. Sci. Technol.*, 26(3), 586-593.

McGechan, M. B., and D. R. Lewis (2002), Transport of particulate and colloid-sorbed contaminants through soil, part 1: General principles, *Biosyst Eng*, 83(3), 255-273.

Mills, A. L., J. S. Herman, G. M. Hornberger, and T. H. Dejesus (1994), Effect of Solution Ionic-Strength and Iron Coatings on Mineral Grains on the Sorption of Bacterial-Cells to Quartz Sand, *Appl. Environ. Microbiol.*, 60(9), 3300-3306.

Morley, L. M., G. M. Hornberger, A. L. Mills, and J. S. Herman (1998), Effects of transverse mixing on transport of bacteria through heterogeneous porous media, *Water Resour. Res.* 34:1901-1908.

Nocito-Gobel, J., and J. E. Tobiason (1996), Effects of ionic strength on colloid deposition and release, *Colloids and surfaces A: Physicochemical and engineering aspects*, 107, 223-231.

Noell, A. L., J. L. Thompson, M. Y. Corapcioglu, and I. R. Triay (1998), The role of silica colloids on facilitated cesium transport through glass bead columns and modeling, *J. Contam. Hydrol.*, 31(1-2), 23-56.

Ochiai, N., E. L. Kraft, and J. S. Selker (2006), Methods for colloid transport visualization in pore networks, *Water Resour. Res.*, 42(12), -.

Pang, L., M. McLeod, J. Aislabie, J. Šimůnek, M. Close, and R. Hector (2008), Modeling transport of microbes in ten undisturbed soils under effluent irrigation, *Vadose Zone J.*, 7(1), 97-111.

Passmore, J. M., D. L. Rudolph, M. M. F. Mesquita, E. E. Cey, and M. B. Emelko (2010), The utility of microspheres as surrogates for the transport of E. coli RS2g in partially saturated agricultural soil, *Water Res.*, 44(4), 1235-1245.

Pivetz, B. E. and T. S. Steenhuis (1995), Soil matrix and macropore biodegradation of 2,4-D, *J. Environ. Qual.*, 24, 564-570.

Pivetz, B. E., I. W. Kelsey, T. S. Steenhuis (1996), and M. Alexander, A procedure to calculate biodegradation during preferential flow through heterogeneous soil columns, *Soil Sci. Soc. Am. J.*, 60, 381-388.

Reynolds, K. A., K. D. Mena, and C. P. Gerba (2008), Risk of waterborne illness via drinking water in the United States, *Rev. Environ. Contam. T.*, 192, 117-158.

Roy, S. B., and D. A. Dzombak (1996), Colloid release and transport processes in natural and model porous media, *Colloids and surfaces A: Physicochemical and engineering aspects*, 107, 245-262.

Ryan, J. N., and P. M. Gschwend (1994), Effects of ionic strength and flow rate on colloid release: Relating kinetics to intersurface potential energy, *Journal of Colloid and Interface Science*, 164(1), 21-34.

Saiers, J. E., G. M. Hornberger, and C. Harvey. 1994. Colloidal silica transport through structured, heterogeneous porous media, *J. Hydrol. (Amsterdam)* 163:271–288.

Sen, T. K., and K. C. Khilar (2006), Review on subsurface colloids and colloid-associated contaminant transport in saturated porous media, *Adv Colloid Interfac*, 119(2-3), 71-96.

Šimůnek, J., C. M. He, L. P. Pang, and S. A. Bradford (2006), Colloid-facilitated solute transport in variably saturated porous media: Numerical model and experimental verification, *Vadose Zone J.*, 5(3), 1035-1047.

Šimůnek, J., and M. Th. van Genuchten, Modeling nonequilibrium flow and transport with HYDRUS (2008), *Vadose Zone J.*, doi:10.2136/VZJ2007.0074, Special Issue "Vadose Zone Modeling", *7*(2).

Šimůnek, J., N.J. Jarvis, M.T. van Genuchten and A. Gardenas. (2003), Review and comparison of models for describing non-equilibrium and preferential flow and transport in the vadose zone. *J. Hydrol.*, 272: 14-35.

Stevik, T. K., K. Aa, G. Ausland, and J. F. Hanssen (2004), Retention and removal of pathogenic bacteria in wastewater percolating through porous media: a review, *Water Res.*, 38(6), 1355-1367.

Tolls, J. (2001), Sorption of veterinary pharmaceuticals in soils: A review, *Environ. Sci. Technol.*, *35*(17), 3397-3406.

Topol, E., et al. (1998), International, randomized, controlled trial of lamifiban (a platelet glycoprotein IIb/IIIa inhibitor), heparin, or both in unstable angina, *Circulation*, *97*(24), 2386-2395.

Torkzaban, S., S. A. Bradford, and S. L. Walker (2007), Resolving the coupled effects of hydrodynamics and DLVO forces on colloid attachment in porous media, *Langmuir*, *23*(19), 9652-9660.

Tosco, T., A. Tiraferri, and R. Sethi (2009), Ionic strength dependent transport of microparticles in saturated porous media: modeling mobilization and immobilization phenomena under transient chemical conditions, *Environ. Sci. Technol.*, 43(12), 4425-4431.

Tufenkji, N., and M. Elimelech (2004), Correlation equation for predicting single-collector efficiency in physicochemical filtration in saturated porous media, *Environ. Sci. Technol.*, *38*(2), 529-536.

Unc, A., and M. J. Goss (2003), Movement of faecal bacteria through the vadose zone, *Water Air Soil Poll.*, 149(1-4), 327-337.

USDA. (1992). National engineering handbook: Agricultural waste management field handbook. Part 651 (210-AWMFH, 4/92). Ch. 3, p 1–29. USDA, Washington, DC.

USEPA. (1998). Environmental impacts of animal feeding operations. U.S. Environ. Protection Agency, Office of Water, Standards and Applied Sci. Div., Washington, DC.

Vinten, A. J. A., B. Yaron, and P. H. Nye (1983), Vertical Transport of Pesticides into Soil When Adsorbed on Suspended Particles, *J. Agr. Food Chem.*, *31*(3), 662-664.

Wang, Y., S.A. Bradford and J. Šimůnek (2013) Transport and fate of microorganisms in soils with preferential flow under different solution chemistry conditions. *Water Resour. Res.*, 49: 2424-2436. doi:10.1002/wrcr.20174.

Wollum, A. G., II, and D. K. Cassel. 1978. Transport of microorganisms in sand columns. *Soil Sci. Soc. Am. J.* 42:72-76.

Yao, K.-M., M. T. Habibian, and C. R. O'Melia (1971), Water and waste water filtration. Concepts and applications, *Environ. Sci. Technol.*, *5*(11), 1105-1112.

Yee, N., J. B. Fein, and C. J. Daughney (2000), Experimental study of the pH, ionic strength, and reversibility behavior of bacteria-mineral adsorption, *Geochim. Cosmochim. Acta*, 64(4), 609-617.

Chapter 2

Transport and Fate of Microorganisms in Soils with Preferential Flow under Different Solution Chemistry Conditions

Abstract

Laboratory and numerical studies were conducted to investigate the transport and fate of

E.coli D21g and coliphage φX174 in saturated soils with preferential flow under different

solution ionic strength (IS=1, 5, 20, and 100 mM) conditions. Preferential flow systems

were created by embedding a coarse sand lens (710 μm) into a finer matrix sand (120

μm). Complementary transport experiments were conducted in homogeneous sand

columns to identify controlling transport and retention processes, and to independently

determine model parameters for numerical simulations in the heterogeneous experiments.

Results from homogeneous and heterogeneous transport experiments demonstrate that

retention of *E. coli* D21g and φX174 increased with IS, while the effect on *E. coli* D21g

in finer sand was much greater than in coarse sand. This microbe transport behavior was

well described by numerical simulations. The importance of preferential flow on microbe

transport was found to be enhanced at higher IS, even though the overall transport

decreased. However, the contribution of preferential flow was much higher for *E. coli*

D21g than φX174. Deposition profiles revealed significant cell retention at the interface

of the coarse sand lens and fine sand matrix as a result of mass transfer. Cell release from

the preferential flow system with a reduction of solution IS exhibited multi-pulse

breakthrough behavior that was strongly dependent on the initial amount of cell retention,

especially at the lens-matrix interface.

2.1 Introduction

Waterborne disease outbreaks associated with drinking water in the United States during 1971–2002 are known to have resulted in 575,457 cases of illness and 79 deaths, with 14% caused by bacteria, 19% by protozoa, 8% by viral pathogens, and 47% by unknown acute gastrointestinal illness [*Reynolds et al.*, 2008]. Wastes from humans, domesticated and wild animals, birds, and insects frequently contain high concentrations of pathogenic microorganisms [*USDA*, 1992; *USEPA*, 1998; *Gerba and Smith*, 2005] that serve as pathogen sources in agricultural settings. Pathogenic microorganisms can be transported to streams by surface water runoff and to ground water by recharge through the vadose zone. These contaminated surface and ground water supplies may eventually serve as drinking water and/or irrigation water for fresh produce. If these contaminated water supplies are not adequately treated before use, ground water typically receives minimal or no treatment, then they can put the public's health at risk.

Much research has examined physical (size of the microbe and the porous medium, microbe concentration, water velocity, water content, and surface roughness) and chemical (surface chemistry of the microbe and soil, and aqueous solution pH, ionic strength, and chemical composition) factors that influence the retention of

microorganisms in homogeneous porous media under relatively uniform flow [*Mills et al.*, 1994; *Mccaulou et al.*, 1995; *Hendry et al.*, 1999; *Yee et al.*, 2000; *Dong et al.*, 2002; *Bradford et al.*, 2006b; *Chen and Walker* 2007]. Mechanisms of microbe retention have been inferred from repacked column breakthrough curves (BTCs) and retention profiles (RPs), batch experiments, and complimentary micromodel studies that allowed for direct microscopic observation [*Ochiai et al.*, 2006]. The mechanisms governing transport and retention of microbes in porous media have been described by several review articles [*Stevik et al.*, 2004; *Sen and Khilar*, 2006; *Bradford and Torkzaban*, 2008].

Field, lysimeter, and undisturbed soil column experiments have frequently revealed that microorganisms, colloids, and other contaminants can travel much deeper and faster than would be predicted based on results from laboratory studies in homogeneous porous media [*Bales et al.*, 1989; *Abu-Ashour et al.*, 1994; *Pivets and Sttenhuis*, 1995; *Pivetz et al.*, 1996; *Jiang et al.*, 2010]. This phenomenon has been ascribed to transport in preferential flow pathways created by plant roots, burrowing earthworms [*Beven and Germann*, 1982; *Madsen and Alexander*, 1982; *Unc and Goss*, 2003; *Cey et al.*, 2009] and/or natural structural heterogeneities [*Wollum, and Cassel*, 1978]. Preferential flow can also occur in soils and aquifers with strong contrasts in

hydraulic conductivity between sediment layers [*Harvey et al*., 1993]. Considerable

research has indicated that colloids and microorganisms can be transported in preferential

flow pathways [*McGechan and Lewis*, 2002; *Jarvis*, 2007; *Pang et al.*, 2008; *Cey et al.*,

2009; *Cey and Rudolph*, 2009; *Passmore et al.*, 2010]. Preferential flow has also been

implicated in the rapid transport of bacteria to field tile drains [*Evans and Owens*, 1972;

Dean and Foran, 1992; *Guzman et al.*, 2009]. However, most of this research is

qualitative in nature because of difficulty in quantifying the physical and chemical

complexities of the soil matrix and macropore system with regard to microbe transport.

This gap in information currently presents a great obstacle to predicting the fate of

microbes in natural environments [*McCarthy and McKay*, 2004].

The exchange rate of water between the macropore and the matrix, or between

layers with contrasting hydraulic conductivities, will likely be a critical factor in

determining the rate of microbe migration in preferential flow systems [*Harvey et al*.,

1993; *Morley et al*.,1998; *Allaire-Leung et al.*, 2000a, 2000b; *Allaire et al.*, 2002a, 2002b]

because of the potential for greater retention of microbes in the matrix as a result of

enhanced chemical interactions, lower hydrodynamic forces, and smaller pore spaces. It

is also possible that microbes may be physically excluded from the matrix, and in this

case transport of microbes would exclusively occur in macropores. Optimum conditions for microbe transport in preferential flow systems will therefore likely depend on a wide variety of chemical and physical factors of both the matrix and macropore domains, but little quantitative research has addressed this issue and the relative importance of these factors has not yet been fully determined [*Fontes et al.*, 1991].

It is important to be able to describe water flow in the preferential flow domain in order to quantitatively simulate the transport of microorganisms in the field. Various conceptual models of preferential flow exist that are dependent on a great number of parameters (e.g., macropore hydraulic properties, mass transfer terms, and macropore geometry) [*Šimůnek and van Genuchten*, 2008]. It is difficult, if not impossible, to independently determine all of the required model parameters under natural conditions [*Šimůnek et al.*, 2003]. Thus, some assumptions have to be made to simplify the preferential flow path for simulation purposes. Artifical macropores can be systematically created by leaving small cylindrical openings in repacked columns [*Pivetz and Steenhuis*, 1995; *Castiglione et al.*, 2003], or by packing different sized sands to generate layers and/or lens with contrasting hydraulic conductivities [*Fontes et al.*, 1991; *Saiers et al.*, 1994; *Morley et al.*, 1998; *Bradford et al.*, 2004]. The study of preferential

flow and transport through artificial macropores provides an opportunity to overcome

many modeling challenges because the macropore geometry and hydraulic properties can

be well defined and controlled in a repeatable manner [*Pivetz and Steenhuis*, 1995;

Castiglione et al., 2003; *Guzman et al.*, 2009; *Arora et al.*, 2011; *Arora et al.*, 2012].

Hence, it is possible to isolate and identify factors that have the greatest influence on

preferential flow and transport in such systems. Furthermore, controlled preferential flow

and transport studies provide valuable information on parameterization that is needed to

help adapt numerical models to complex natural systems.

Most studies of colloid and/or microbe transport through artificial macropores

have focused on understanding the influence of physical heterogeneity on BTCs [*Fontes

et al.*, 1991; *Saiers et al.*, 1994; *Morley et al.*, 1998] and RPs [*Bradford et al.*, 2004].

Numerical simulations of collected data demonstrate the importance of transverse mixing

at the interface between the coarse-sand lens and fine-sand matrix [*Saiers et al.*, 1994;

Morley et al., 1998] and the spatial distribution of retained colloids [*Bradford et al.*,

2004]. Relatively little research has investigated the influence of microbe size and

solution chemistry in preferential flow systems. *Fontes et al.* [1991] studied bacteria

transport under two different ionic strength (IS) conditions in a column with a coarse

sand lens imbedded in a finer soil matrix, and demonstrated decreasing transport potential with an increase in IS. However, bacteria RPs were not determined in this study, and the data was not modeled. Furthermore, no published research has examined the release behavior of microbes with a reduction of solution IS in systems with artificial macropores. Consequently, our understanding of the effects of solution chemistry on microbe transport in preferential flow systems is still incomplete.

The objective of this research was to study the coupled influence of physical and chemical factors on the transport of microorganisms in preferential flow systems. Transport experiments were conducted for two different sized microorganisms (*E. coli* D21g and coliphage φX174) in packed columns with an artificial macropore at various IS conditions. Complementary transport experiments were also conducted with these microorganisms in homogeneously packed columns to independently determine many of the model parameters. Retention profiles and the release of retained microorganisms after altering the IS of the soil solution were additionally studied for heterogeneous columns. Numerical simulation of the flow and transport behavior of the preferential flow system with HYDRUS (2D/3D) facilitated the quantification of flow and transport processes, especially the mass transfer and release behavior at the matrix/macropore interface.

2.2 Materials and Methods

2.2.1 Sands and Electrolyte Solutions

Two sizes of Ottawa (quartz) sand were used in the column experiments described below. The median grain size (d_{50}) of these sands were 120 and 710 μm (referred to as fine sand and coarse sand below) and their corresponding coefficients of uniformity were equal to 1.6 and 1.3, respectively. A salt cleaning procedure was employed to remove kaolinite clay from the sand surfaces [*Bradford and Kim*, 2010] before use in the experiments to eliminate any background interference from clay particles.

Electrolyte solutions that were used in column experiments consisted of autoclaved, deionized (DI) water with its pH=5.8 and the IS level adjusted to 0, 1, 5, 20, and 100 mM using NaCl or NaBr. These IS levels were selected to create a range of adhesive conditions between the microorganisms and sand. Bromide served as a conservative tracer in the column experiments. The effluent concentration of bromide was determined using a Bromide-Selective Electrode (Thermo Scientific Orion bromide electrode ionplus® Sure-Flow®).

2.2.2 Microbes

Escherichia coli D21g and coliphage φX174 were selected as representative

microorganisms for column transport experiments. *E. coli* D21g is a Gram-negative,

nonmotile bacterial strain, which has minimal lipopolysaccharides (LPS), and negligible

amounts of extra-cellular polymeric substances (EPS) [*Walker et al.*, 2004]. The effective

diameter of *E. coli* D21g is 1.84 μm [*Walker et al.*, 2004]. Coliphage φX174 is

considered to be a conservative indicator for human virus transport. It is a spherical,

single stranded DNA coliphage with a 27-nm diameter and low hydrophobicity [*Dowd et

al.*, 1998].

E. coli D21g was cultured in Luria-Bertani broth (LB Broth, Fisher Scientific,

Fair Lawn, NJ) containing 0.03 mg/L gentamycin (Sigma, St. Louis, MO) on a rotary

shaker overnight (12-18 h) at 37°C. Then 2 mL of liquid culture was transferred onto a

LB media plate containing 0.03 mg/L gentamycin, and the plates were cultured overnight

(12-18h) at $37\,^{o}$C. Sterile water was placed on the plates and the colonies were gently

harvested using a sterile glass rod to release the colonies into solution. The bacteria

suspension was then centrifuged to separate whole cells from the solution. The

supernatant was decanted and the bacteria were resuspended. These processes were

repeated two times before diluting the concentrated suspension into the desired

electrolyte solution to ensure that all traces of the growth medium were removed. A fresh

cell suspension was prepared right before the start of each experiment. The

concentrations of *E.coli* D21g in influent, effluent, and soil solution were determined

using a spectrophotometer (Unico UV-200, United Products & Instruments, Dayton, NJ)

at 600 nm [*Torkzaban et al.*, 2008], and by the spread plating method [*Clesceri et al.*,

1989] when necessary (e.g., low concentration).

Coliphage φX174 was propagated at 37^oC overnight on bacterial host *E. coli* CN-13

(ATCC 700609) at mid-exponential growth phase in Typtic soy broth supplemented with

1% nalixidic acid. The lysate was centrifuged (5000× g for 20 min) and filtered (0.45 μm

filter) to remove the cell debris and to recover the coliphage. The concentration of

coliphage φX174 in aqueous solutions was determined using the double agar overlay

Method 1601 [*USEPA*, 2001] with bacterial host *E. coli* CN-13. The number of plaque

forming units (PFU) was determined by counting the plaque density. All coliphage assays

were run in duplicate and diluted as necessary.

E. coli D21g and coliphage φX174 were added to the NaBr solutions to achieve

influent concentrations (C_0) of ∼1.0×10^8 cells/mL and ∼1.0×10^7 pfu/mL, respectively.

The suspension was continuously mixed during the column experiment using a magnetic stirrer. The values of C_0 for both microbes were measured three times during the course of a transport experiment to assess the reproducibility of the measurements and microbial survival. The spectrophotometer readings for *E. coli* D21g were within 1% of C_0, and the standard deviation of the spread plating method was 14.3% of C_0. The standard deviation of repeated measurements of φX174 was 13.1% of C_0. No systematic decrease in C_0 was observed over the duration of the column experiments, and this indicates that little inactivation occurred during this interval.

2.2.3 DLVO Calculations

The zeta potential of coliphage φX174, *E. coli* D21g, and Ottawa sand crushed to a powder in the various solution chemistries (Table 2.1) was calculated from experimentally measured electrophoretic mobilities using a ZetaPALS instrument (Brookhaven Instruments Corporation, Holtsville, NY) and the Smoluchowski equation. The total interaction energy of the φX174 and *E. coli* D21g upon approach to the Ottawa sand under the various solution chemistries was subsequently calculated (Table 2.1) using Derjaguin-Landau-Verwey-Overbeek (DLVO) theory and a sphere-plate assumption

[*Verwey and Overbeek*, 1948; *Derjaguin*, 1954]. Electrostatic double layer interactions were quantified using the expression of *Hogg et al.* [1966] using zeta potentials in place of surface potentials. The retarded London-van der Waals attractive interaction force was determined from the expression of *Gregory* [1981]. Values of the Hamaker constant used in these calculations were 4E-21 J [*Penrod et al.*, 1996] and 6.5E-21 J [*Rijnaarts et al.*, 1995] for φX174 and *E. coli* D21g, respectively.

Table 2.1. Measured zeta potentials and calculated mean interaction energy barrier height and depth of the secondary minima for *E. coli* D21g and φX174 on approach to the quartz sand.

	Zeta potential (mV)				Energy barrier height (kT)				Secondary minima (kT)			
IS	Fine	Coarse	*E. coli*	φX174	*E. coli* D21g		φX174		*E. coli* D21g		φX174	
(mM)	Sand	Sand	D21g		Fine	Coarse	Fine	Coarse	Fine	Coarse	Fine	Coarse
					Sand	Sand	Sand	Sand	Sand	Sand	Sand	Sand
1	-80	-83	-60	-20	5520	5657	11.2	11.2	N/A	N/A	N/A	N/A
5	-81	-75	-52	-15	4317	4149	6.5	6.4	-0.5	-0.5	-0.01	-0.01
20	-80	-63	-43	-8.5	2920	2502	1.6	1.6	-2.6	-2.7	-0.03	-0.03
100	-40	-30	-13	-6.4	59	15.7	NB	NB	-23.4	-26.4	NB	NB

NB – Denotes no energy barrier

N/A – Denotes not applicable

2.2.4 Homogeneous Column Experiments

Glass chromatography columns (15 cm long and 4.8 cm inside diameter) were used in homogeneous transport experiments. A schematic of the experimental setup is given by *Bradford et al.* [2002]. The columns were wet packed with a given size of Ottawa sand. The porosity of the packed columns was between 0.36 and 0.38, and the length of the columns was about 13 cm. Aqueous solutions were pumped upward through the vertically oriented columns at a steady flow rate using a peristaltic pump. The pore water velocities in the homogeneous column experiments (Table 2.2) were selected to be consistent with those measured in the heterogeneous column experiments described below.

Two pore volumes (PVs) of a selected NaCl solution were flushed through a column, and the sand was allowed to equilibrate with this solution (phase 0) before initiating a microbial transport experiment. Microbial transport experiments were carried out in two phases. First, several PVs of microbe suspension and NaBr were introduced into the column at a constant rate and IS (phase 1). Second, NaCl solution was flushed through the column at the same flow rate and IS as in phase 1 until the effluent microbe concentration returned to a baseline level (phase 2). Effluent samples were continuously

collected during the transport experiment at selected intervals using a fraction collector.

The effluent samples were then analyzed for Br and microbe concentrations as described

above. Replicate transport experiments were conducted for the different solution

chemistry conditions.

Table 2.2. Experimental (pore water velocity, v) and fitted model (bromide dispersivity, λ; microbe attachment rate coefficient, k_{att}; and maximum solid phase concentration of microbes, S_{max}) parameters from the homogeneous fine and coarse sand column experiments with *E. coli* D21g and φX174 at different solution IS conditions. The goodness of the model fit is quantified by the coefficient of linear regression (R^2) on breakthrough data unless otherwise noted.

	IS (mM)	v (cm/min)	λ (cm)	*E. coli* D21g			φX174		
				k_{att}	S_{max}	R^2	k_{att}	S_{max}	R^2
Fine Sand	1	0.33	0.10	0.0004	0.01	0.99	0.33	0.17	0.98
	5	0.31	0.10	0.066	1.1	0.99	ND	ND	ND
	20	0.34	0.13	0.2	3.5	0.95	ND	ND	ND
	100	0.37	0.14	0.48	4.8	0.99^a	0.68^b 0.034^c	0.16^b 0.54^c	0.96
Coarse Sand	20	10.3	0.52	0.001	0.1	1.00	ND	ND	ND
	100	10.3	0.59	0.005	0.4	0.97	ND	ND	ND

[a]determined using retention profile information.

[b]parameters for site 1

[c]parameters for site 2

ND – denotes not determined

The microbial RPs in the sand of some columns were determined following

completion of phases 1 and 2. The saturated sand was carefully excavated into tubes

containing excess DI water. The tubes were shaken for 15 minutes to liberate any

reversibly retained microbes and the concentrations of *E. coli* D21g and coliphage φX174

in the excess solution were determined as described above. The volume of solution and

mass of dry sand was determined from mass balance. The microbe mass recovery (%)

was subsequently determined during phases 1 and 2 and for the RPs from mass balance

and the injected amount (Table 2.3).

Table 2.3. Mass balance information (effluent, sand, and total) for homogeneous fine and coarse sand column experiments with *E. coli* D21g and φX174 at different solution IS conditions.

| | IS (mM) | Recovery (%) | | | | | |
| | | *E. coli* D21g | | | φX174 | | |
		Effluent	Sand	Total	Effluent	Sand	Total
Fine Sand	1	103	ND	103	69	1	70
	5	44	58	102	ND	ND	ND
	20	12	83	95	ND	ND	ND
	100	2	85	87	36	1	37
Coarse Sand	20	98	3	101	ND	ND	ND
	100	92	12	104	ND	ND	ND

ND—denotes not determined.

2.2.5 Heterogeneous Column Experiments

Heterogeneous column experiments were conducted in a plexiglass (acrylic)

column, 22 cm long and 13.2 cm inside diameter. A polyester membrane (Saatifil PES

18/13) with an 18 μm nominal pore size was placed at the bottom of the column and

connected to a hanging water column (tube) to control the bottom boundary pressure.

Preferential flow systems were created by packing the fine (120 μm) and coarse (710 μm)

sands into the column as follows: (i) the column was filled with autoclaved DI water to

about one third of the column height, and a 30 cm long plastic tube with outside diameter

of 1.14 cm was held in the center of the column; (ii) the fine sand was incrementally wet

packed into the matrix portion of the column (outside the plastic tube) to a height of 20

cm; (iii) excess water in the plastic tube was drained from the bottom; (iv) the tube was

carefully pulled out from the column without disturbing the surrounding fine matrix sand

and leaving a 1.14 cm diameter hole in the center of the column; (v) the hole was then

filled to a height of 20 cm with the coarse sand using a funnel to create a preferential flow

lens; (vi) the column was then saturated with water from the bottom. The porosity of the

columns ranged from 0.34 to 0.36. Figure 2.1 shows an example of the artificial

preferential flow path.
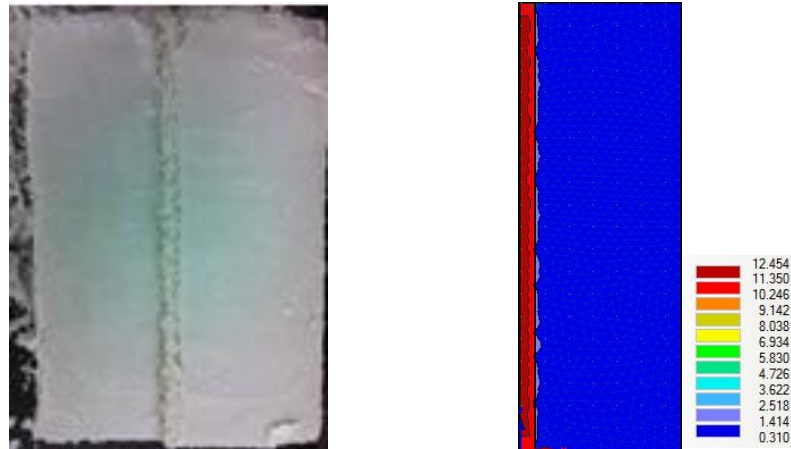
Figure 2.1. A representative picture of heterogeneous column with lens in the center (left) and simulated flow field (right).

Solutions were delivered onto the surface of the heterogeneous column at a steady flow rate using a rain simulator connected to a peristaltic pump. The water velocity was selected in order to just maintain saturated conditions (several mm of ponding at the surface) in the column through the experiments. Figure 2.2 shows a schematic of the experimental setup used for the preferential bromide and microbial transport experiments. Similar procedures were carried out to collect and analyze effluent samples in the homogeneous and heterogeneous column experiments. Furthermore, phases 0, 1, and 2 were conducted in an analogous fashion. After recovery of the BTCs, the distribution of retained microbes in the heterogeneous column was quantified as follows. Sand samples

were taken at six equally spaced depths and three locations, namely: the lens, the matrix

in the vicinity of the lens, and the bulk matrix. The determination of the amount of

retained microbes in the sand was then determined in a similar manner to the

homogeneous column experiments. Phases 1 and 2 of the heterogeneous column

experiments were replicated for most solution chemistry conditions.
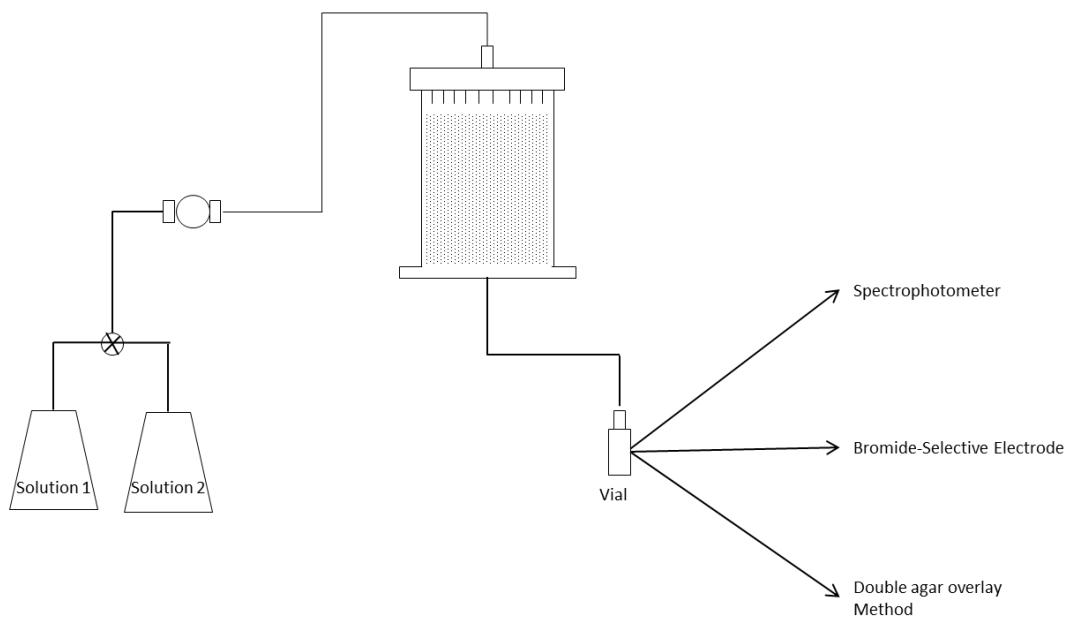
Figure 2.2. A schematic of the setup for transport experiments in heterogeneous columns.

Following recovery of the breakthrough curve (BTC) for the microbes and bromide,

some of the columns underwent an additional experimental phase 3 to determine the

release of retained microbes with a reduction in solution IS. In this case, columns were

flushed with autoclaved DI water at the same velocity as during phases 1 and 2 until the

released microbe concentration in the effluent returned to a baseline level. The effluent

samples were collected and analyzed using the same protocols as during phases 1 and 2.

The saturated hydraulic conductivity (K_s) for the fine and coarse sands was

directly measured to be 0.3 cm/min and 11 cm/min, respectively. However, the value of

K_s in the matrix and lens was observed to vary somewhat for each heterogeneous column

experiment due to small differences in packing and porosity. A more representative value

of K_s for the matrix and lens was determined as follows. The value of K_s for the matrix

was determined from the breakthrough time of the Br tracer from the matrix. The value of

K_s for the lens was subsequently determined as the difference in the measured total flow

rate and the matrix flow rate.

2.3 Numerical Modeling

The HYDRUS-1D and HYDRUS (2D/3D) [*Šimůnek et al.*, 2008] codes were

used to simulate the transport of bromide and microbes in the homogeneous and

heterogeneous column experiments, respectively. The HYDRUS codes simulate water

flow using the Richards equation. Bromide transport was simulated using the advection-

dispersion equation (ADE). Microbe transport and retention was simulated using the

ADE with first-order terms for kinetic retention and release as shown below for the 2D

case:

$$\frac{\partial(\theta C)}{\partial t} = \frac{\partial}{\partial x_i}\left(\theta D_{ij}\frac{\partial C}{\partial x_j}\right) - \frac{\partial q_i C}{\partial x_i} - \theta \psi k_{att} C + \rho k_{det} S \qquad [1]$$

$$\frac{\partial(\rho S)}{\partial t} = \theta \psi k_{att} C - \rho k_{det} S \qquad [2]$$

where subscripts i and j denote coordinate directions, C [N_c L^{-3}; L and N_c denote the units

of length and number of microbes, respectively] is the microbe concentration in the

aqueous phase, S [N_c M^{-1}; M denotes units of mass of soil] is the microbe concentration

on the solid phase, D_{ij} [L^2 T^{-1}] is the hydrodynamic dispersion coefficient, q_i [L T^{-1}] is the

Darcy water velocity in i direction, k_{det} [T^{-1}] is the microbe detachment rate coefficient,

k_{att} [T^{-1}] is the microbe attachment rate coefficient, θ [$-$] is the water content, and ρ [M L^{-}

^{3}] is the bulk density. The parameter ψ [-] accounts for time and concentration dependent

blocking using a Langmuirian approach as [*Adamczyk et al.*, 1994]:

$$\psi = 1 - \frac{S}{S_{max}} \qquad [3]$$

where S_{max} [N_c M^{-1}] is the maximum solid phase concentration of microbes. In the case of

φX174 at solution IS = 100 mM, a similar two site kinetic retention was employed.

The homogeneous column transport experiments were simulated using a third-type

boundary condition at the inlet, and a zero concentration gradient at the outlet. The

HYDRUS codes include a nonlinear least squares optimization routine to inversely

estimate model parameters by fitting to experimental data. This option was used to

determine Br and microbe transport parameters by fitting the experimental data from the

homogeneous column experiments. In particular, the dispersivity was determined from

the Br BTC and the transport parameters (S_{max}, k_{att}, k_{det}) for microbes at given solution

chemistry conditions were determined from measured microbe BTCs and/or RPs (Table

2.2).

Bromide and microbe transport parameters obtained from the homogeneous

column experiments were subsequently used in HYDRUS simulations of the

heterogeneous column experiments with preferential flow. In this case, a 2D

axisymmetrical geometry was employed and the model domain was 20 by 6.6 cm. This

domain was subdivided into two vertical regions, with the left region representing the

coarse lens in the center of the column with a radius of 0.57 cm and the remaining region

representing the fine matrix sand. Domain discretization was designed to reduce

simulation times while minimizing mass balance errors. A constant water flux boundary

condition was employed at the soil surface, and a constant head was applied at the bottom boundary. A third-type boundary was chosen for the solute transport boundary condition at the inlet, and a zero concentration gradient was selected at the column outlet.

2.4 Results and Discussion

2.4.1 Bromide

Representative plots of observed and simulated BTCs (C/C_0 verse pore volume) for the Br tracer in the homogeneous fine sand and coarse sand columns are shown in Figure 2.3. Bromide acted as a good conservative tracer, with good mass recovery and breakthrough at 1 pore volume. The 1D advection-dispersion equation provided an excellent description of the homogeneous Br BTCs (Fig. 2.3) when the dispersivity was inversely optimized to the data (R^2>0.98). Dispersivities were around 0.12 and 0.55 cm (Table 2.2) for fine and coarse sand columns, respectively.
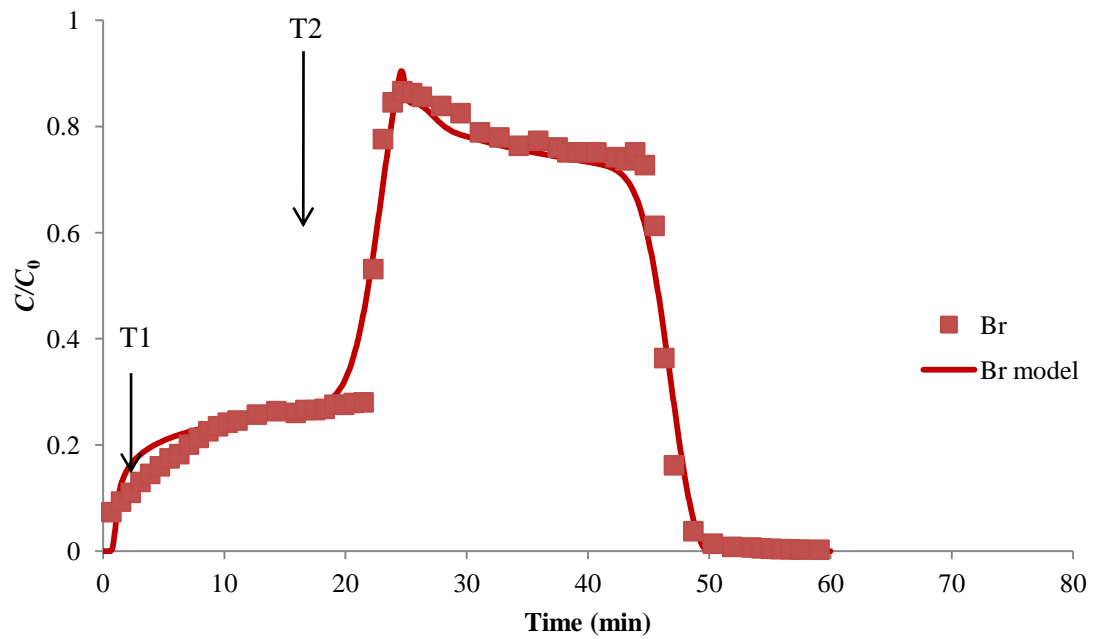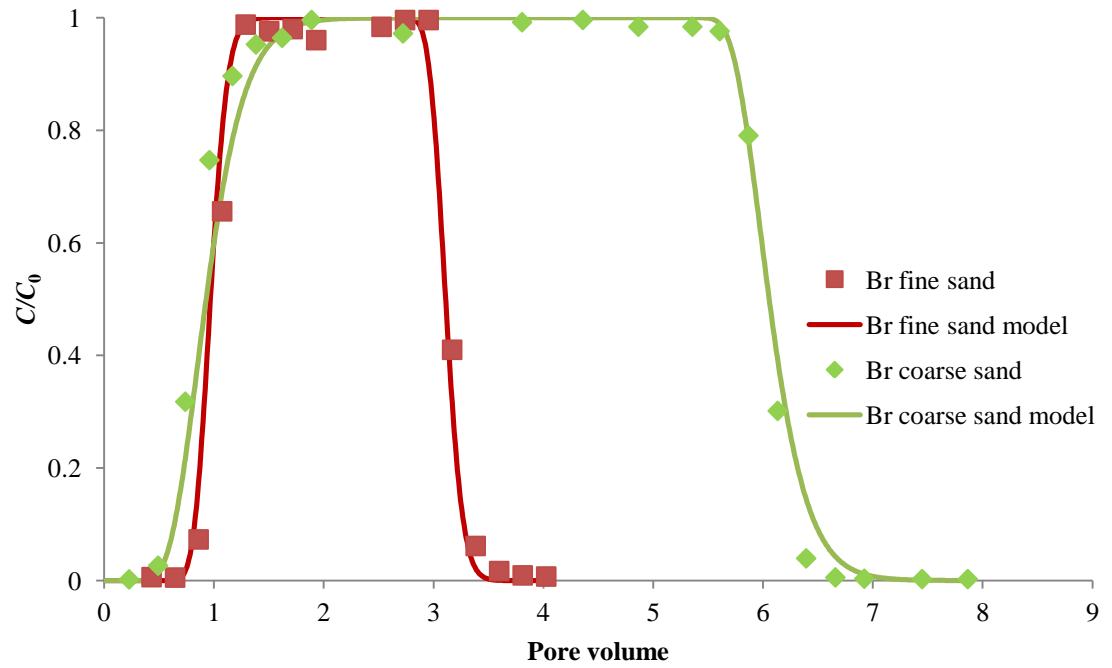
Figure 2.3. Representative plots of observed and simulated (model) normalized Br concentrations (C/C_0) in homogeneous fine sand and coarse sand columns as a function of pore volume (top), and in the heterogeneous column as a function of time (bottom). Parameter values are given in Tables 2.2 and 2.4.

45

Fig. 2.3 also provides representative observed and simulated BTCs for Br in a

heterogeneous column that exhibited preferential flow. The very early breakthrough of Br

(labeled as T1) demonstrated the extremely fast movement of water and solute through

the artificial macropore. The peak value of C/C_0 in this first pulse was around 0.20-0.27,

indicating that 20-27% of the total water flux occurred through the macropore (Table 2.4).

A second, higher (C/C_0 =0.83 to 0.90) Br pulse (labeled as T2) occurred after about 22

minutes due to breakthrough of Br from the matrix material. The value of C/C_0 does not

reach 1 for the matrix pulse because of the difference in arrival/ending times of the

matrix and lens pulses; e.g., the matrix pulse is diluted by NaCl solution from the lens. As

mentioned earlier, the measured Br breakthrough times for the lens and matrix regions

were used to refine estimates of the hydraulic properties in the heterogeneous column

experiments. Table 2.2 provides a summary of the solute transport parameters that were

used in subsequent HYDRUS simulations for each column. The values of the lens and

matrix K_s (Table 2.4) and water fluxes (Table 2.4) were very consistent for the different

column experiments and this indicates that the artificial macropore was highly duplicable

and had limited variation. Furthermore, the agreement between observed and simulated

Br BTCs was very good (R^2>0.92 in Table 2.4). Simulations therefore provided an

excellent description of water flow and Br transport in the heterogeneous systems.

Table 2.4. Experimental values of the local (lens and matrix) saturated hydraulic conductivity (K_s), the percentage of local flux to total flux, and the percentage of local transport to total transport in the heterogeneous column experiments for *E. coli* D21g at different solution IS conditions.

IS (mM)	Lens			Matrix		
	K_s (cm/min)	Flux %	Transport %	K_s (cm/min)	Flux %	Transport %
1	11.2	25	26	0.31	75	74
5	11.8	27	38	0.31	73	62
20	10.5	27	68	0.31	73	32
100	10.6	20	99	0.33	80	1

2.4.2 *E. coli* D21g

Figure 2.4a presents observed and simulated BTCs for *E. coli* D21g in

homogeneous fine sand when the solution IS equaled 1, 5, 20, and 100 mM. Figure 2.4b

gives similar information for the coarse sand when the IS was 20 mM and 100 mM.

Corresponding RPs and mass balance information for these systems are presented in Fig.

2.5 and Table 2.3, respectively. Retention profiles are plotted in Figure 2.5 as the

normalized retained concentration of cells in the sand (S/C_0) as a function of the distance

from the column inlet. Retention parameters (k_{att}, k_{det}, and S_{max}) were estimated by nonlinear least squares optimization to the experimental data (Table 2.2).

Less breakthrough was observed for both fine sand and coarse sand as the IS increased (Fig. 2.4). The effluent recovery rate for *E. coli* D21g decreased from 103% to 2% in the fine sand as the IS increased from 1 to 100 mM (Table 2.3). A similar trend occurred in the coarse sand, but changes in IS had a much less significant influence on the transport of *E. coli* D21g in coarse than in fine sand (Table 2.2). For example, when the IS=100 mM, the recovery in the effluent was equal to 2% and 92% in the fine and coarse sands, respectively. Similar *E. coli* D21g transport experiments in the coarse sand were not conducted at IS=1 and 5 mM because almost complete breakthrough occurred at IS= 20 and 100 mM. The RPs for *E. coli* D21g in the fine and coarse sand (Fig. 2.5) followed complimentary trends to the BTCs shown in Figure 2.4, with increasing cell retention with IS and in the finer sand. The RPs tended to decrease exponentially with depth as predicted by the filtration theory [*Yao et al.*, 1971].
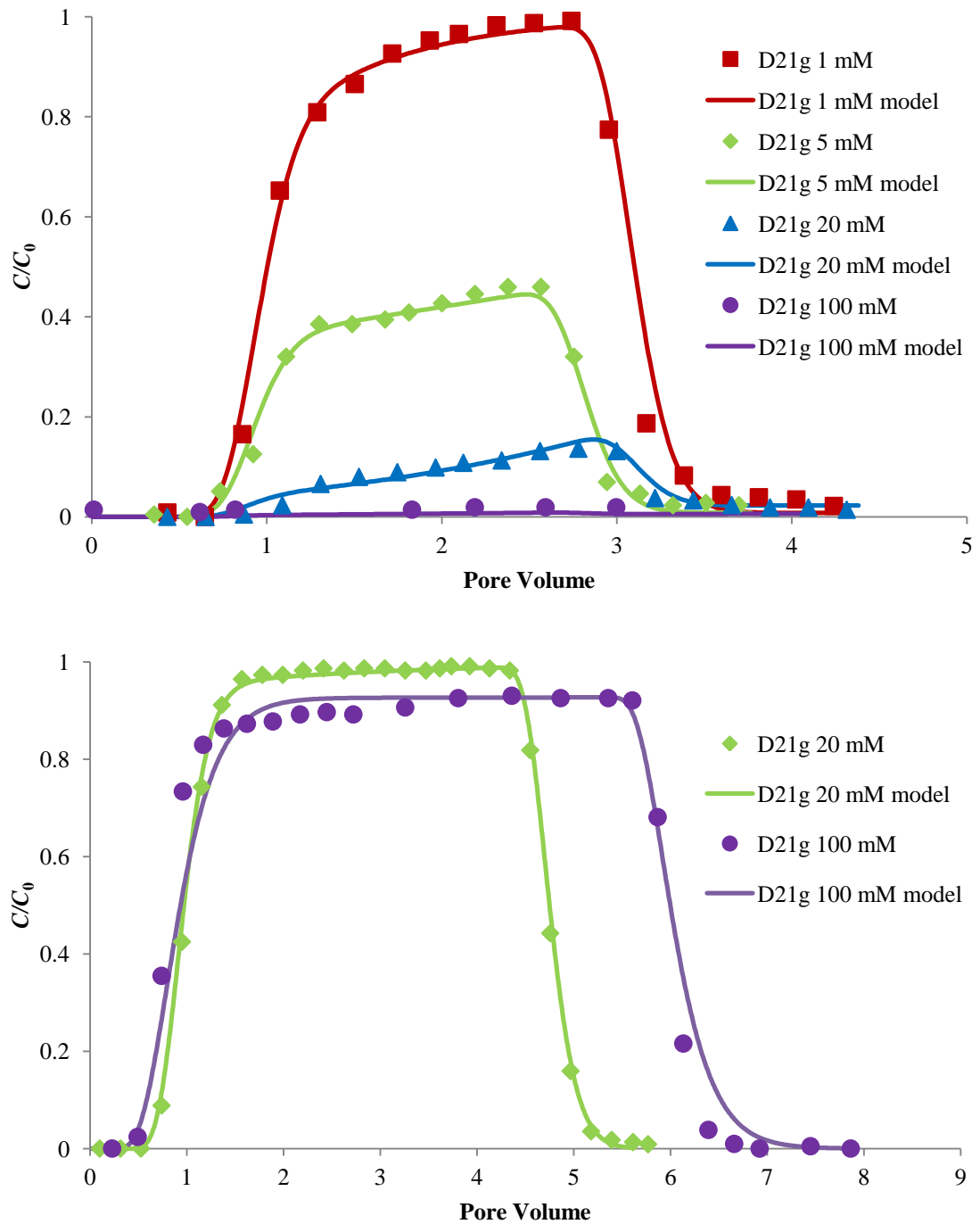
Figure 2.4. Observed and simulated (model) normalized effluent concentrations (C/C_0) of *E. coli* D21g as a function of pore volume in homogeneous fine sand (top) and coarse sand columns (bottom) at selected solution IS conditions. Parameter values are given in Table 2.2.

Figure 2.5. Observed and simulated (model) normalized solid phase concentrations (S/C_0) of *E. coli* D21g as a function of depth in homogeneous fine sand (top) and coarse sand columns (bottom) at selected solution IS conditions. Parameter values are given in Table 2.2.

Simulations provided a good description of the *E. coli* D21g BTC and RP data

(R^2>0.95 in Table 2.2), including the blocking behavior at intermediate IS conditions.

Similar to experimental observations, the values of k_{att} and S_{max} increased with IS, and

were larger in the finer than the coarser sand (Table 2.2). The value of k_{det} was low in all

cases, thus k_{det} was set as 0 for all simulations.

A partial explanation for differences in the *E. coli* D21g transport behavior in

coarse and fine sand is obtained from the filtration theory [*Yao et al.*, 1971], which

predicts that *E. coli* D21g mass transfer to the sand surface is greater for the finer than the

coarser sand. Table 2.1 presents the calculated mean interaction energy height and depth

of the secondary minimum for *E. coli* D21g on approach to the quartz sand. Unfavorable

attachment conditions (i.e., the presence of a significant energy barrier in Table 2.1) are

predicted to occur for all the solution IS. However, the depth of the secondary energy

minimum increased with IS (Table 2.1) and followed a qualitatively similar trend to the

amount of cell retention (Table 2.3).

It should be mentioned that mean interaction energies do not reflect the

potentially significant influence of microscopic heterogeneities on cell retention

[*Duffadar and Davis*, 2008]. Evidence for the potential role of microscopic

heterogeneities is obtained from the mass balance information (Table 2.3) and from fitted

model parameters (Table 2.2). In particular, values of S_{max} increased with IS and in the

finer sand (Table 2.2). Furthermore, the total mass recovery in the fine sand decreased

from around 100% at IS=1 mM to around 87% at IS=100 mM (Table 2.3). This

observation suggests that a small amount (<13%) of *E. coli* D21g were irreversibly

retained (primary minimum) in the fine sand at IS=100 mM. Conversely, mass balance

information indicates that *E. coli* D21g reversibly interacted in a secondary minimum

(>95%) at lower IS and in the coarse sand.

Figure 2.6 presents observed and simulated BTCs for *E. coli* D21g in the

heterogeneous columns when the solution IS equaled 1, 5, 20, and 100 mM.

Corresponding mass balance information for these systems is presented Table 2.5. Recall

that the first pulse in the BTC is associated with transport through the lens, whereas the

second pulse is controlled by the matrix. When the IS=1 mM the effluent recovery of *E.*

coli D21g was 96% (Table 2.5) and the BTCs for *E. coli* D21g (Fig. 2.6) and Br (Fig. 2.3)

were very similar. However, the matrix breakthrough time for *E. coli* D21g was slightly

earlier than for Br (21.5 compared to 23.0 minute). This suggests that size exclusion may

increases the transport velocity of *E. coli* D21g by constraining cells to faster flow

domains and larger pore networks than Br [*Fontes, et al.* 1991; *Ryan and Elimelech*, 1996; *Morley, et al.* 1998; *Ginn*, 2002].
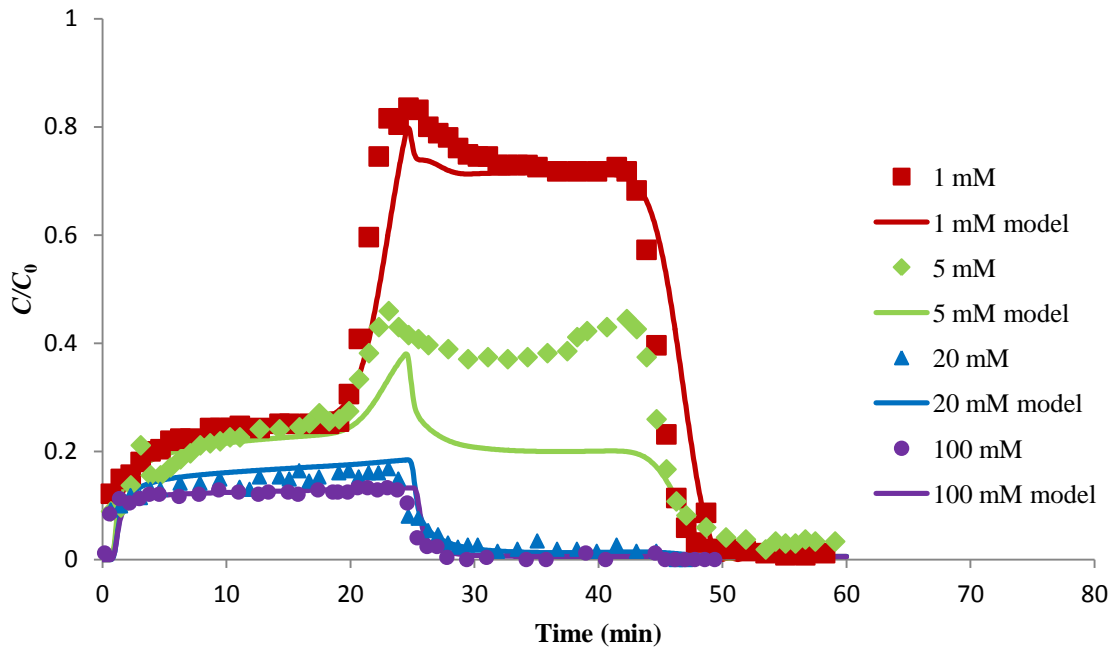
Figure 2.6. Observed and simulated (model) normalized effluent concentrations (C/C_0) of *E. coli* D21g as a function of time in heterogeneous columns at selected solution IS conditions. Parameter values are given in Tables 2.2 and 2.4.

Similar to homogeneous columns (Fig. 2.4), the recovery of *E. coli* D21g in the effluent of the heterogeneous columns decreased from 96% to 13% (Table 2.5) as the solution IS increased from 1 to 100 mM (Fig. 2.6). This trend is consistent with data presented by *Fontes et al.* [1991]. The peak value of C/C_0 in the first pulse of the BTC

53

for the lens decreased over a narrow range from 25 to 13% as the IS increased from 1 to

100 mM. In contrast, the peak value of C/C_0 in the second pulse of the BTC for the

matrix decreased over a larger range from 77 to almost 0% as the IS increased from 1 to

100 mM. The contribution of preferential flow for the overall transport of *E. coli* D21g

increased from 26 to 99% as IS changed from 1 mM to 100 mM (Table 2.4). This shows

an interesting phenomenon that has not been reported by other researchers. Increasing the

solution IS decreased the overall transport, but increased the relative importance of

preferential flow.

Table 2.5. Experimental mass balance information (effluent during phases 1 and 2, with DI flush during phase 3, and total) for the heterogeneous column experiments with *E. coli* D21g and φX174 under different solution IS conditions. The goodness of the model fit is also quantified by the coefficient of linear regression (R^2) on breakthrough data using model parameters in Tables 2.2 and 2.4.

IS (mM)	R^2			Recovery (%)					
				E. coli D21g			φX174		
	Br	*E. coli* D21g	φX174	Effluent	DI	Total	Effluent	DI	Total
1	0.92	0.98	0.85	96	ND	96	98	ND	98
5	0.98	0.71	ND	61	32	93	ND	ND	ND
20	0.96	0.9	ND	32	61	93	ND	ND	ND
100	0.94	0.88	0.95	13	68	81	50	2	52

ND – denotes not determined

Figure 2.7 shows the RPs for *E. coli* D21g in the lens, in the matrix adjacent to the lens, and in the bulk matrix sand when the IS=100 mM. Similar to the homogeneous column experiments, greater amounts of *E. coli* D21g retention occurred in the matrix than the lens. Furthermore, the RPs in the lens and bulk matrix sands were quite similar to those observed in the corresponding homogeneous coarse and fine sand column experiments (Fig. 2.5), respectively. The RPs of the matrix in the vicinity of lens provided strong evidence for the interaction between the lens and matrix sands. Simulation results presented by *Morley et al.* [1998] are consistent with this finding. In particular, retained concentrations of *E. coli* D21g in the matrix were higher next to the lens than in the bulk matrix at all depths. Deviation in the amount of *E. coli* D21g retention in the matrix adjacent to the lens and the bulk matrix was especially significant at depths greater than 6 cm. These observations demonstrate significant amounts of cell transport from the lens to the surrounding matrix and enhanced cell retention in the matrix than the lens.
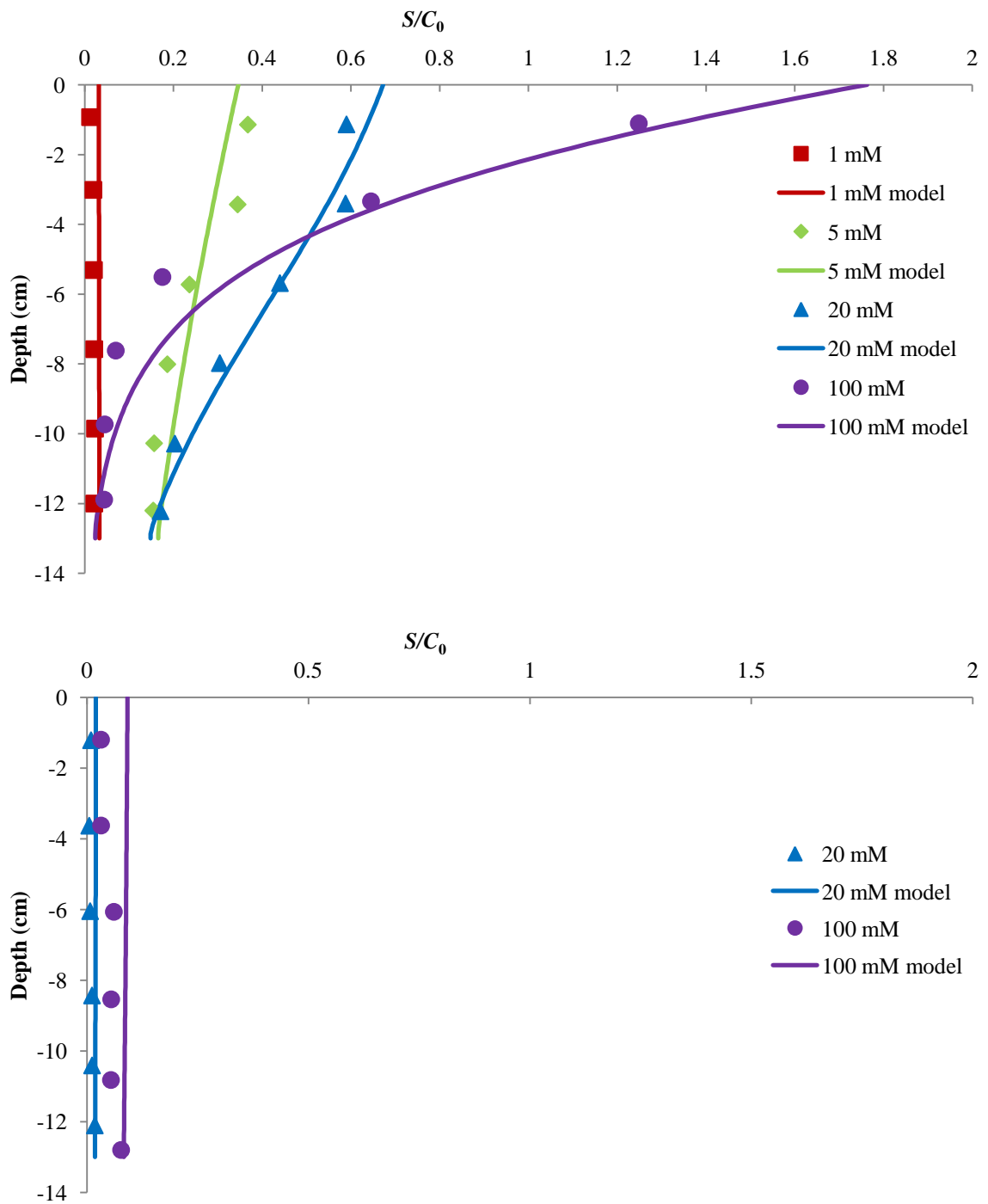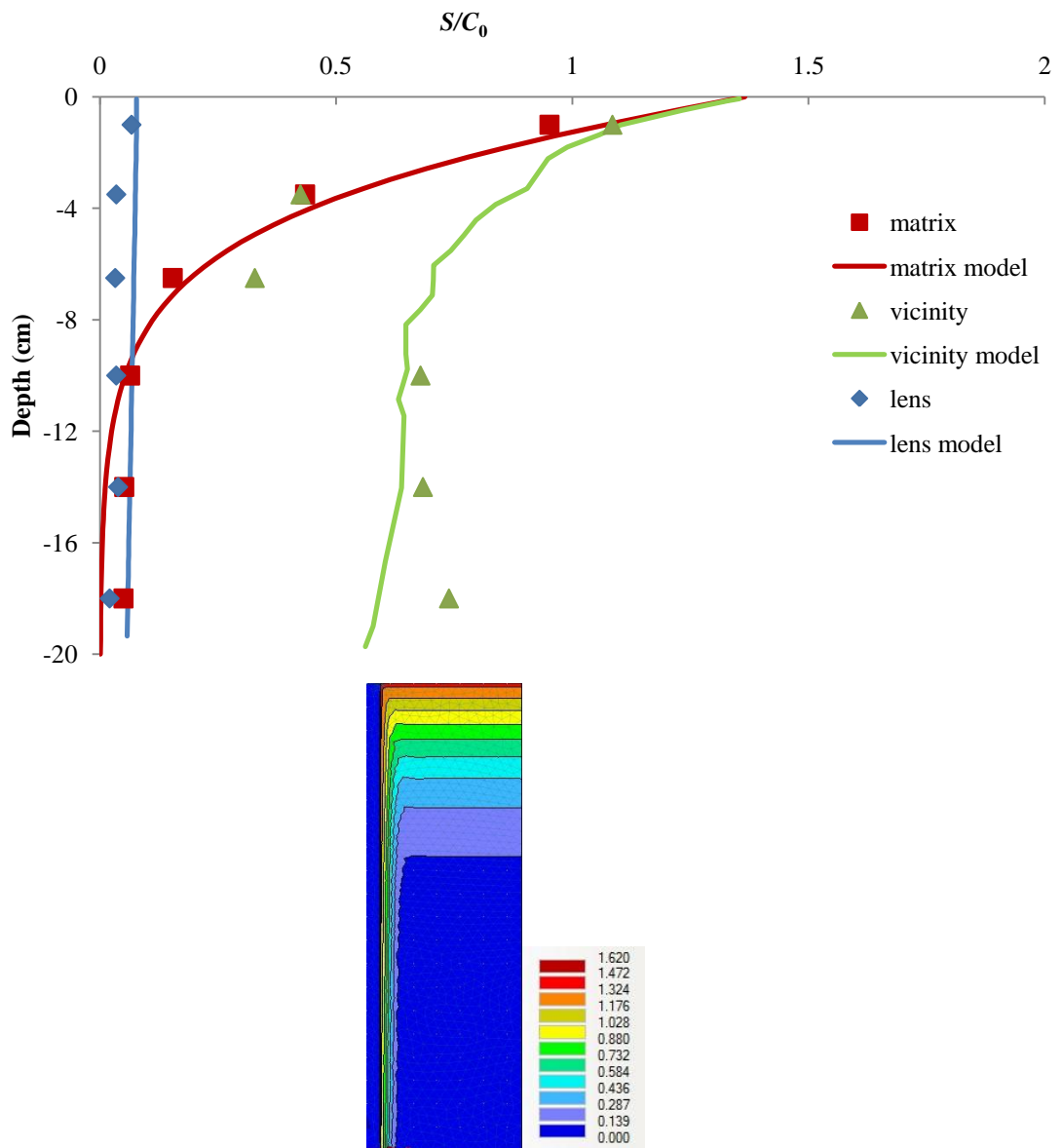
Figure 2.7. Observed and simulated (model) normalized solid phase concentrations (S/C_0) of *E. coli* D21g as a function of depth in heterogeneous column at three different locations (lens, matrix in the vicinity of lens, and matrix) (top), and simulated spatial distribution of *E. coli* D21g in HYDRUS (bottom) at solution IS = 100 mM.

The transport and retention of *E. coli* D21g in the heterogeneous columns were again simulated using HYDRUS. Parameters values used in these simulations were obtained from corresponding Br data and *E. coli* D21g data in the homogeneous columns (Table 2.2). Longitudinal dispersivities of coarse and fine sand were set as the average values obtained from homogeneous experiments (0.55 cm and 0.12 cm) for all columns. Transverse dispersivity was set to be one tenth of the longitudinal dispersivity. The simulated BTCs (Fig. 2.6) matched with the observed BTCs reasonably well for all IS conditions (R^2>0.71 in Table 2.5). The simulations also provided a reasonable description of the measured RPs in the heterogeneous column (Fig. 2.7). No significant water flow was observed at the interface of the lens and matrix in the simulation. Mass transfer at the lens-matrix interface was not very sensitive to the longitudinal dispersivity, but was controlled by the transverse dispersivity and especially the concentration gradient.

Additional experiments were conducted to better understand the significance of cell retention at the lens-matrix interface. In particular, after completion of phases 1 and 2 the heterogeneous columns were eluted with DI water (phase 3) to study cell release when the secondary minimum was eliminated. The release process was not simulated because of the coupling between cell retention parameters and variable IS. Figure 2.8

presents the release curves for *E. coli* D21g during phase 3. Similar to Fig. 2.6, early

breakthrough from the lens was observed just after switching to DI water. Release curves

in homogeneous column experiments typically produce a sharp spike [*Bradford et al.*,

2007; *Torkzaban et al.*, 2010a]. In contrast, the first pulse of the release curve in the

heterogeneous columns was more gradual and of a longer duration. This observation

supports the above conclusion about the interaction and mass transfer at the lens-matrix

interface. A second sharp spike with extremely high cell concentrations came out from

the matrix at about 22 minutes (consistent with the breakthrough time for the matrix).

Greater release was obtained by flushing with DI water in systems with higher IS and

greater cell retention during phases 1 and 2. The overall recovery rates of *E. coli* D21g

(breakthrough and release) are provide in Table 2.5. Similar to the homogeneous columns,

the overall recovery was lower than 100% and decreased with increasing IS.
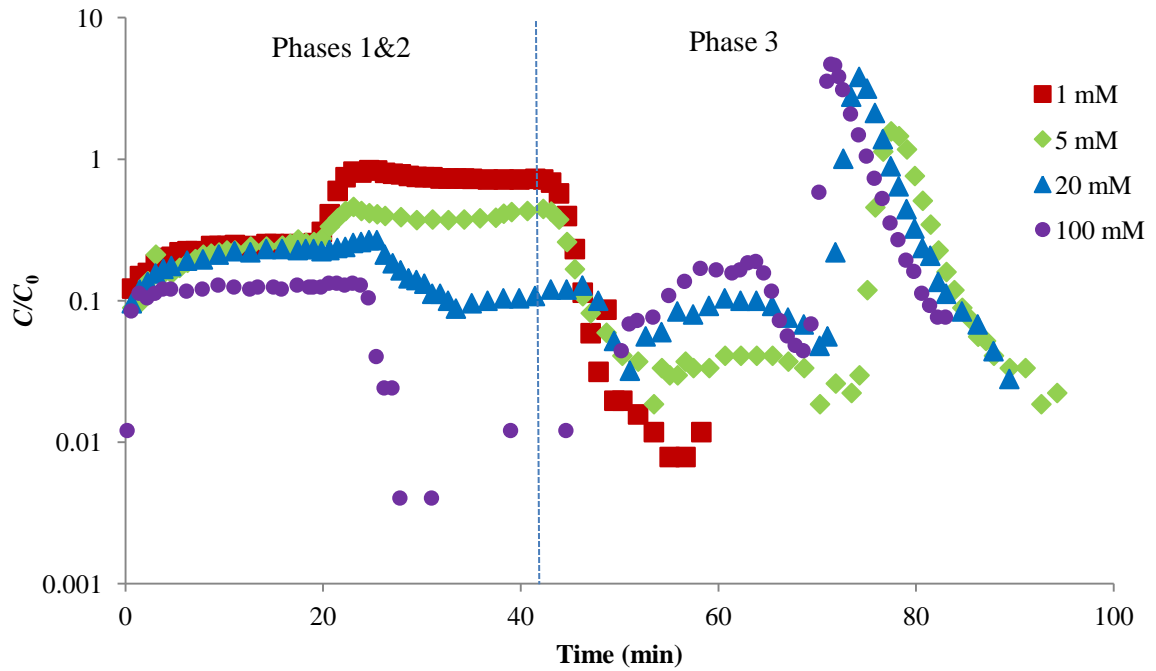
Figure 2.8. Semi-log plots of observed normalized effluent concentrations (C/C_0) of *E. coli* D21g as a function of time in heterogeneous columns at selected solution IS conditions including phase 3.

2.4.3 Coliphage φX174

Figure 2.9 presents observed and simulated BTCs for φX174 in homogeneous fine sand when the IS equaled 1 and 100 mM. In contrast to *E. coli* D21g, the BTCs for φX174 were slightly retarded and the amount of retardation increased with IS. Similar behavior has been observed for other nanoparticles [*Torkzaban et al.*, 2010a]. The recovered φX174 in the column effluent was equal to 69 and 36% when the IS was 1 and 100 mM, respectively. The two site kinetic model was selected for φX174 when IS = 100

mM for better performance. The transport simulation provided a good description of this

data (R^2>0.96). The parameter k_{det} was not needed to describe this data on a non-log scale,

suggesting mainly irreversible retention. Similarly, very small amounts of φX174 were

recovered from the sand (<2%). The RPs for φX174 could therefore not be accurately

determined. The effect of microscopic heterogeneities on colloid retention has been

reported to increase as the colloid size decreases [*Duffadar and Davis*, 2008]. These

observations suggest that φX174 was subject to irreversible, primary minimum

attachment to a larger extent than *E. coli* D21g.
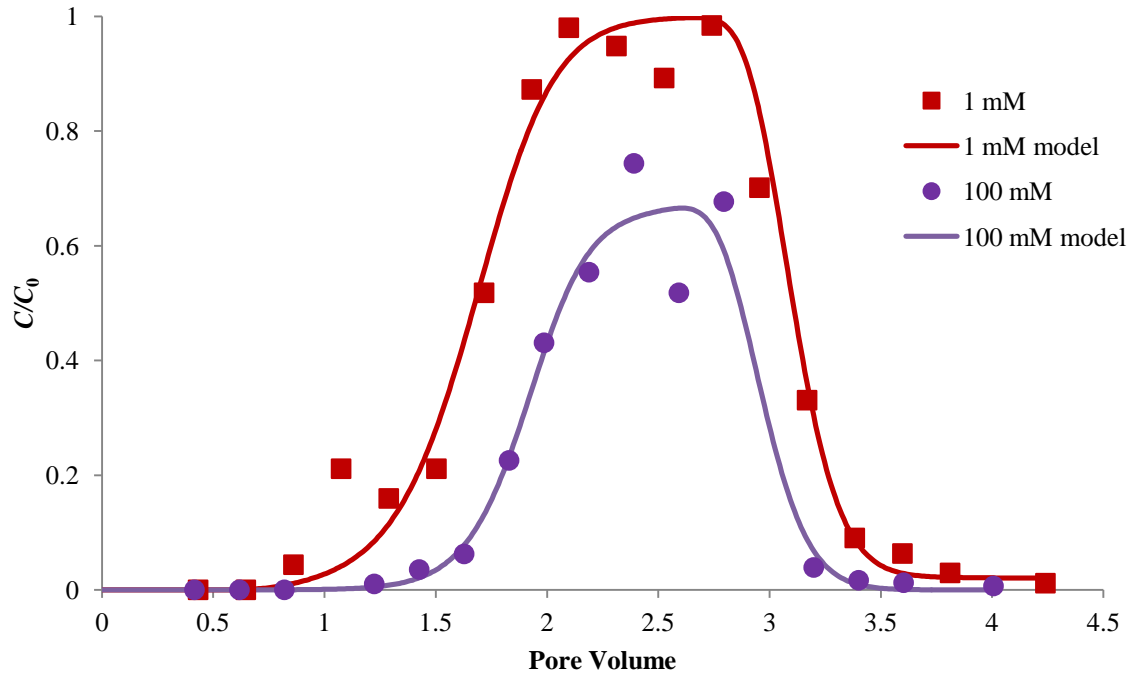
Figure 2.9. Observed and simulated (model) normalized effluent concentrations (C/C_0) of φX174 as a function of pore volume in homogeneous fine sand columns at solution IS =1 and 100 mM. Parameter values are given in Table 2.2.

Retention of φX174 was less than *E. coli* D21g when the IS=100 mM, but greater than *E. coli* D21g when the IS= 1 mM. These differences in the retention depend on the values of k_{att} and S_{max} given in Table 2.2. Filtration theory [*Yao et al.*, 1971] predicts that k_{att} is proportional to the product of the colloid collector efficiency (η) and the sticking efficiency (α). The value of η was predicted [*Tufenkji and Elimelech*, 2003] to be much larger for φX174 (η=0.28) than *E. coli* D21g (η=0.02). Conversely, α and S_{max} depend in a complex manner on the depth of the secondary minimum and hydrodynamic forces

[*Shen et al.*, 2010], surface macromolecules [*Kim et al.*, 2009], and physical and chemical heterogeneity [*Bendersky and Davis*, 2011]. Furthermore, the influence of the secondary minimum and chemical heterogeneity changes with IS and colloid size.

Transport experiments for φX174 in the fine sand when the IS=5 and 20 mM were not conducted because the expected differences in the BTCs (intermediate to 1 and 100 mM data shown in Fig. 2.9) were within the analytic error. Similarly, φX174 retention in the coarse sand at IS equal to 1 and 100 mM was initially assumed to be zero because the *E. coli* D21g data (Fig. 2.4) exhibited much less retention in the coarse than the fine sand for given IS conditions (Table 2.3). The validity of this assumption will be verified in the heterogeneous column experiments discussed below.

Figure 2.10 presents BTCs for φX174 in heterogeneous columns when the IS equaled 1 and 100 mM. Chemistry had a very similar influence on the transport of φX174 as for *E. coli* D21g (Fig. 2.6). In particular, the overall transport decreased with an increase in the IS, but the contribution of preferential flow increased. The recovery changed from 98 to 50% when the IS was 1 and 100 mM, respectively. The peak value of C/C_0 in the lens (first) and matrix (second) pulses changed from 28 to 18% and 99 to 58% when the IS was 1 and 100 mM, respectively. In contrast to *E. coli* D21g, higher values

of C/C_0 were observed for φX174 at comparable IS conditions and the contribution of

preferential flow was much lower (26% to 34% with an increase in IS). This observation

suggests that φX174 is less influenced by physical heterogeneity than *E. coli* D21g, and

thereby behave more similar to Br because of its smaller size.

The simulation could not provide a good description of the φX174 data in the

heterogeneous column when using parameter values from the homogeneous fine sand

column experiments. Large variations in C_0 and the degree of sand cleaning could cause

significant difference in S_{max} for the fine sand in the homogeneous and heterogeneous

column experiments. Therefore, we used the same values of k_{att} from the homogeneous

fine sand column and optimized separate values of S_{max} to the heterogeneous matrix data.

Values of R^2 were greater than 0.85 with the optimized S_{max}.

In contrast to *E. coli* D21g (Fig. 2.8), only small amounts of φX174 were released

from the lens and matrix during phase 3 when the IS was reduced from 100 mM to DI

water. Similar to the minimal recovery of φX174 from the sand, this observation reflects

that φX174 was mainly irreversibly retained in a primary minimum.
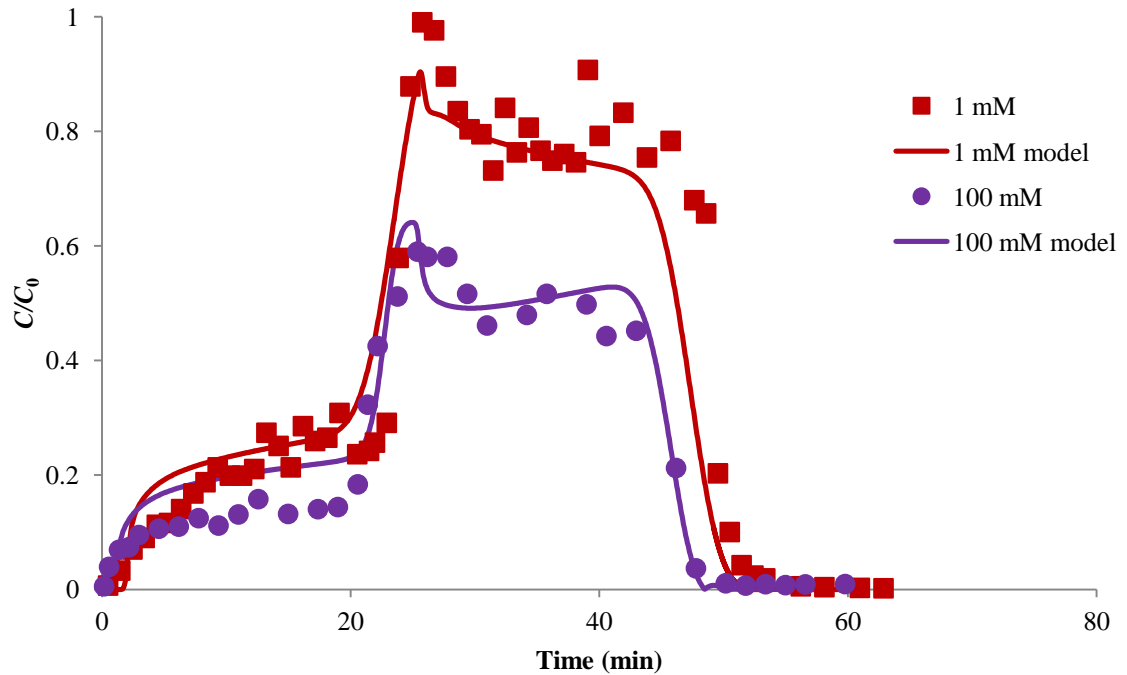
Figure 2.10. Observed and simulated (model) normalized effluent concentrations (C/C_0) of φX174 as a function of time in heterogeneous columns at solution IS =1 and 100 mM. Parameter values are given in Tables 2.2 and 2.4. For the IS=100 mM experiment the values of S_{max} were optimized to 0.04 and 0.15 for the two sites.

2.4.4 Limitations of the Mathematical Model

It needs to be emphasized that the mathematical model used here to describe the

transport and fate of microorganisms has its limitations with respect to the complexity of

processes involved in the transport of microorganisms in soils, as well as with respect to

modeling preferential transport. The model considers attachment/detachment as first-

order processes and neglects other processes such as straining and/or size exclusion.

Additionally, only Langmuirian-type blocking was considered, while other blocking models could have been used as well. Microbes were treated as having a uniform size distribution, and aggregation and other biological activities were not considered in the model. Note that the analysis of the effects of these various processes can be found elsewhere (e.g., *Bradford et al.* [2003] for straining and size exclusion; *Bradford et al.* [2006a] for different blocking mechanisms; *Bradford et al.* [2005] for ripening behavior; *Bradford et al.* [2006b] for cell aggregation; *Gargiulo et al.* [2006] for cell growth; and *Bradford et al.* [2006c] for virus inactivation).

It should also be stressed that application of our 2D model for preferential flow in natural systems is difficult, because it requires detailed information on the spatial distribution of soil hydraulic properties which produce preferential flow paths. To overcome this limitation, flow and transport in preferential pathways is sometimes described using a dual permeability model that divides flow into fast and slow regimes (e.g., *Jarvis* [2007]; *Šimůnek and van Genuchten*, [2008]). However, this approach is more common for variably-saturated conditions than for fully saturated conditions.

2.5 Summary and Conclusions

DLVO calculations indicate that the depth of the secondary minimum increased and that the height of the energy barrier deceased with an increase in IS. Consequently, retention of *E. coli* D21g and φX174 was enhanced as the solution IS increased in both homogeneous and heterogeneous sand columns. This effect of IS was found to be especially significant for *E. coli* D21g in the finer sand. In general, *E. coli* D21g was mainly reversibly retained in the sand as a result of interactions in a secondary minima, whereas φX174 was largely irreversible retained as a result of primary minima interactions. HYDRUS proved to be a powerful tool to simulate the transport and deposition behavior of *E. coli* D21g and φX174 in both homogenous and preferential flow systems under the different IS conditions.

The relative amount of preferential transport of microbes through the lens increased with IS. This indicates that preferential transport of microbes became more important under conditions of higher overall retention. Cell RPs demonstrated significant amounts of mass transfer at the interface between the lens and matrix. Cell release with a reduction in solution IS exhibited multi-peaked breakthrough in the preferential flow systems. The amount of cell release was sensitive to the initial distribution of retained

cells, especially at the lens-matrix interface. Accurate predictions of microorganism

transport and fate in fields with preferential flow and transients in solution chemistry

require information on BTCs, RPs and release behavior.

The artificial macropore method proved to be a reliable and repeatable way to

study transport processes in systems with preferential flow. Further study will be done to

investigate the influence of macropore geometry with the artificial macropore method,

which can help improve our understanding of natural environments. Numerical models

still need to be improved to better characterize mass transfer at the matrix-lens interface

and the release of microorganisms with transients in solution IS. Furthermore, alternative

mathematical models are warranted to predict transport behavior in more complicated

systems and at larger scales in order to connect the studies in idealized artificial

macropore system with the real processes in natural systems.

2.6 References

Abu-Ashour, J., D. M. Joy, H. LEE, H. R. Whiteley, and S. Zelin, Transport of microorganisms through soil, *Water, Air and Soil Pollution*, *75*, 141-158, 1994.

Adamczyk, Z., B. Siwek, M. Zembala, and P. Belouschek (1994), Kinetics of localized adsorption of colloid particles, *Adv Colloid Interfac*, 48(0), 151-280. doi:10.1016/0001-8686(94)80008-1.

Allaire-Leung, S. E., S. C. Gupta, and J. F. Moncrief (2000a), Water and solute movement in soil as influenced by macropore characteristics - 1. Macropore continuity, *J Contam Hydrol*, 41(3-4), 283-301.

Allaire-Leung, S. E., S. C. Gupta, and J. F. Moncrief (2000b), Water and solute movement in soil as influenced by macropore characteristics - 2. Macropore tortuosity, *J Contam Hydrol*, 41(3-4), 303-315.

Allaire, S. E., S. C. Gupta, J. Nieber, and J. F. Moncrief (2002a), Role of macropore continuity and tortuosity on solute transport in soils: 2. Interactions with model assumptions for macropore description, *J Contam Hydrol*, 58(3-4), 283-298.

Allaire, S. E., S. C. Gupta, J. Nieber, and J. F. Moncrief (2002b), Role of macropore continuity and tortuosity on solute transport in soils: 1. Effects of initial and boundary conditions, *J Contam Hydrol*, 58(3-4), 299-321.

Arora, B., B. P. Mohanty, and J. T. McGuire (2011), Inverse estimation of parameters for multidomain flow models in soil columns with different macropore densities, *Water Resour. Res.*, 47(4), W04512, doi:10.1029/2010wr009451.

Arora, B., B. P. Mohanty, and J. T. McGuire (2012), Uncertainty in dual permeability model parameters for structured soils, *Water Resour. Res.*, 48(1), W01524, doi:10.1029/2011wr010500.

Bales, R. C., C. P. Gerba, G. H. Grondin, and S. L. Jensen, Bacteriophage transport in sandy soil and fractured tuff, *Appl. Environ. Microbiol.*, 55(8), 2061-2067,1989.

Bendersky, M., and J. M. Davis (2011), DLVO interaction of colloidal particles with topographically and chemically heterogeneous surfaces, *Journal of Colloid and Interface Science*, 353(1), 87-97. doi:10.1016/j.jcis.2010.09.058.

Beven, K., and P. Germann (1982), Macropores and Water-Flow in Soils, *Water Resour. Res.*, 18(5), 1311-1325.

Bradford, S. A., and H. Kim (2010), Implications of Cation Exchange on Clay Release and Colloid-Facilitated Transport in Porous Media, *J Environ Qual*, 39(6), 2040-2046. doi:10.2134/Jeq2010.0156.

Bradford, S. A., J. Šimůnek, M. Bettahar, M. Th. van Genuchten, and S. R. Yates. (2003). Modeling colloid attachment, straining, and exclusion in saturated porous media. *Environ. Sci. Technol.* 37, 2242-2250.

Bradford, S. A., J. Šimůnek, M. Bettahar, M. Th. van Genuchten, and S. R. Yates. (2006a). Significance of straining in colloid deposition: Evidence and implications. *Water Resour. Res.* 42, W12S15, doi:10.1029/2005WR004791.

Bradford, S. A., M. Th. van Genuchten, and J. Šimůnek. (2005). Modeling of colloid transport and deposition in porous media. In: Workshop on HYDRUS: Advanced modeling of water flow and solute transport in the vadose zone, University of Utrecht, Utrecht, The Netherlands, October 17-19, pp. 1-5.

Bradford, S. A., and S. Torkzaban (2008), Colloid transport and retention in unsaturated porous media: A review of interface-, collector-, and pore-scale processes and models, *Vadose Zone J*, 7(2), 667-681.

Bradford, S. A., S. R. Yates, M. Bettahar, and J. Šimůnek (2002), Physical factors affecting the transport and fate of colloids in saturated porous media, *Water Resour. Res.*, 38(12), 1327. doi:10.1029/2002wr001340.

Bradford, S. A., M. Bettehar, J. Šimůnek, and M. Th. van Genuchten (2004), Straining and attachment of colloids in physically heterogeneous porous media, *Vadose Zone Journal*, *3*(2), 384-394.

Bradford, S. A., J. Šimůnek, and S. L. Walker (2006b), Transport and straining of E-coli O157 : H7 in saturated porous media, *Water Resour. Res.*, 42(12), doi:10.1029/2005WR004805.

Bradford, S. A., Y. F. Tadassa, and Y. Jin. (2006c). Transport of coliphage in the presence and absence of manure suspension. *J. Environ. Qual.* 35, 1692-1701.

Bradford, S. A., S. Torkzaban, and S. L. Walker (2007), Coupling of physical and chemical mechanisms of colloid straining in saturated porous media, *Water Res.*, 41(13), 3012-3024. doi:10.1016/j.watres.2007.03.030.

Castiglione, P., B. P. Mohanty, P. J. Shouse, J. Šimůnek, M. T. van Genuchten, and A. Santini (2003), Lateral Water Diffusion in an Artificial Macroporous System, *Vadose Zone J*, 2(2), 212-221. doi:10.2113/2.2.212.

Cey, E. E., and D. L. Rudolph (2009), Field study of macropore flow processes using tension infiltration of a dye tracer in partially saturated soils, *Hydrol Process*, 23(12), 1768-1779.

Cey, E. E., D. L. Rudolph, and J. Passmore (2009), Influence of macroporosity on preferential solute and colloid transport in unsaturated field soils, *J Contam. Hydrol*, 107(1-2), 45-57.

Chen, G. X., and S. L. Walker (2007), Role of solution chemistry and ion valence on the adhesion kinetics of groundwater and marine bacteria, *Langmuir*, 23(13), 7162-7169.

Clesceri, L. S., A. E. Greenberg, and R. R. Trussel (1989), Standard methods for the examination of water and waste water, 17th ed., *American Public Health Assoc.*, Washington DC.

Dean, D. M., and M. E. Foran (1992), The Effect of Farm Liquid Waste Application on Tile Drainage, *J Soil Water Conserv*, 47(5), 368-369.

Derjaguin, B. V. (1954), A theory of the heterocoagulation, interaction and adhesion of dissimilar particles in solutions of electrolytes, *Discussions of the Faraday Society*, 18, 85-98.

Dong, H. L., T. C. Onstott, M. F. Deflaun, M. E. Fuller, T. D. Scheibe, S. H. Streger, R. K. Rothmel, and B. J. Mailloux (2002), Relative dominance of physical versus chemical effects on the transport of adhesion-deficient bacteria in intact cores from South Oyster, Virginia, *Environ Sci Technol*, 36(5), 891-900.

Dowd, S. E., S. D. Pillai, S. Y. Wang, and M. Y. Corapcioglu (1998), Delineating the specific influence of virus isoelectric point and size on virus adsorption and transport through sandy soils, *Appl Environ Microb*, 64(2), 405-410.

Duffadar, R. D., and J. M. Davis (2008), Dynamic adhesion behavior of micrometer-scale particles flowing over patchy surfaces with nanoscale electrostatic heterogeneity, *Journal of Colloid and Interface Science*, 326(1), 18-27. doi:10.1016/j.jcis.2008.07.004.

Evans, M. R., and J. D. Owens (1972), Factors Affecting the Concentration of Faecal Bacteria in Land-drainage Water, *J Gen Microbiol*, 71(3), 477-485. doi:10.1099/00221287-71-3-477.

Fontes, D. E., A. L. Mills, G. M. Hornberger and J. S. Herman (1991), Physical and chemical factors influencing transport of microorganisms through porous media, *Appl. Environ. Microbiol.* 57(9):2473-2481.

Gargiulo, G., S. A. Bradford, J. Šimunek, H. Vereecken, and E. Klumpp. (2006). Transport and deposition of metabolically active and stationary phase Deinococcus Radiodurans in unsaturated porous media. *Environ. Sci. Technol.* 41, 1265-1271.

Gerba, C.P. and J.E. Smith. (2005), Sources of Pathogenic Microorganisms and Their Fate during Land Application of Wastes. *J. Environ. Qual.* 34: 42-48. doi:10.2134/jeq2005.0042.

Ginn, T. R. (2002), A travel time approach to exclusion on transport in porous media, *Water Resour. Res.*, 38(4), -.

Gregory, J. (1981), Approximate expressions for retarded van der waals interaction, *Journal of Colloid and Interface Science*, 83(1), 138-145. doi:10.1016/0021-9797(81)90018-7.

Guzman, J. A., G. A. Fox, R. W. Malone, and R. S. Kanwar, *Escherichia coli* transport from surface-applied manure to subsurface drains through artificial biopores, *J. Environ. Qual.*, 38, 2412–2421, 2009.

Harvey, R. W., N. E. Kinner, D. MacDonald, E. W. Metge, and A. Bunn, Role of physical heterogeneity in the interpretation of small scale laboratory and field observations of bacteria, microbial-sized microsphere, and bromide transport through aquifer sediments, *Water Resour. Res.*,29(8), 2713-2721, 1993.

Hendry, M. J., J. R. Lawrence, and P. Maloszewski (1999), Effects of velocity on the transport of two bacteria through saturated sand, *Ground Water*, 37(1), 103-112.

Hogg, R., T. W. Healy, and D. W. Fuerstenau (1966), Mutual coagulation of colloidal dispersions, *Transactions of the Faraday Society*, 62, 1638-1651.

Jarvis, N. J. (2007), A review of non-equilibrium water flow and solute transport in soil macropores: principles, controlling factors and consequences for water quality, *Eur J Soil Sci*, 58(3), 523-546.

Jiang, S., L. Pang, G. D. Buchan, J. Šimůnek, M. J. Noonan, and M. E. Close, Modeling water flow and bacterial transport in undisturbed lysimeters under irrigations of dairy shed effluent and water using HYDRUS-1D, *Water Research*, special issue, doi:10.1016/j.watres.2009.08.039, *44*, 1050-1061, 2010.

Kim, H. N., S. A. Bradford, and S. L. Walker (2009), Escherichia coli O157:H7 Transport in Saturated Porous Media: Role of Solution Chemistry and Surface Macromolecules, *Environ Sci Technol*, 43(12), 4340-4347. doi:10.1021/Es8026055.

Madsen, E. L., and M. Alexander (1982), Transport of Rhizobium and Pseudomonas through Soil1, *Soil Sci. Soc. Am. J.*, 46(3), 557-560.

McCarthy, J. F., and L. D. McKay, Colloid transport in the subsurface: Past, present, and future challenges, *Vadose Zone Journal*, *3*, 326–337, 2004.

Mccaulou, D. R., R. C. Bales, and R. G. Arnold (1995), Effect of Temperature-Controlled Motility on Transport of Bacteria and Microspheres through Saturated Sediment, *Water Resour. Res.*, 31(2), 271-280.

McGechan, M. B., and D. R. Lewis (2002), Transport of particulate and colloid-sorbed contaminants through soil, part 1: General principles, *Biosyst Eng*, 83(3), 255-273.

Mills, A. L., J. S. Herman, G. M. Hornberger, and T. H. Dejesus (1994), Effect of Solution Ionic-Strength and Iron Coatings on Mineral Grains on the Sorption of Bacterial-Cells to Quartz Sand, *Appl Environ Microb*, 60(9), 3300-3306.

Morley, L. M., G. M. Hornberger, A. L. Mills, and J. S. Herman (1998), Effects of transverse mixing on transport of bacteria through heterogeneous porous media, *Water Resour. Res.* 34:1901-1908.

Ochiai, N., E. L. Kraft, and J. S. Selker (2006), Methods for colloid transport visualization in pore networks, *Water Resour. Res.*, 42(12), -.

Pang, L., M. McLeod, J. Aislabie, J. Šimůnek, M. Close, and R. Hector (2008), Modeling transport of microbes in ten undisturbed soils under effluent irrigation, *Vadose Zone J*, 7(1), 97-111.

Passmore, J. M., D. L. Rudolph, M. M. F. Mesquita, E. E. Cey, and M. B. Emelko (2010), The utility of microspheres as surrogates for the transport of E. coli RS2g in partially saturated agricultural soil, *Water Res.*, 44(4), 1235-1245.

Pivetz, B. E. and T. S. Steenhuis, Soil matrix and macropore biodegradation of 2,4-D, *J. Environ. Qual.*, 24, 564-570, 1995.

Pivetz, B. E., I. W. Kelsey, T. S. Steenhuis, and M. Alexander, A procedure to calculate biodegradation during preferential flow through heterogeneous soil columns. *Soil Sci. Soc. Am. J.*, 60, 381-388, 1996.

Penrod, S. L., T. M. Olson, and S. B. Grant (1996), Deposition Kinetics of Two Viruses in Packed Beds of Quartz Granular Media, *Langmuir*, 12(23), 5576-5587. doi:10.1021/la950884d.

Reynolds, K. A., K. D. Mena, and C. P. Gerba (2008), Risk of waterborne illness via drinking water in the United States, *Rev Environ Contam T*, 192, 117-158.

Rijnaarts, H. H. M., W. Norde, E. J. Bouwer, J. Lyklema, and A. J. B. Zehnder (1995), Reversibility and mechanism of bacterial adhesion, *Colloids and Surfaces B: Biointerfaces*, 4(1), 5-22. doi:10.1016/0927-7765(94)01146-v.

Ryan, J. N., and M. Elimelech (1996), Colloid mobilization and transport in groundwater, *Colloid Surface A*, 107, 1-56.

Saiers, J. E., G. M. Hornberger, and C. Harvey. 1994. Colloidal silica transport through structured, heterogeneous porous media, *J. Hydrol. (Amsterdam)* 163:271–288.

Sen, T. K., and K. C. Khilar (2006), Review on subsurface colloids and colloid-associated contaminant transport in saturated porous media, *Adv Colloid Interfac*, 119(2-3), 71-96.

Shen, C., Y. Huang, B. Li, and Y. Jin (2010), Predicting attachment efficiency of colloid deposition under unfavorable attachment conditions, *Water Resour. Res.*, 46(11), W11526. doi:10.1029/2010wr009218.

Šimůnek, J., and M. Th. van Genuchten, Modeling nonequilibrium flow and transport with HYDRUS, *Vadose Zone Journal*, doi:10.2136/VZJ2007.0074, Special Issue "Vadose Zone Modeling", *7*(2), 782-797, 2008.

Šimůnek, J., N.J. Jarvis, M.T. van Genuchten and A. Gardenas. (2003), Review and comparison of models for describing non-equilibrium and preferential flow and transport in the vadose zone. *J Hydrol*, 272: 14-35.

Šimůnek, J., M. T. van Genuchten, and M. Sejna (2008), Development and applications of the HYDRUS and STANMOD software packages and related codes, *Vadose Zone J*, 7(2), 587-600. doi:10.2136/Vzj2007.0077.

Stevik, T. K., K. Aa, G. Ausland, and J. F. Hanssen (2004), Retention and removal of pathogenic bacteria in wastewater percolating through porous media: a review, *Water Res.*, 38(6), 1355-1367.

Torkzaban, S., S. S. Tazehkand, S. L. Walker, and S. A. Bradford (2008), Transport and fate of bacteria in porous media: Coupled effects of chemical conditions and pore space geometry, *Water Resour. Res.*, 44(4), W04403, doi:10.1029/2007wr006541.

Torkzaban, S., H. N. Kim, J. Šimůnek, and S. A. Bradford (2010a), Hysteresis of Colloid Retention and Release in Saturated Porous Media During Transients in Solution Chemistry, *Environ Sci Technol*, 44(5), 1662-1669. doi:Doi 10.1021/Es903277p.

Torkzaban, S., Y. Kim, M. Mulvihill, J. Wan, and T. K. Tokunaga (2010b), Transport and deposition of functionalized CdTe nanoparticles in saturated porous media, *J. Contamin. Hydrol.*, 118, 208-217:

Tufenkji, N., and M. Elimelech (2003), Correlation Equation for Predicting Single-Collector Efficiency in Physicochemical Filtration in Saturated Porous Media, *Environ Sci Technol*, 38(2), 529-536. doi:10.1021/es034049r.

Unc, A., and M. J. Goss (2003), Movement of faecal bacteria through the vadose zone, *Water Air Soil Poll*, 149(1-4), 327-337.

USDA. (1992). National engineering handbook: Agricultural waste management field handbook. Part 651 (210-AWMFH, 4/92). Ch. 3, p 1–29. USDA, Washington, DC.

USEPA. (1998). Environmental impacts of animal feeding operations. U.S. Environ. Protection Agency, Office of Water, Standards and Applied Sci. Div., Washington, DC.

USEPA. (2001). Method 1601: Male-specifi c (F+) and somatic coliphage in water by two-step enrichment procedure. EPA-821-R-01–030. U.S. Environ. Protection Agency , Offi ce of Water, Engineering and Analysis Div., Washington, DC.

Verwey, E.J.W., and J.T.G. Overbeek. (1948), Theory of the stability of lyophobic colloids. Elsevier, Amsterdam.

Walker, S. L., J. A. Redman, and M. Elimelech (2004), Role of cell surface lipopolysaccharides in Escherichia coli K12 adhesion and transport, *Langmuir*, 20(18), 7736-7746. doi:10.1021/La049511f.

Wollum, A. G., II, and D. K. Cassel. 1978. Transport of microorganisms in sand columns. *Soil Sci. Soc. Am. J.* 42:72-76.

Yao, K.-M., M. T. Habibian, and C. R. O'Melia (1971), Water and waste water filtration. Concepts and applications, *Environ Sci Technol*, 5(11), 1105-1112. doi:10.1021/es60058a005.

Yee, N., J. B. Fein, and C. J. Daughney (2000), Experimental study of the pH, ionic strength, and reversibility behavior of bacteria-mineral adsorption, *Geochim Cosmochim Ac*, 64(4), 609-617.

Chapter 3

Physical and Chemical Factors Influencing the Transport and Fate of *E. coli* D21g in Soils with Preferential Flow

ABSTRACT

Laboratory and numerical studies were conducted to investigate the transport of *E.coli*

D21g in preferential flow systems with artificial macropores of different lengths and

configurations under two solution ionic strengths. The release process of *E.coli* D21g

under transient chemistry conditions was also studied. The length of an artificial

macropore proved to have a great impact on the transport of *E.coli* D21g, especially

under high ionic strength conditions. The configuration with a discontinuous artificial

macropore (Type IV) was found to have less preferential transport of *E.coli* D21g than

configurations with a continuous macropore opened to either top (Type II) or bottom

(Type III) boundary. At low ionic strength, more extensive transport in the preferential

path and earlier arrival time were observed for *E.coli* D21g compared to bromide as a

result of size exclusion. Two release pulses (one from the preferential path and the other

from the matrix) were observed following a reduction of the solution ionic strength for

Type II and III configurations, whereas three pulses (two from the preferential path and

another from the matrix) were observed for the Type IV configuration. Numerical

simulations of *E. coli* D21g under both constant and transient solution chemistry

conditions had very high agreement with the experiment data, except for their capability

to predict some subtle differences in transport between the various lens configurations.

3.1 INTRODUCTION

The vadose zone serves as an important barrier to protect groundwater from pathogenic microorganisms that can cause waterborne disease outbreaks [*Runnells*, 1976; *National Research Council*, 1994; *Jamieson et al.*, 2002]. The capability of the vadose zone to remove pathogens depends on properties of the porous media, the microbes, and the soil solution. An understanding and ability to simulate the influence of various factors that enhance the transport potential of pathogens in the vadose zone is especially needed to protect water resources from contamination. In this research we consider three factors that are known to enhance the transport potential of microbes in soils: (i) preferential flow; (ii) transients in solution chemistry; and (iii) size exclusion. Research pertaining to each of these issues will be briefly reviewed below, followed by a description of our research objectives.

Rapid water flow may occur in the vadose zone as a result of plant roots, burrowing earthworms, cracks, or natural structural heterogeneities [*Wollum and Cassel*, 1978; *Beven and Germann*, 1982; *Madsen and Alexander*, 1982; *Unc and Goss*, 2003; *Cey et al.*, 2009]. Accurate descriptions of contaminant transport in the vadose zone is hampered by these preferential flow pathways [*Šimůnek et al.*, 2003] that by-pass a large

part of the soil matrix [*Jury and Flühler*, 1992]. In particular, it is extremely difficult to characterize physical features (e.g., the length and configuration) of preferential flow pathways in natural systems and the exchange of water and contaminants at the interface between the preferential pathway and the soil matrix. Both of these factors are expected to have a critical influence on the transport and fate of contaminants in preferential flow systems but are still poorly quantified [*Harvey et al.*, 1993; *Morley et al.*, 1998; *Allaire-Leung et al.*, 2000a, 2000b; *Allaire et al.*, 2002a, 2002b].

Many studies have investigated the transport of colloids and microorganisms in the field, or undisturbed soil columns with preferential flow [*Bales et al.*, 1989; *Dean and Foran*, 1992; *Jarvis*, 2007; *Pang et al.*, 2008; *Cey et al.*, 2009; *Cey and Rudolph*, 2009; *Guzman et al.*, 2009]. Preferential pathways have been found to be a major contributor to the overall transport of microbes because they are typically strongly retained in the soil matrix [*Bales et al.*, 1989; *Abu-Ashour et al.*, 1994; *Jiang et al.*, 2010]. However, most of these researches are qualitative in nature because of difficulty in quantifying the physical and chemical complexities of the soil matrix and macropore system. Studies using artificial macropores provide an opportunity to overcome many of these experimental and modeling limitations because the macropore geometry and hydraulic

properties can be well defined and controlled [*Fontes et al.*, 1991; *Pivetz and Steenhuis*, 1995; *Castiglione et al.*, 2003; *Guzman et al.*, 2009; *Arora et al.*, 2011; *Arora et al.*, 2012; *Wang et al.*, 2013]. However, systematic studies investigating the influence of the length and configuration of artificial macropores on the preferential transport of bacteria still have not yet been reported.

Solution chemistry (pH, ionic strength and composition) has proven to be an important factor that influnces the transport and retention of microorganisms in porous media [*Mills et al.*, 1994; *Yee et al.*, 2000; *Dong et al.*, 2002; *Chen and Walker*, 2007] and in systems with preferential flow [*Fontes et al.*, 1991; *Wang et al.*, 2013]. The solution chemistry may change dramatically in the vadose zone during infiltration and drainage events as a result of differences in water quality at the soil surface (rain, irrigation, and runoff), evapotranspiration, and the mineral composition of the soil and groundwater. Such transients in solution chemistry are well-known to induce the release of colloids and microbes in homogeneous porous media [*Bales et al.*, 1989; *McDowell-Boyer*, 1992; *Ryan and Gschwend*, 1994; *Nocito-Gobel and Tobiason*, 1996; *Roy and Dzombak*, 1996; *Grolimund et al.*, 2001; *Lenhart and Saiers*, 2003; *Cheng and Saiers*, 2009; *Tosco et al.*, 2009; *Bradford and Kim*, 2010; *Bradford et al.*, 2012]. Consequently, transients in

solution chemistry may jeopardize the purification capability of the vadose zone by inducing microbial release. There is presently a great need to understand processes that influence microbial remobilization, especially in soils with preferential flow. *Wang et al.* [2013] demonstrated that transients in solution chemistry can remobilize retained microbes and rapidly transport them in a preferential flow system. However, numerical modeling of this microbe release and transport still has not yet been reported.

In addition to preferential flow and transients in solution chemistry, size exclusion may also enhance the transport potential of microbes in soils by physically restricting their transport to larger, more conductive, pore spaces [*Ryan and Elimelech*, 1996; *Ginn*, 2002]. It is possible that size exclusion will be more pronounced in systems with preferential flow because of the wide difference in pore sizes between the soil matrix and the high permeability domain. However, this issue has not yet been systematically investigated.

The objectives of this research were to: 1) investigate the influence of the length and configuration (as shown in Figure 3.1) of artificial macropores on the preferential transport of microorganisms under different ionic strength conditions; 2) simulate the release behavior of microbes with transients in solution chemistry in systems with

preferential flow; and 3) study the effect of size exclusion on microbial transport in systems with preferential flow.
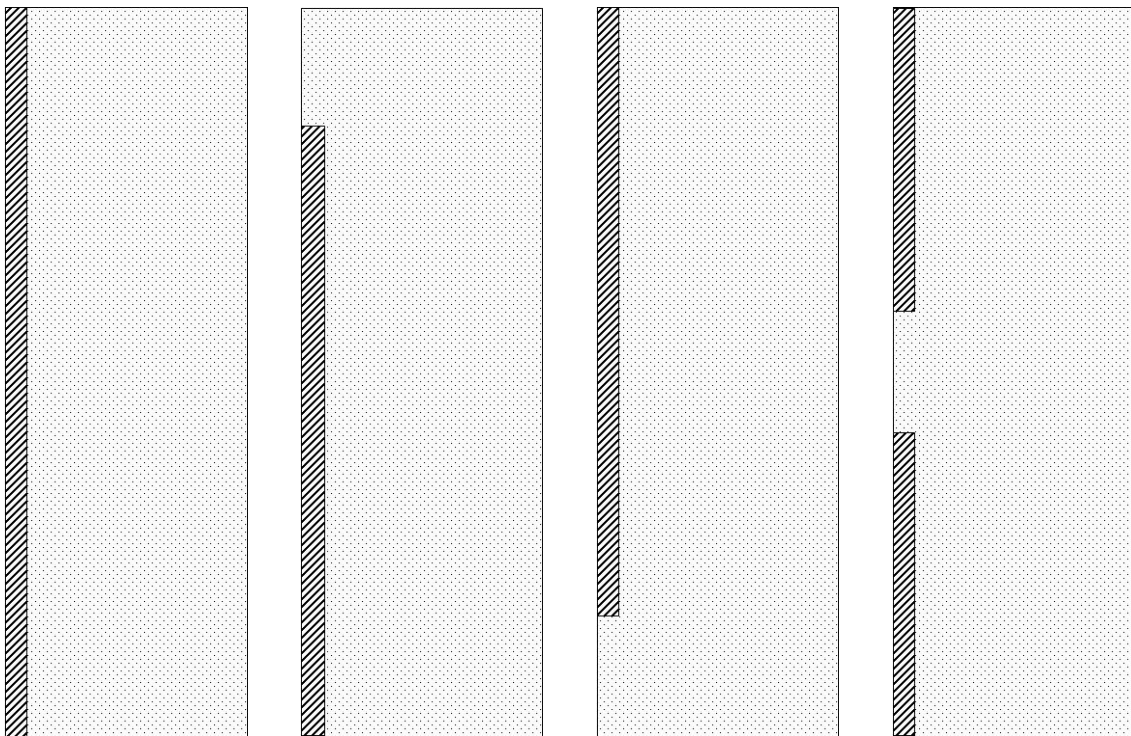
Figure 3.1. Axi-symmetric representation of the four types of lens structures (column center is on the left hand side) studied in this research: Type I - one lens through the whole column, Type II - one lens opened to the bottom boundary, Type III - one lens opened to the top boundary, and Type IV - a discontinuous lens opened to both boundaries (diagonal pattern represents coarse sand and point pattern represents fine sand).

3.2 Experimental Information

3.2.1 Porous Media and Electrolyte Solutions

Two sizes of Ottawa (quartz) sand were used in the column experiments. The median grain sizes (d_{50}) of these sands were 120 and 710 μm. In order to eliminate any background interference from clay particles, the sand was treated by a salt cleaning procedure described by Bradford and Kim [2010].

Electrolyte solutions for the column experiments consisted of autoclaved deionized (DI) (pH=5.8) water with the ionic strength (IS) adjusted to 0, 1, 5, 20, and 100 mM using NaCl and NaBr to create a range of adhesive conditions between the bacteria and sand. The concentration of the conservative tracer bromide was determined in the column effluent using a Bromide-Selective Electrode (Thermo Scientific Orion bromide electrode ionplus® Sure-Flow®).

3.2.2 Escherichia coli D21g

We selected Escherichia coli D21g, a Gram-negative, nonmotile bacterial strain [*Walker et al.*, 2004], as a representative microorganism for the column transport experiments. The culture and harvest procedures used in this study have been described

by *Wang et al.* [2013]. In brief, *E. coli* D21g was cultured overnight (12-18 h) at 37°C in Luria-Bertani broth (LB Broth, Fisher Scientific, Fair Lawn, NJ) containing 0.03 mg/L gentamycin (Sigma, St. Louis, MO), transferred onto a LB media plate containing 0.03 mg/L gentamycin, and the plates were cultured overnight (12-18h) at 37°C. The colonies were harvested into sterile water, and then the bacteria suspension was centrifuged and resuspended two times to remove all traces of the growth medium. A fresh cell suspension at the desired electrolyte solution was prepared right before the start of each experiment. The concentrations of E.coli D21g in influent, effluent, and soil solution were determined using a spectrophotometer (Unico UV-200, United Products & Instruments, Dayton, NJ) at 600 nm [*Torzaban et al.*, 2008] or with the spread plating method [*Clesceri et al.*, 1989] when necessary (e.g., low concentration).

The NaBr solution containing *E. coli* D21g at a concentration of ~1.0 × 10^8 cells/mL was continuously mixed during the column experiment using a magnetic stirrer. The value of the influent concentration (C_0) was measured three times during the course of a transport experiment to assess the reproducibility of the measurements and microbial survival. The spectrophotometer readings for *E. coli* D21g were within 1% of C_0, and the standard deviation of the spread plating method was 14.3% of C_0. No systematic decrease

87

in C_0 was observed over the duration of the column experiments, and this indicates that little death occurred during this interval.

3.2.3 Column Experiments

Preferential transport experiments were conducted in a plexiglass (acrylic) column that was 22 cm long and had an inside diameter of 13.2 cm. Preferential flow systems were created by packing fine (120 μm) and coarse (710 μm) sands into the column as follows: (i) the column was filled with autoclaved DI water to about one third of the column height, and a 30 cm long plastic tube with outside diameter of 1.14 cm was held in the center of the column; (ii) the fine sand was incrementally wet packed into the matrix portion of the column (outside the plastic tube) to a height of 20 cm; (iii) excess water in the plastic tube was drained from the bottom; (iv) the tube was carefully pulled out from the column without disturbing the surrounding fine matrix sand and leaving a 1.14 cm diameter hole in the center of the column; (v) the hole was then filled to a height of 20 cm with various combinations of coarse and fine sands (Figure 3.1) using a funnel to create the desired preferential flow lens structure; and (vi) the column was then saturated with water from the bottom. Four lens configurations were considered (Figure

3.1) that are denoted as Types I (continuous coarse sand throughout the column), II

(coarse sand lens of variable length that is open at the bottom boundary), III (coarse sand

lens of variable length that is open at the top boundary), and IV (coarse sand lens of

variable length that is open at both boundaries but discontinuous in the center).

A polyester membrane (Saatifil PES 18/13) with a 18 μm nominal pore size was

placed at the bottom of the column and connected to a hanging water column (tube) to

control the bottom boundary pressure. Solutions were delivered onto the surface of the

heterogeneous column at a steady flow rate using a rain simulator connected to a

peristaltic pump. The water velocity was selected in order to just maintain saturated

conditions (several mm of ponding at the surface) in the column through the experiments.

Two pore volumes (PVs) of a selected NaCl solution were flushed through the column,

and the sand was allowed to equilibrate with this solution (phase 0) before initiating a

microbial transport experiment.

Microbial transport experiments were carried out in two phases. First, several PVs of

microbe suspension and NaBr were introduced into the column at a constant rate and IS

(phase I). Second, NaCl solution was flushed through the column at the same flow rate

and IS as in phase 1 until the effluent microbe concentration returned to a baseline level

(phase II). Effluent samples were continuously collected during the transport experiment at selected intervals using a fraction collector. The effluent samples were then analyzed for Br and microbe concentrations as described above.

Following recovery of the breakthrough curves (BTC) for the microbes and bromide, some of the columns underwent an additional experimental phase III to examine the release of retained microbes with a reduction in solution IS. In this case, columns were flushed with autoclaved DI water at the same velocity as during phases I and II until the released microbe concentration in the effluent returned to a baseline level. The effluent samples were collected and analyzed using the same protocols as during phases I and II.

In some cases the distribution of retained microbes in the heterogeneous columns was quantified after recovery of the BTCs (phases I and II). Sand samples were taken at seven depths (spaced according to the position of the interrupting fine sand layer in the lens) and three locations, namely: the lens, the matrix in the vicinity of the lens, and the bulk matrix. The length and position of preferential paths were determined during extraction. The sand samples were carefully excavated into tubes containing excess DI water. The tubes were shaken for 15 minutes to liberate any reversibly retained microbes

and the concentrations of *E. coli* D21g in the excess solution were determined as

described above.

3.3 Numerical Models

A two-dimensional finite element mathematic model was created using the

COMSOL software package and used to simulate the transport, retention, and release of

E. coli D21g in the heterogeneous column experiments based on the solution of the

Richards equation and the advection-dispersion equation (ADE) with terms for kinetic

retention and release. The microbial transport equations are given as:

$$\frac{\partial(\theta C)}{\partial t} = \frac{\partial}{\partial x_i}\left(\theta D_{ij}\frac{\partial C}{\partial x_j}\right) - \frac{\partial q_i C}{\partial x_i} - \theta \psi k_{att} C + \rho k_{det} H_o (S - f_c S_3)(S - f_c S_3) \qquad [1]$$

$$\frac{\partial(\rho S)}{\partial t} = \theta \psi k_{att} C - \rho k_{det} H_o (S - f_c S_3)(S - f_c S_3) \qquad [2]$$

where subscripts *i* and *j* denote coordinate directions, C [N_c L^{-3}; L and N_c denote the units

of length and number of microbes, respectively] is the microbe concentration in the

aqueous phase, S [N_c M^{-1}; M denotes units of mass of soil] is the microbe concentration

on the solid phase, S_3 [$N_c M^{-1}$] is the value of S before a reduction of IS during phase III, f_c

(dimensionless) is the fraction of microbes on the solid phase that still remains

immobilized after a reduction in IS, D_{ij} [L^2 T^{-1}] is the hydrodynamic dispersion

coefficient, q_i [L T^{-1}] is the Darcy water velocity in the i direction, k_{det} [T^{-1}] is the

microbe detachment rate coefficient, k_{att} [T^{-1}] is the microbe attachment rate coefficient,

θ [$-$] is the water content, and ρ [M L^{-3}] is the bulk density. The parameter ψ [-] accounts

for time and concentration dependent blocking using a Langmuirian approach as

[*Adamczyk et al.*, 1994]:

$$\psi = 1 - \frac{S}{S_{max}} \qquad [3]$$

where S_{max} [N_c M^{-1}] is the maximum solid phase concentration of microbes.

We followed a step-by-step procedure presented by Wang et al. [2013] to

determine hydraulic properties and microbe transport parameters for simulations in

preferential flow systems during phases I and II. In short, the saturated water content

(θ) and bulk density (ρ) were directly calculated, and the saturated hydraulic

conductivities (K_s) for both sands were determined from homogeneous column

experiments. Due to the variation caused by the column packing process, the hydraulic

conductivity of the matrix was calculated based on the breakthrough time of bromide.

And then, the hydraulic conductivity of the lens was inversely estimated based on the

total flow rate and the hydraulic conductivity of the matrix. We adopted the

hydrodynamic dispersion coefficient (D_{ij}) and the transport parameters (S_{max}, k_{att}, k_{det}) for

D21g at given solution chemistry conditions from *Wang et al.* [2013]. In this case, $k_{det}=0$

and k_{att} was a constant for given solution chemistry conditions.

The last term on the right hand side of Equations [1] and [2] accounts for the

release of *E. coli* D21g with a reduction in IS during phase III in a manner similar to

Bradford et al. [2012]. In addition to Eqs. [1]-[3], the solution IS (1:1 electrolyte) was

also simulated during phase III using an ADE for a conservative tracer. In the presence

of DI water, k_{att} was set equal to 0 based upon data presented in *Wang et al.* [2013] for

low IS conditions, f_c was determined from mass balance information following

completion of phase III, and k_{det} was estimated by optimization (trial and error) to the

experimental data. The Heaviside function (H_o) was equal to 0 when $S < f_c S_3$ and 1 when

$S \geq f_c S_3$. The above approach allowed a known amount of retained *E. coli* D21g to be

released upon arrival of the DI water front at a particular location.

3.4 Results and Discussions

3.4.1 Bromide

Figure 3.2 shows the normalized effluent concentrations (C/C_0) of bromide as a function of time from columns with Type I and II lens when the length of the coarse sand lens ranged from 10 to 20 cm. Two pulses of bromide were observed at the outlet of all columns. The first pulse travelled through the lens and arrived much earlier than the second pulse from the matrix. The length of the lens had a great impact on the arrival times of the first pulse. Specifically, the arrival time of the first pulse increased from 2 to 12 minutes with a decrease in the length of the Type II lens from 20 to 10 cm as shown in Table 3.1. Type III and IV lenses also exhibited this same trend (Table 3.1). As the length of the lens decreased, water and bromide had to travel a longer distance through the fine sand which decreased the average velocity of both water and bromide, and delayed the arrival of bromide at the outlet. This decrease in velocity produced a corresponding decrease in the relative amount of bromide that was transported through the preferential pathway (the first pulse) with a decrease in the lens length. Conversely, the velocity of the matrix was almost the same for all columns and the arrival time of the second pulse was therefore similar (21.1 to 23.8 minutes).

Table 3.1. Breakthrough information for bromide.

Type of lens configuration	Length of lens (cm)	Arrival time of first pulse (min)	Arrival time of second pulse (min)	Peak concentration in first pulse $(100*C/C_0)$	Total recovery (%)
Type I	20	1.4	23.8	24.7	99.4
Type II	19	3.2	21.9	19.5	99.6
	18	3.7	21.5	17.8	100.1
	16	5.3	21.8	16.8	100.2
	10	11.1	21.1	16.3	98.9
Type III	19	3.1	22.2	20.6	99.5
Type IV	19	6.6	22.5	16.6	99.6
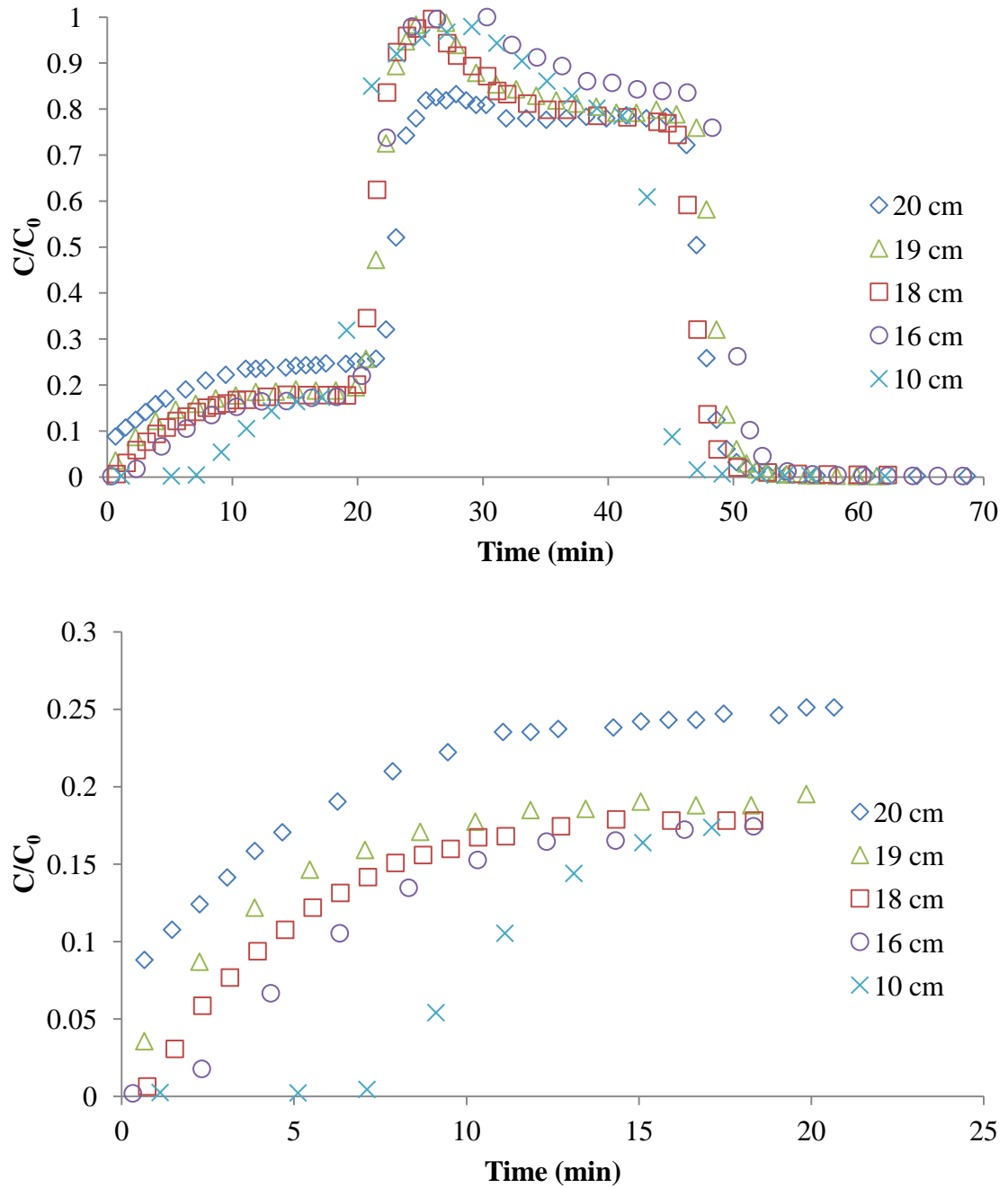
Figure 3.2. Observed effluent concentrations of Br as a function of time for columns with Type I (20 cm) and Type II lens configurations of different lengths (19 cm, 18 cm, 16 cm, and 10 cm). The bottom figure zooms on the early arrival of Br through the lens.
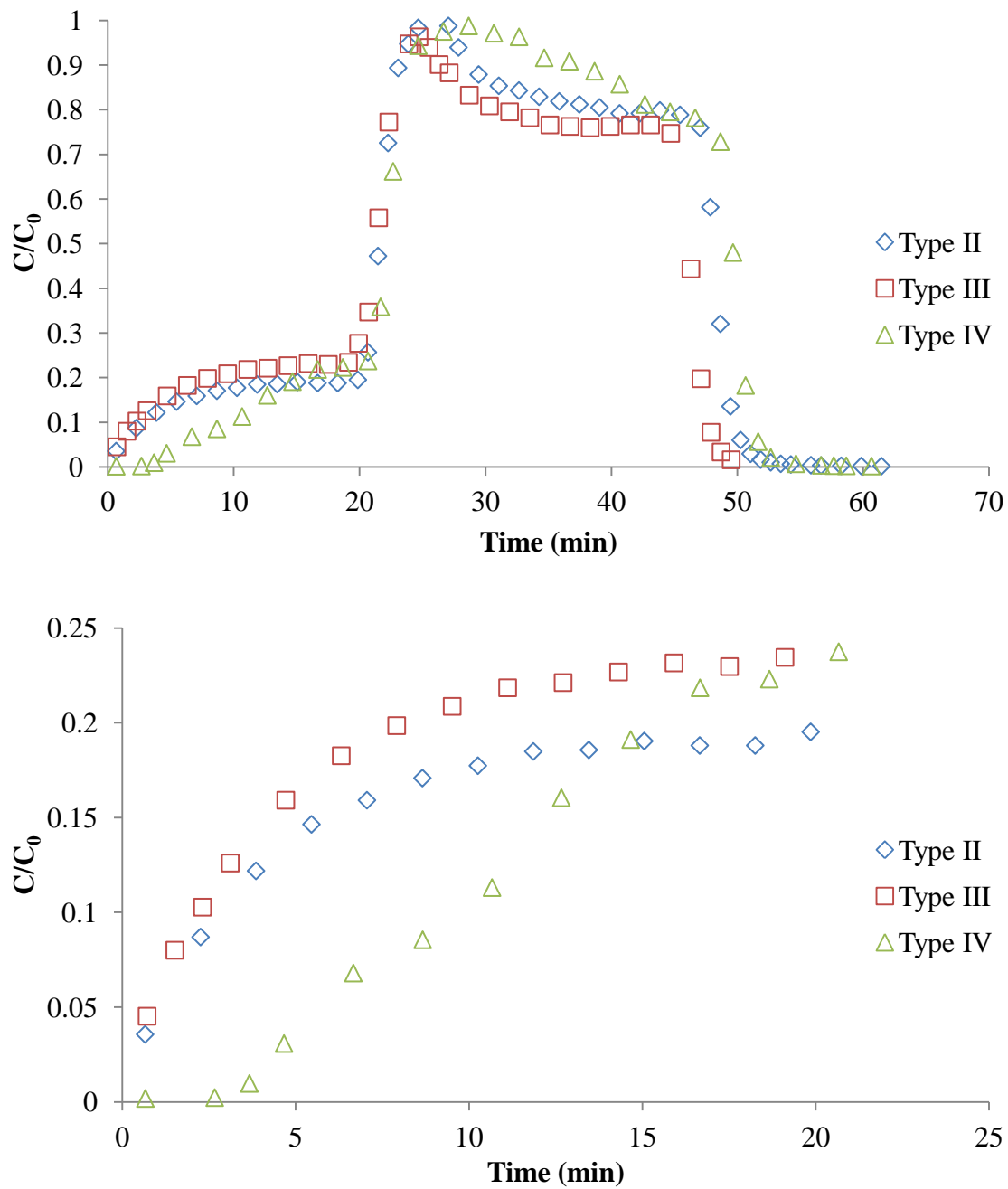
Figure 3.3. Observed effluent concentrations of Br as a function of time for columns with the same lens length (19 cm long) but with different lens configurations. The bottom figure zooms on the early arrival of Br through the lens.

The influence of lens configuration (Types II, III, and IV) on bromide transport is shown in Figure 3.3 when the lens length equaled 19 cm. Differences in the bromide BTCs for Type II (lens continuous at the column bottom) and III (lens continuous at the column top) lens configurations were rather minor. Conversely, the Type IV (lens is discontinuous in the center) lens configuration produced significantly different BTCs from Types II and III, especially with respect to the pulse from the preferential pathway (Figure 3.3). The pulse of bromide from the preferential path had more dispersion and arrived slightly later for Type IV heterogeneity compared with the other two lens configurations. This observation indicates that the discontinuous lens created more disruptions to flow and transport pathways.

3.4.2 E. coli D21g

3.4.2.1 Constant Solution Chemistry Condition

A high energy barrier limited the retention of *E. coli* D21g in both fine and coarse sand when the IS equaled 1 mM [*Wang et al.*, 2013]. Thus, the influence of lens length and configuration was very similar for *E. coli* D21g and bromide when the IS=1 mM (Figure 3.4). Similar to bromide, the first pulse of *E. coli* D21g arrived later and had less

mass when the length of the lens decreased, and was more dispersed for Type IV than II and III lens configurations. Conversely, the arrival time for *E. coli* D21g in the second pulse (from the matrix) was about one and half minutes (0.07 pore volumes) earlier than for bromide in the same experiments (Table 3.1 and Table 3.2; Figure 3.4). This observation was ascribed to size exclusion [*Fontes et al.*, 1991; *Ryan and Elimelech*, 1996; *Morley et al.*, 1998; *Ginn*, 2002], which can increase the transport velocity of particles by constraining them to larger pore networks. It was not possible to tell whether *E. coli* D21g also had an earlier arrival time than bromide in the first pulse (lens), because of the very rapid arrival for both bromide and *E. coli* D21g. However, the relative concentration of *E. coli* D21g was higher than that of bromide in the first pulse (Tables 3.1 and 3.2). Since bromide was a conservative tracer and some *E. coli* D21g was retained in the sand, this observation suggests that size exclusion may have also enhanced the transport of *E. coli* D21g in the lens in comparison to bromide.
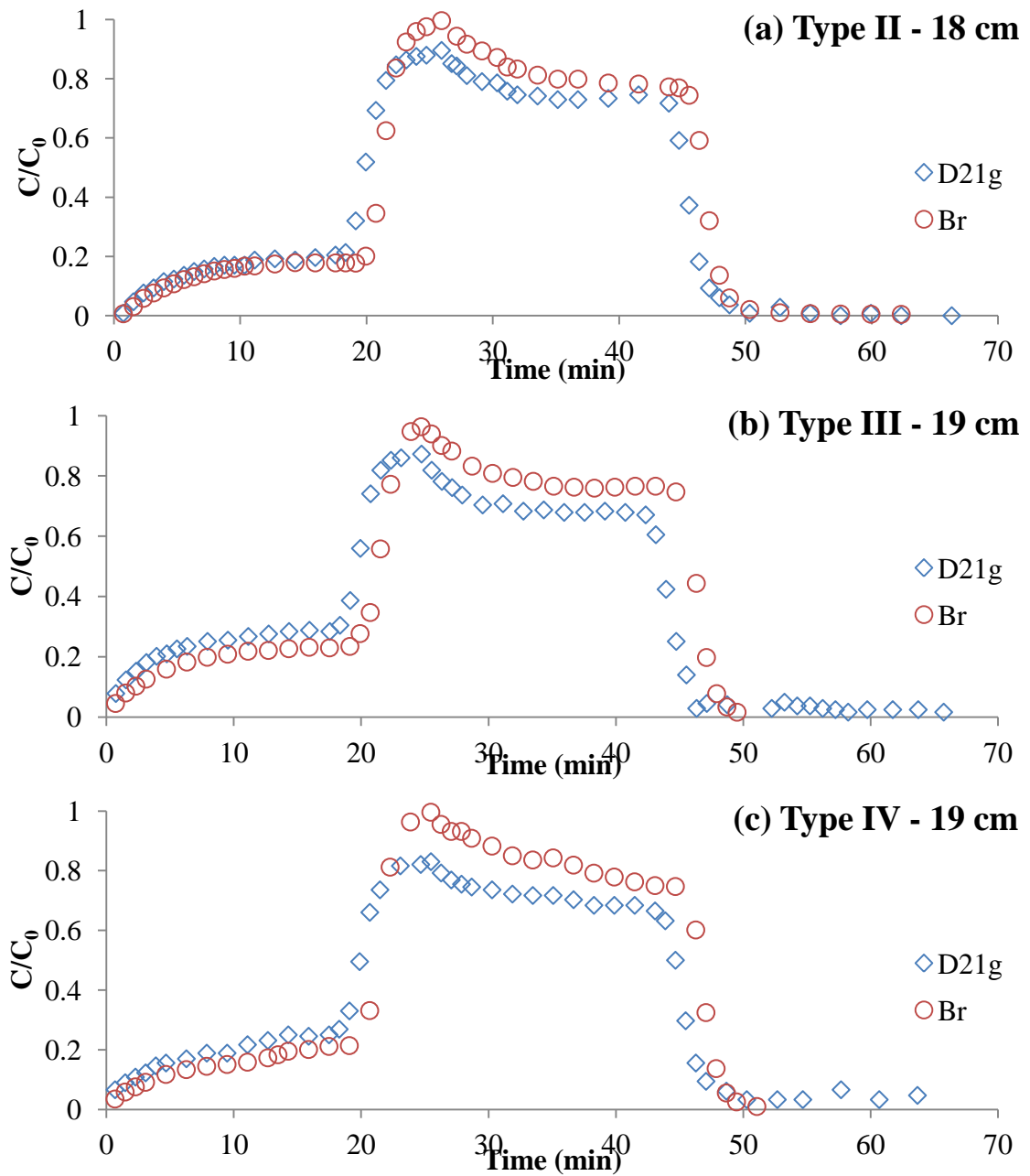
Figure 3.4. Observed effluent concentrations of *E. coli* D21g at IS=1 mM and Br as a function of time for (a) Type II lens configuration with a length of 18 cm, (b) Type III lens configuration with a length of 19 cm, and (c) Type IV lens configuration with a length of 19 cm.

Table 3.2. Breakthrough information for *E. coli* D21g at 1 mM and 20 mM.

Type of lens configuration	Length of lens (cm)	IS (mM)	Arrival time of first pulse (min)	Arrival time of second pulse (min)	Peak concentration in first pulse $(100*C/C_0)$	Total recovery (%)
Type II	18	1	3.6	19.9	18.7	97.4
Type III	19	1	2.2	20.7	28.4	96.4
Type IV	19	1	3.0	21.4	24.5	96.5
Type III	19	20	2.3	NA	13.8	13.9
Type IV	19	20	3.0	NA	11.2	10.0
Type II	18	20	6.5	NA	9.1	8.2
Type II	16	20	NA	NA	4.2	2.9
Type IV	16	20	NA	NA	NA	0

Figure 3.5 shows representative BTCs for *E. coli* D21g when the IS=20 mM and the lens configuration was Type II. In comparison to IS=1 mM, the height of the energy barrier deceased and the depth of the secondary minimum increased when the IS=20 mM [*Wang et al.*, 2013]. Consequently, the retention of *E. coli* D21g in the fine matrix sand became much greater and no detectable amount of *E. coli* D21g was transported through the 20 cm long matrix (data not shown). However, *E. coli* D21g was able to travel

through the preferential path for most of the studied conditions. The concentration of *E. coli* D21g in the effluent decreased dramatically when the lens length decreased, and only a trace amount of *E. coli* D21g was detected in the effluent when the lens length was equal to 16 cm (Table 3.2). The preferential flow pathway was the major or even the only route for *E. coli* D21g transport under high IS conditions. Consequently, the lens length had a much greater impact on the transport of *E. coli* D21g through the preferential path when the IS=20 mM than when the IS=1 mM (Table 3.2).
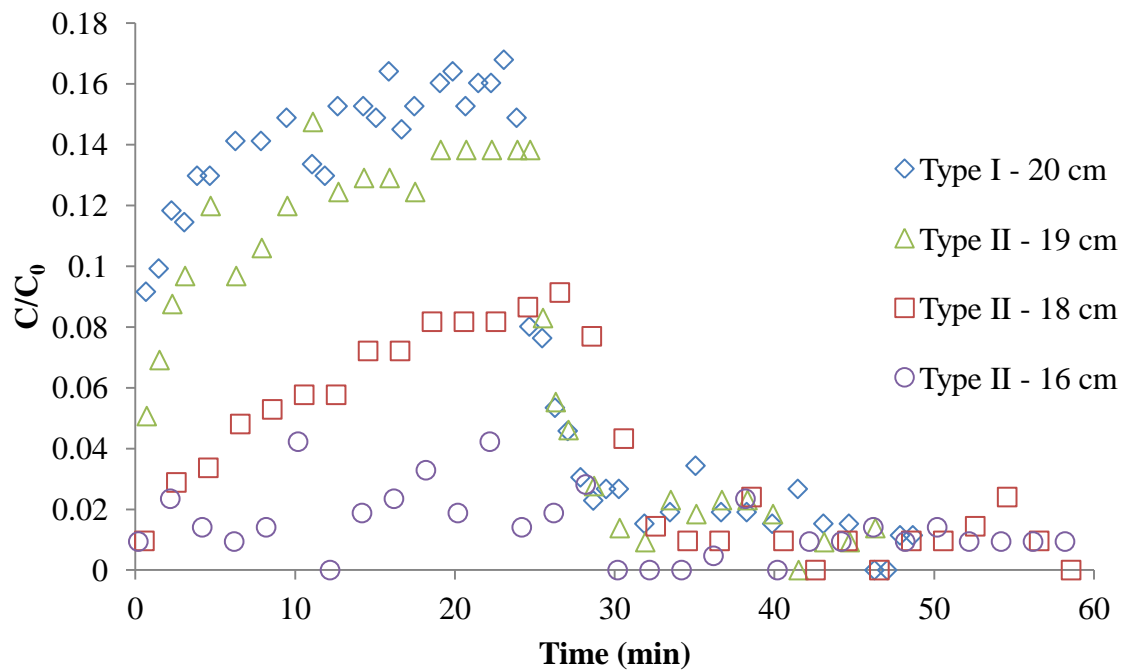
Figure 3.5. Observed effluent concentrations of *E. coli* D21g at IS = 20 mM as a function of time for Type I lens configuration (20 cm) and Type II lens configuration with a length of 19, 18, and 16 cm.

Figure 3.6 demonstrates that the transport of *E. coli* D21g was also influenced by the lens configuration (Types II, III, and IV). In comparison with the Type II and III configurations, the Type IV heterogeneity enhanced the mixing and delayed the arrival of *E. coli* D21g in the first pulse when the IS=1 mM. Similar behavior was observed for bromide (Fig. 3.3). At a higher IS=20 mM, the enhanced mixing of the two flow domains in the Type IV configuration produced greater retention of *E. coli* D21g in the

preferential flow path, and corresponding less recovery of *E. coli* D21g in the first pulse

(Table 3.2).
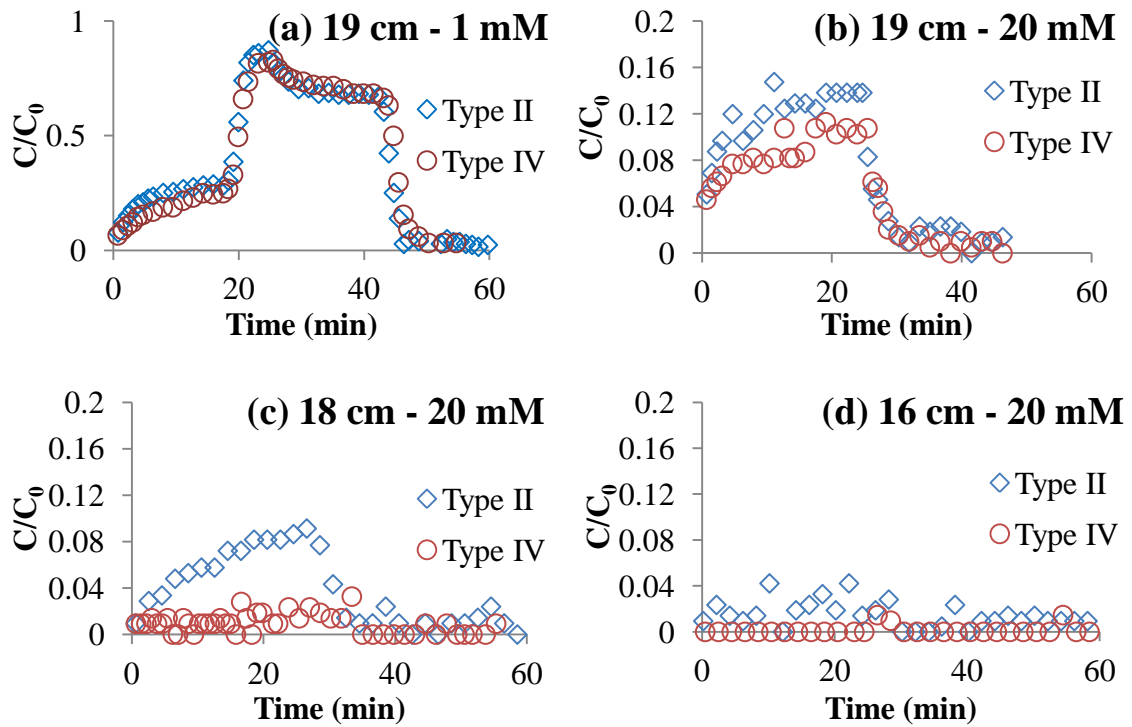
Figure 3.6. Observed effluent concentrations of *E. coli* D21g for Type II and Type IV

lens configurations as a function of time for (a) a lens length of 19 cm and IS=1 mM; (b)

a lens length of 19 cm and IS=20 mM; (c) a lens length of 18 cm and IS=20 mM; and (d)

a lens length of 16 cm and IS=20 mM.

The spatial distribution of retained mass is also very important for understanding

the transport and retention behavior of *E. coli* D21g in systems with preferential flow.

Figure 3.7 shows representative retention profiles for *E. coli* D21g for Type II, III, and IV lens configurations when the lens length was 19 cm and the solution IS=20 mM. Three locations were considered for each case: (i) in the lens (including the fine sand); (ii) in the matrix adjacent to the lens; and (iii) in the bulk matrix sand.

In the matrix, most retained cells were in the top few centimeters of the column and S/C_0 rapidly decreased with an increase in distance from the column inlet. Conversely, values of S/C_0 in the coarse sand portions of the lenses were very low. For Type II lens configuration, the fine sand disruption in the preferential path was located at the top. Thus, the value of S/C_0 was about the same as in the matrix at this location (Figure 3.7a). For Type III lens configuration, the fine sand disruption in the preferential path was located at the bottom, and the value of S/C_0 in this region was as high as that in the top matrix (Figure 3.7b). For Type IV lens configuration, a high value of S/C_0 was located in the middle of the preferential flow path where the fine sand disruption occurred (Figure 3.7c).
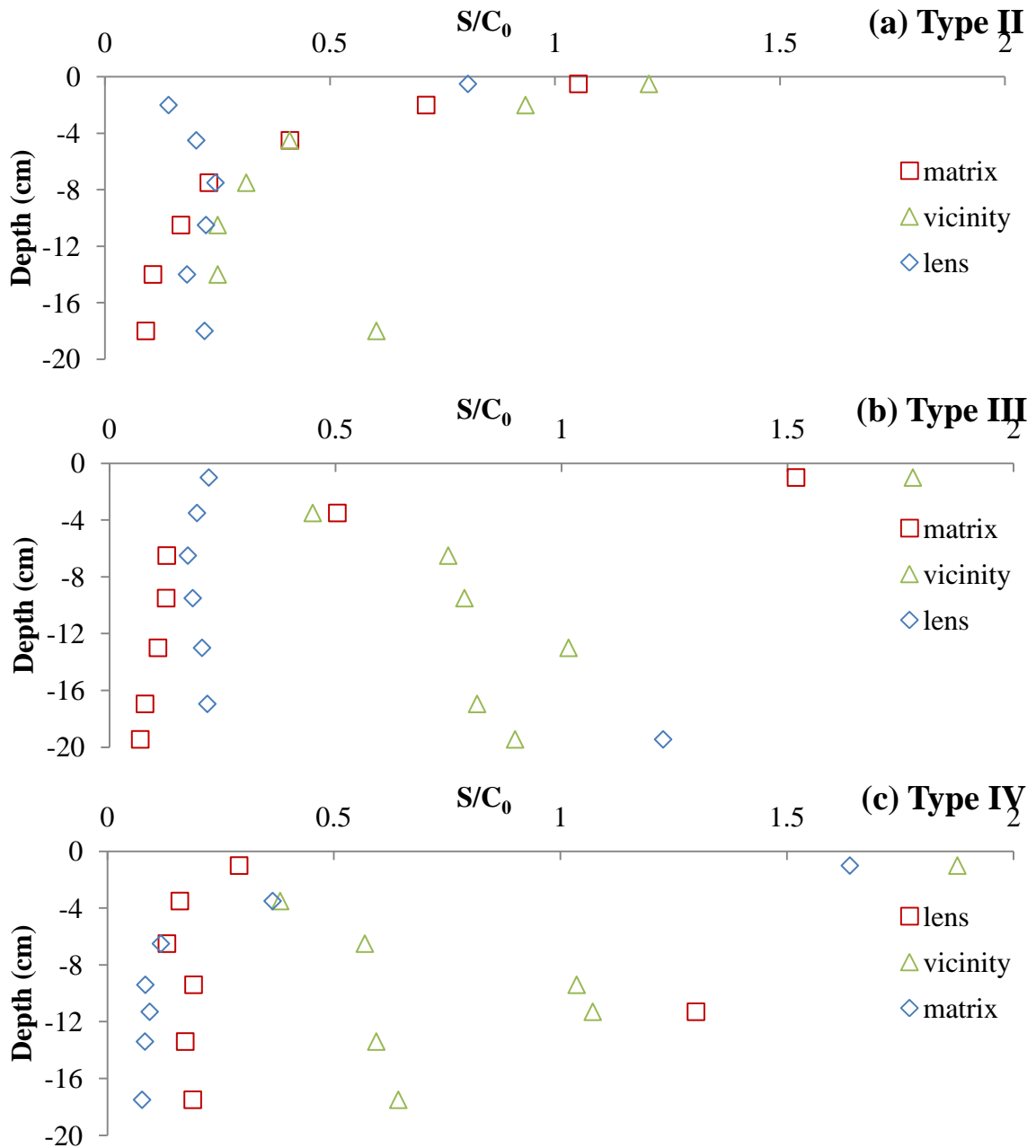
Figure 3.7. Normalized solid phase concentrations (S/C_0) of *E. coli* D21g as a function of depth for (a) Type II lens, (b) Type III lens, and (c) Type IV lens of 19 cm. Three locations are considered, namely: (i) in the lens; (ii) in the matrix in the immediate vicinity of the lens; and (iii) in the matrix away from the lens.

The greatest amount of cell retention tended to occur in the matrix adjacent to the lens. This location reflects the influence of mass exchange between the lens and matrix, as well as retention in the matrix. Similar high values of S/C_0 occurred near the column inlet for the three lens configurations because retention was mainly controlled by the matrix in this location. Conversely, distinct differences in the amount of cell retention occurred with increasing depth for the various lens configurations because of differences in the amount of mass transfer between the lens and matrix. The higher values of S/C_0 with increasing depth in the Type III and IV configurations indicates that discontinuities to lenses that are open at the column top will increase the subsequent mass transfer from the lens to the matrix, and thereby enhance *E. coli* D21g retention. On the other hand, cell retention adjacent to the lens in the Type II configuration was lower because the cells had to initially travel through the matrix, and many were therefore retained in the matrix, before reaching the lens.

3.4.2.2 Transients in Solution Chemistry

Figure 3.8 presents the release behavior of *E. coli* D21g during phase III when the influent solution IS was switched from 20 mM to DI water. Type II, III, and IV lens

configurations were considered and the lens length was 16 cm. Table 3.3 gives the arrival times and mass balance information for the release process. Similar to transport during phases I and II, multiple pulses of released cells were observed during phase III because of preferential flow. The highest pulse of released *E. coli* D21g arrived at the outlet about 21 minutes after the start of DI water flushing. This arrival corresponds with the travel time of bromide through the matrix (Figs. 3.2 and 3.3), and therefore indicates that this high peak mainly reflects cell release from the matrix. This peak was highest because most of the cells were retained in the matrix (Fig. 3.7). Conversely, the smaller earlier pulses mainly reflect mass transfer from the matrix to the lens, because little cell retention occurred in the coarse sand lens at an IS=20 mM [*Wang et al.*, 2013]. The lens configuration (Types II, III, and IV) had a significant influence on the number and magnitude of these earlier pulses. There was only one small pulse of released *E. coli* D21g for Type II and III lens configurations at earlier times (6.9 to 7.2 minutes), whereas the Type IV configuration produced two small pulses that arrived after 6.2 and 14.7 minutes. This observation suggests that mass transfer from the matrix to the lens was most efficient in the Type II and III configurations, and less efficient in the discontinuous Type IV configuration.
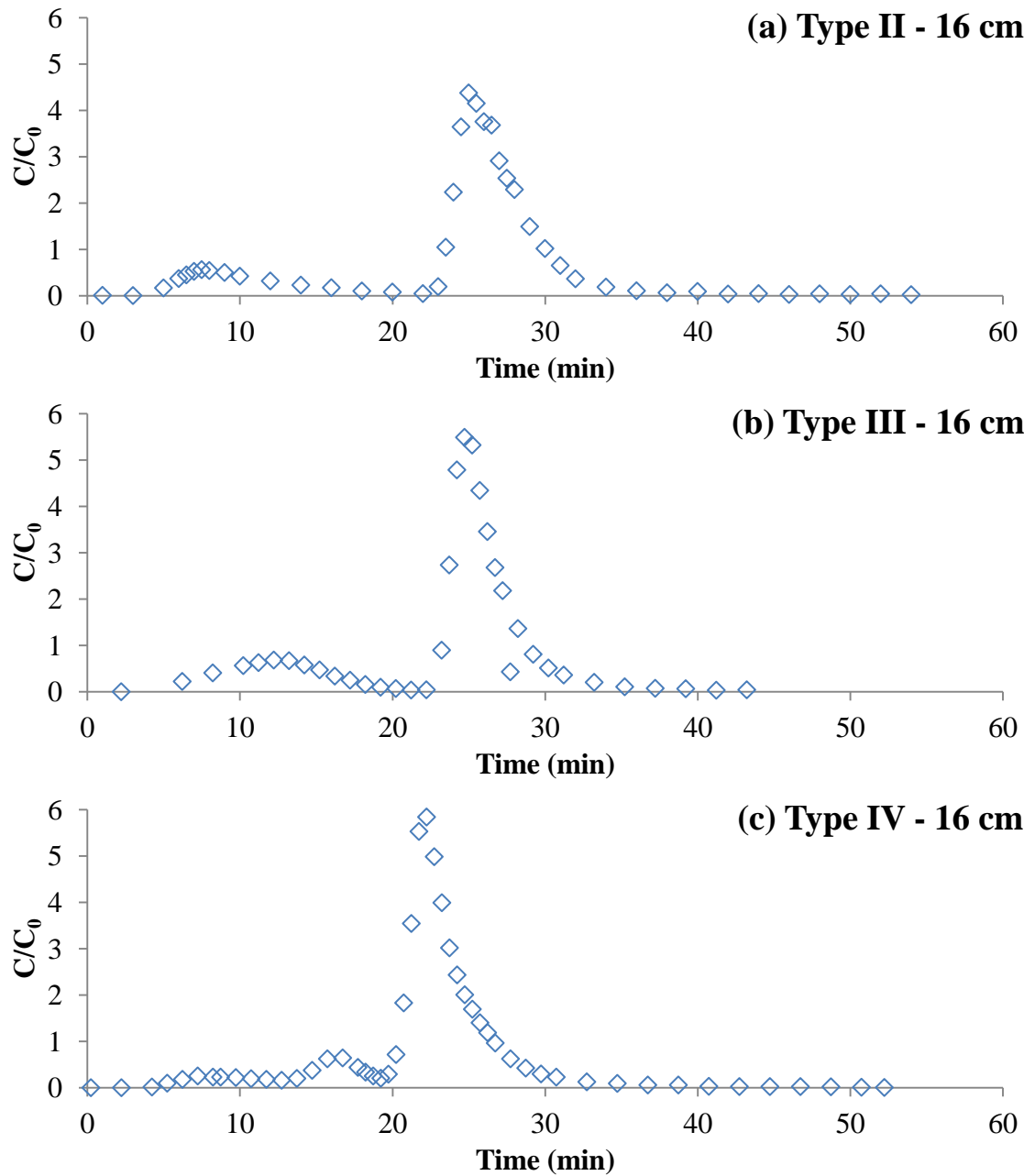
Figure 3.8. Observed effluent concentrations of *E. coli* D21g as a function of time during the release process for (a) Type II lens of 16 cm length; (b) Type III lens of 16 cm length; and (c) Type IV lens of 16 cm length. The time when the influent solution was switched from 20 mM solution to DI water was labeled as 0 at the start of phase III.

Table 3.3. Release information of *E. coli* D21g.

Type of lens configuration	Length of lens	Arrival time of first small pulse (min)	Arrival time of second small pulse (min)	Peak concentration of first small pulse $(100*C/C_0)$	Peak concentration of second small pulse $(100*C/C_0)$	Recovery of first or first and second pulse (%)	Arrival time of major pulse (min)	Peak concentration of major pulse $(100*C/C_0)$	Recovery of major pulse (%)
Type II	16	6.9	NA	56.4	NA	17.8	23.0	437.5	78.0
Type III	16	7.2	NA	68.3	NA	22.4	23.2	548.7	69.5
Type IV	16	6.2	14.7	25.3	64.2	14.6	20.7	583.9	76.8

3.4.3 Simulations with Numerical Models

Figure 3.9 shows examples of simulated BTCs of bromide and *E. coli* D21g at an IS=1 mM during phases I and II. Figure 3.10 shows examples of simulated BTCs of *E. coli* D21g at an IS=20 mM during phases I and II, and cell release during phase III when the IS was reduced to DI water. The model was able to simulate the transport of bromide and *E. coli* D21g with very high accuracy during phases I and II when the IS was 1 or 20 mM. The release behavior of *E. coli* D21g from the matrix (the high pulse that arrived at later times) and the earlier pulse for Type II and III configurations were also well simulated by the model. Conversely, the model was not able to capture the subtle differences in the early release behavior for Type II, III, and IV configurations. In particular, the model failed to predict the enhanced dispersion during phases I and II, and the arrival times of the two earlier pulses associated with mass transfer from the matrix to the lens in the Type IV configuration. These differences may arise because cell retention processes that occurred at textural interfaces were incompletely quantified in the model [*Bradford et al.*, 2005].
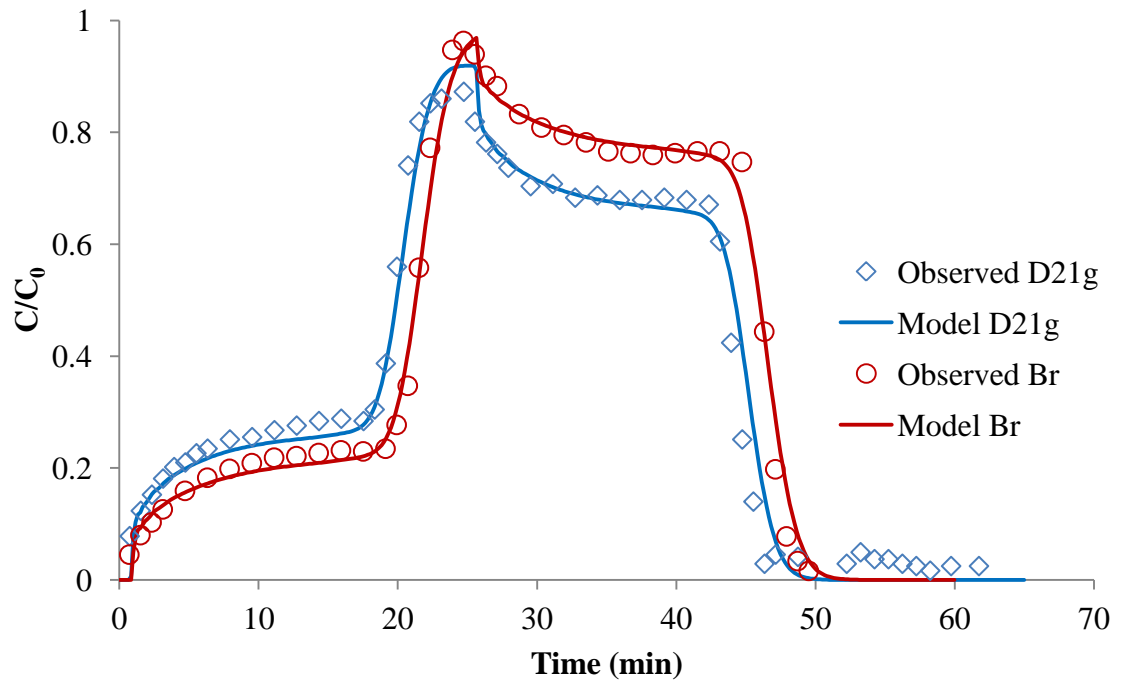
Figure 3.9. Examples of observed and simulated effluent concentrations as a function of time for Br and *E. coli* D21g of Type III lens with a 19 cm length and IS=1 mM.
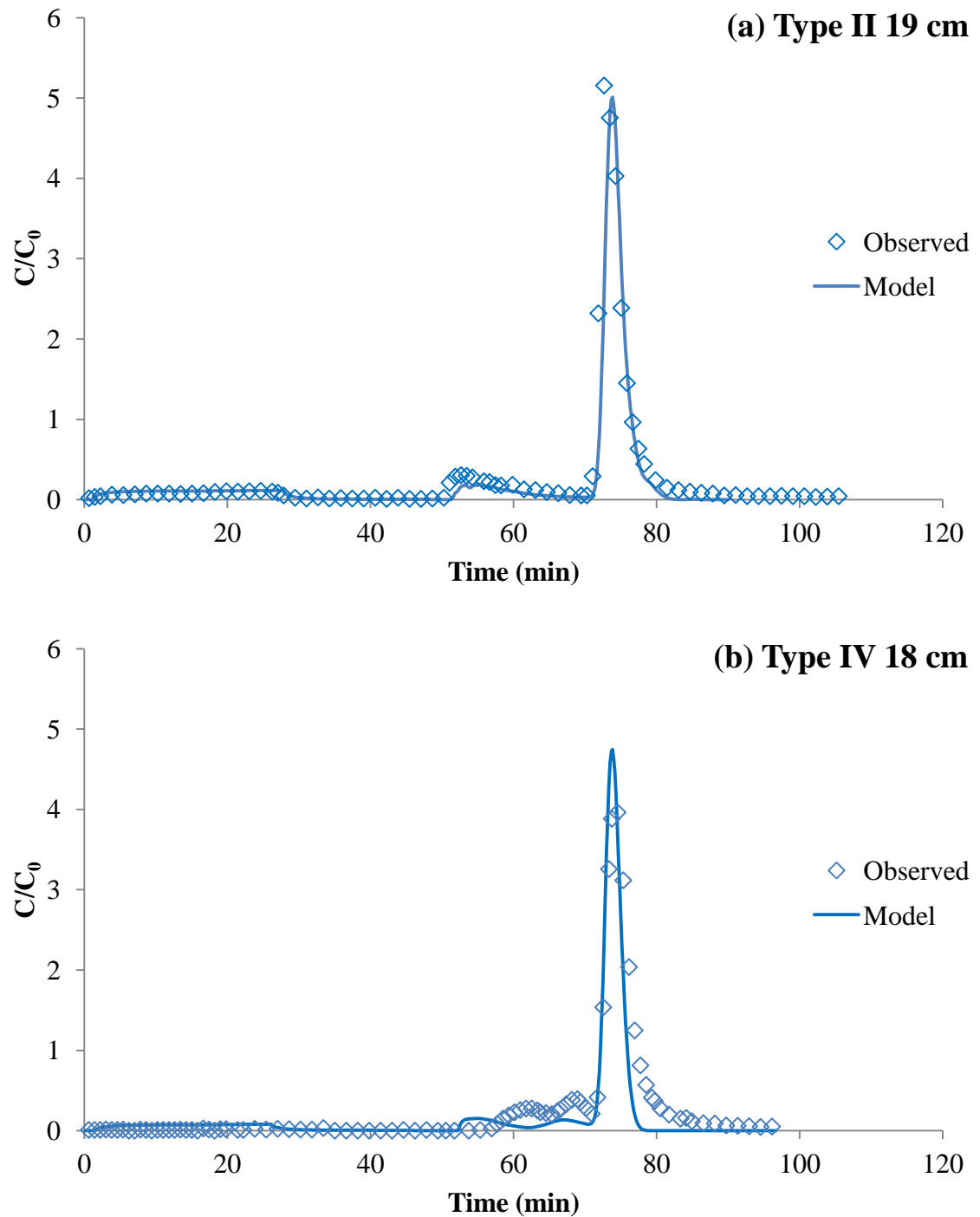
Figure 3.10. Examples of observed and simulated effluent concentrations of *E. coli* D21g as a function of time for (a) Type II lens of 19 cm length; and (b) Type IV lens of 18 cm length. The IS was 20 mM during phases I and II.

3.5 Summary and Conclusions

The length of the lens affected the water flow and transport of bromide and *E. coli* D21g. In particular, a decrease in the lens length produced later arrival times and lower effluent concentrations through the preferential pathway. This effect became more pronounced for *E. coli* D21g at a high IS because of increased cell retention in the matrix. The Type IV (lens is discontinuous in the center) lens configuration produced a larger dispersivity and later arrival time in the preferential path than Type II (lens is open at the bottom) and III (lens is open at the top) configurations, and it also yielded less transport of *E. coli* D21g at high IS due to enhanced mixing of the flow through the preferential path and matrix compared to the other two configurations. Size exclusion not only increased the travel speed of *E. coli* D21g in both the matrix and preferential path, but also increased the relative amount of *E. coli* D21g that was transported in the preferential path in comparison to bromide.

Numerical simulations of *E. coli* D21g under both constant and transient solution chemistry conditions had very high agreement with the experiment data. However, the model wasn't capable of simulating some of the subtle differences in transport between the various lens configurations. In particular, the model could not simulate the enhanced dispersion behavior in the early preferential flow pulse for the Type IV configuration during phases I and II. It also failed to predict the arrival times and transport amounts in the two earlier release peaks during phase III for the Type IV configuration. Hence, model improvements are needed to better characterize cell transport and retention processes at the interface between the preferential path and matrix.

3.6 References:

Abu-Ashour, J., D. M. Joy, H. Lee, H. R. Whiteley, and S. Zelin (1994), Transport of microorganisms through soil, *Water Air Soil Pollut.*, 75(1-2), 141-158

Allaire-Leung, S. E., S. C. Gupta, and J. F. Moncrief (2000a), Water and solute movement in soil as influenced by macropore characteristics - 1. Macropore continuity, *J. Contam. Hydrol.*, 41(3-4), 283-301.

Allaire-Leung, S. E., S. C. Gupta, and J. F. Moncrief (2000b), Water and solute movement in soil as influenced by macropore characteristics - 2. Macropore tortuosity, *J. Contam. Hydrol.*, 41(3-4), 303-315.

Allaire, S. E., S. C. Gupta, J. Nieber, and J. F. Moncrief (2002a), Role of macropore continuity and tortuosity on solute transport in soils: 2. Interactions with model assumptions for macropore description, *J. Contam. Hydrol.*, 58(3-4), 283-298.

Allaire, S. E., S. C. Gupta, J. Nieber, and J. F. Moncrief (2002b), Role of macropore continuity and tortuosity on solute transport in soils: 1. Effects of initial and boundary conditions, *J. Contam. Hydrol.*, 58(3-4), 299-321.

Arora, B., B. P. Mohanty, and J. T. McGuire (2011), Inverse estimation of parameters for multidomain flow models in soil columns with different macropore densities, *Water Resour. Res.*, 47(4), W04512.

Arora, B., B. P. Mohanty, and J. T. McGuire (2012), Uncertainty in dual permeability model parameters for structured soils, *Water Resour. Res.*, 48(1), W01524.

Bales, R. C., C. P. Gerba, G. H. Grondin, and S. L. Jensen (1989), Bacteriophage transport in sandy soil and fractured tuff, *Appl. Environ. Microb.*, 55(8), 2061-2067.

Beven, K., and P. Germann (1982), Macropores and water flow in soils, *Water Resour. Res.*, 18(5), 1311-1325.

Bradford, S. A., and M. Bettahar (2005), Straining, attachment, and detachment of Cryptosporidium oocysts in saturated porous media, *J. Contam. Hydrol.*, 34(2), 469-478.

Bradford, S. A., and H. Kim (2010), Implications of Cation Exchange on Clay Release and Colloid-Facilitated Transport in Porous Media, *J. Contam. Hydrol.*, 39(6), 2040-2046.

Bradford, S. A., S. Torkzaban, H. Kim, and J. Šimůnek (2012), Modeling colloid and microorganism transport and release with transients in solution ionic strength, *Water Resour. Res.*, 48(9), W09509.

Castiglione, P., B. Mohanty, P. Shouse, J. Šimůnek, M. T. Van Genuchten, and A. Santini (2003), Lateral water diffusion in an artificial macroporous system, *Vadose Zone J.*, 2(2), 212-221.

Cey, E. E., and D. L. Rudolph (2009), Field study of macropore flow processes using tension infiltration of a dye tracer in partially saturated soils, *Hydrol. Processes*, 23(12), 1768-1779.

Cey, E. E., D. L. Rudolph, and J. Passmore (2009), Influence of macroporosity on preferential solute and colloid transport in unsaturated field soils, *J. Contam. Hydrol.*, 107(1-2), 45-57.

Chen, G. X., and S. L. Walker (2007), Role of solution chemistry and ion valence on the adhesion kinetics of groundwater and marine bacteria, *Langmuir*, 23(13), 7162-7169.

Cheng, T., and J. E. Saiers (2009), Mobilization and transport of in situ colloids during drainage and imbibition of partially saturated sediments, *Water Resour. Res.*, 45(8), W08414.

Clesceri, L. S., A. E. Greenberg, and R. R. Trussel (1989), Standard methods for the examination of water and waste water, 17th edn. *American Public Health Association*, Washington DC

Dean, D. M., and M. E. Foran (1992), The Effect of Farm Liquid Waste Application on Tile Drainage, *J. Soil Water Conserv.*, 47(5), 368-369.

Dong, H. L., T. C. Onstott, M. F. Deflaun, M. E. Fuller, T. D. Scheibe, S. H. Streger, R. K. Rothmel, and B. J. Mailloux (2002), Relative dominance of physical versus chemical effects on the transport of adhesion-deficient bacteria in intact cores from South Oyster, Virginia, *Environ. Sci. Technol.*, 36(5), 891-900.

Fontes, D. E., A. L. Mills, G. M. Hornberger, and J. S. Herman (1991), Physical and chemical factors influencing transport of microorganisms through porous media, *Appl. Environ. Microbiol.*, 57(9), 2473-2481.

Ginn, T. R. (2002), A travel time approach to exclusion on transport in porous media, *Water Resour. Res.*, 38(4), -.

Grolimund, D., K. Barmettler, and M. Borkovec (2001), Release and transport of colloidal particles in natural porous media: 2. Experimental results and effects of ligands, *Water Resour. Res.*, 37(3), 571-582.

Guzman, J. A., G. A. Fox, R. W. Malone, and R. S. Kanwar (2009), Transport from Surface-Applied Manure to Subsurface Drains through Artificial Biopores, *J. Environ. Qual.*, 38(6), 2412-2421.

Harvey, R. W., N. E. Kinner, D. MacDonald, D. W. Metge, and A. Bunn (1993), Role of physical heterogeneity in the interpretation of small-scale laboratory and field observations of bacteria, microbial-sized microsphere, and bromide transport through aquifer sediments, *Water Resour. Res.*, 29(8), 2713-2721.

Jamieson, R., R. Gordon, K. Sharples, G. Stratton and A. Madani (2002), Movement and persistence of fecal bacteria in agricultural soils and subsurface drainage water: A review, *Canadian Biosystems Engineering*, 44: 1-9.

Jarvis, N. J. (2007), A review of non-equilibrium water flow and solute transport in soil macropores: principles, controlling factors and consequences for water quality, *Eur. J. Soil. Sci.*, 58(3), 523-546.

Jiang, S., L. P. Pang, G. D. Buchan, J. Šimůnek, M. J. Noonan, and M. E. Close (2010), Modeling water flow and bacterial transport in undisturbed lysimeters under irrigations of dairy shed effluent and water using HYDRUS-1D, *Water Res.*, 44(4), 1050-1061.

Jury, W. A., and H. Flühler (1992), Transport of Chemicals Through Soil: Mechanisms, Models, and Field Applications, *Adv. Agron.*, 47, 141-201.

Lenhart, J. J., and J. E. Saiers (2003), Colloid mobilization in water-saturated porous media under transient chemical conditions, *Environ. Sci. Technol.*, 37(12), 2780-2787.

Madsen, E. L., and M. Alexander (1982), Transport of Rhizobium and Pseudomonas through Soil1, *Soil Sci. Soc. Am. J.*, 46(3), 557-560.

McDowell-Boyer, L. M. (1992), Chemical mobilization of micron-sized particles in saturated porous media under steady flow conditions, *Environ. Sci. Technol.*, 26(3), 586-593.

Mills, A. L., J. S. Herman, G. M. Hornberger, and T. H. Dejesus (1994), Effect of Solution Ionic-Strength and Iron Coatings on Mineral Grains on the Sorption of Bacterial-Cells to Quartz Sand, *Appl. Environ. Microbiol.*, 60(9), 3300-3306.

Morley, L. M., G. M. Hornberger, A. L. Mills, and J. S. Herman (1998), Effects of transverse mixing on transport of bacteria through heterogeneous porous media, *Water Resour. Res.*, 34(8), 1901-1908.

National Research Council (1994), Ground water recharge using waters of impaired quality, *Natl Academy Pr.*

Nocito-Gobel, J., and J. E. Tobiason (1996), Effects of ionic strength on colloid deposition and release, *Colloids and surfaces A: Physicochemical and engineering aspects*, 107, 223-231.

Pang, L., M. McLeod, J. Aislabie, J. Šimůnek, M. Close, and R. Hector (2008), Modeling transport of microbes in ten undisturbed soils under effluent irrigation, *Vadose Zone J.*, 7(1), 97-111.

Pivetz, B., and T. Steenhuis (1995), Soil matrix and macropore biodegradation of 2, 4-D, *J. Environ. Qual.*, 24(4), 564-570.

Roy, S. B., and D. A. Dzombak (1996), Colloid release and transport processes in natural and model porous media, *Colloids and surfaces A: Physicochemical and engineering aspects*, 107, 245-262.

Runnells, D.D. (1976), Wastewaters in the Vadose Zone of Arid Regions: Geochemical Interactionsa, *Ground Water*, 14: 374-385. doi:10.1111/j.1745-6584.1976.tb03131.x.

Ryan, J. N., and P. M. Gschwend (1994), Effects of ionic strength and flow rate on colloid release: Relating kinetics to intersurface potential energy, *Journal of Colloid and Interface Science*, 164(1), 21-34.

Ryan, J. N., and M. Elimelech (1996), Colloid mobilization and transport in groundwater, *Colloids and surfaces A: Physicochemical and engineering aspects*, 107, 1-56.

Šimůnek, J., and M. Th. van Genuchten, Modeling nonequilibrium flow and transport with HYDRUS (2008), *Vadose Zone J.*, doi:10.2136/VZJ2007.0074, Special Issue "Vadose Zone Modeling", *7*(2).

Šimůnek, J., N. J. Jarvis, M. T. van Genuchten, and A. Gardenas (2003), Review and comparison of models for describing non-equilibrium and preferential flow and transport in the vadose zone, *J. Hydrol.*, 272(1-4), 14-35.

Torkzaban, S., S. S. Tazehkand, S. L. Walker, and S. A. Bradford (2008), Transport and fate of bacteria in porous media: Coupled effects of chemical conditions and pore space geometry, *Water Resour. Res.*, 44(4), W04403.

Tosco, T., A. Tiraferri, and R. Sethi (2009), Ionic strength dependent transport of microparticles in saturated porous media: modeling mobilization and immobilization phenomena under transient chemical conditions, *Environ. Sci. Technol.*, 43(12), 4425-4431.

Unc, A., and M. J. Goss (2003), Movement of faecal bacteria through the vadose zone, *Water Air Soil Pollut.*, 149(1-4), 327-337.

Walker, S. L., J. A. Redman, and M. Elimelech (2004), Role of cell surface lipopolysaccharides in Escherichia coli K12 adhesion and transport, *Langmuir*, 20(18), 7736-7746.

Wang, Y., S. A. Bradford, and J. Šimůnek (2013), Transport and fate of microorganisms in soils with preferential flow under different solution chemistry conditions, *Water Resour. Res.*, 49(5), 2424-2436. doi:10.1002/wrcr.20174.

Wollum, A., and D. Cassel (1978), Transport of microorganisms in sand columns, *Soil Sci. Soc. Am. J.*, 42(1), 72-76.

Yee, N., J. B. Fein, and C. J. Daughney (2000), Experimental study of the pH, ionic strength, and reversibility behavior of bacteria-mineral adsorption, *Geochim. Cosmochim. Acta*, 64(4), 609-617.

Chapter 4

Estimation and Upscaling of Dual-Permeability Model Parameters for the Transport of *E.coli* D21g in Soils with Preferential Flow

ABSTRACT

Dual-permeability models are increasingly used to quantify the transport of solutes and microorganisms in soils with preferential flow. An ability to accurately determine the model parameters and their variation with preferential pathway characteristics is crucial for predicting the transport of microorganisms in the field. The dual-permeability model with optimized parameters was able to accurately describe the transport of *E. coli* D21g in columns with artificial macropores of different configurations and lengths at two ionic strength levels (1 and 20 mM NaCl). Correlations between the model parameters and the structural geometry of the preferential flow path were subsequently investigated. Decreasing the macropore length produced a decrease in the apparent saturated hydraulic conductivity of the fracture domain and an increase in the mass transfer between the fracture and matrix domains. The mass transfer coefficient was also found to be dependent on the configuration of the preferential flow pathway. A linear superposition approach was used to estimate field scale preferential transport behavior for hypothetical fields with different amounts and configurations of macropores. Upscaling procedures were numerically investigated to predict this field scale transport behavior from column scale parameters. The upscaling method provided a satisfactory prediction of the field results under the tested scenarios. This information will be useful in assessing the risks of microbial transport due to preferential flow.

4.1 Introduction

Surface and groundwater contamination by pathogenic microorganisms has been reported across the United States, which put the public's health at risk [*Wang et al.*, 2013a]. Water entering groundwater has to pass through porous media in the vadose and saturated zones in the subsurface. Soil passage, such as riverbank filtration, dune recharge, infiltration basins and trenches, and sand filters, is also used to treat surface water to meet demands for drinking water. Therefore, an accurate understanding of the transport and fate of pathogens in porous media is needed to protect our drinking water resources.

Many studies have been conducted to quantify the influence of physical (size of the microbe and the porous medium, microbe concentration, water velocity, water content and surface roughness) and chemical (surface chemistry of the microbe and soil, and aqueous solution pH, ionic strength, and chemical composition) factors on microorganism transport in homogeneous porous media [*Mills et al.*, 1994; *Mccaulou et al.*, 1995; *Hendry et al.*, 1999; *Yee et al.*, 2000; *Dong et al.*, 2002; *Bradford et al.*, 2006; *Chen and Walker*, 2007]. However, field experiments have frequently revealed that preferential pathways are a major contributor to the overall transport of microbes because they are typically strongly retained in the soil matrix [*Bales et al.*, 1989; *Abu-Ashour et al.*, 1994; *Jiang et al.*, 2010].

The occurrence of preferential flow is found to be the rule rather than the exception in most field soils [*Flury et al.*, 1994; *Singh and Kanwar*, 1991], which may occur as a result of plant roots, burrowing earthworms, cracks, or natural structural

heterogeneities [*Wollum and Cassel*, 1978; *Beven and Germann*, 1982; *Madsen and Alexander*, 1982; *Unc and Goss*, 2003; *Cey et al.*, 2009]. Preferential flow has been identified as a major problem hampering accurate predictions of contaminant transport in soils because of difficulty in quantifying the physical and chemical complexities of the soil matrix and macropore system [*Šimůnek et al.*, 2003].

Several approaches have been developed to simulate preferential flow and transport [*Köhne et al.*, 2009a, b]. One method is to construct a 2D/3D simulation profile explicitly defining the heterogeneities or the preferential pathways of the domain. *Wang et al.* [2013a, b] successfully applied Hydrus 2D/3D to simulate microorganism transport in columns with artificial macropores. A map of the structural geometry must be known in order to conduct the simulation. Some lab-scale mapping methods have been developed to accurately measure pore sizes and connectivity of macropore-type preferential pathways [*Anderson et al.*, 2003; *Monga et al.*, 2007], but it is extremely difficult, if not impossible, for field-scale.

Other physically based models, such as dual-porosity and dual-permeability models, mostly divide the soil into two or multiple domains, and assume uniform flow within each flow domain. Both dual-porosity and dual-permeability models assume that the porous medium consists of two interacting regions, one associated with the inter-aggregate, macropore, or fracture system, and one comprising intra-aggregate pores inside soil aggregates. While dual-porosity models assume that water in the matrix is stagnant, dual-permeability models allow for water flow in the matrix as well. The mass exchange between the two regions normally is assumed to be linear [*Leij and Bradford*,

123

2009]. Dual-permeability models are increasingly used for analysis of preferential transport both on the laboratory column scale [e.g., *Gwo et al.*, 1995, 1996; *Allaire et al.*, 2002a, b; *Greco*, 2002; *Castiglione et al.*, 2003] and on the plot or field scale [e.g., *Jarvis et al.*, 1991; *Andreu et al.*, 1994; *Larsson and Jarvis*, 1999a, b; *Kohler et al.*, 2001]. However, the difficulty in determination of the many dual-permeability model parameters largely limits the application of these models [*Köhne et al.*, 2009a, b].

Stochastic models have also been employed to simulate preferential flow and transport in soils. A variety of stochastic methods have been used to describe solute transport in heterogeneous flow fields [e.g., *Gelhar and Axness*, 1983; *Dagan*, 1984; *Freyberg*, 1986; *Sposito and Barry*, 1987; *Kabala and Sposito*, 1991; *Russo*, 1991]. In a simplified stochastic modeling approach the field may be viewed as a series of independent stream tubes with their hydraulic conductivity and/or other selected parameters described using probability density functions (PDFs) [*Jury and Roth*, 1990; *Dagan*, 1993]. However, no methodology has been developed to directly characterize the PDF, especially when preferential flow pathways are presented. *Kung et al.* [2005] proposed an indirect method to determine pore-size spectrum of macropore-type preferential pathways, but quantification of PDFs remains to be a challenge for the application of stochastic models to preferential flow and transport.

The objectives of this study were to link the parameters of the dual-permeability model with geometry information of the macropore, and then investigate methods to upscale behavior from the column to field scales. In particular, the dual-permeability model was employed to simulate bromide and microorganism transport in columns with

124

preferential pathways of different lengths and configurations. Correlations were then established between macropore geometry information (length, configuration) and parameters of the dual-permeability model. A linear superposition approach was used to estimate field scale preferential transport behavior for hypothetical PDFs. Upscaling procedures were numerically investigated to predict the field scale transport behavior.

4.2 Experiment Information

Transport experiments of *E. coli* D21g were conducted in columns with artificial preferential flow pathways as described by *Wang et al.* [2013a, b]. Detail information about the column experiments can be found in these publications, and will be briefly summarized below. Two types of Ottawa (quartz) sand with the median grain size of 120 and 710 μm (referred to as fine sand and coarse sand below) were used in the column experiments after being cleaned using a salt cleaning method [*Bradford and Kim*, 2010] to eliminate any background interference from clay particles. A 13.2 cm diameter by 22 cm long plexiglass column with an 18 μm nominal pore size polyester membrane at the bottom was used in the experiment. The fine sand was wet packed in the column with a plastic tube (with outside diameter of 1.14 cm) in the center. Then the coarse sand and fine sand were filled into to the hole created by pulling out the plastic tube from the column to make the desired preferential flow path as described in Figure 4.1. Various NaCl and NaBr solutions at selected IS (1 and 20 mM) with pH=5.8 were prepared for the experiment. These IS levels were selected to create a range of adhesive conditions between the microorganisms and sand.

Solutions were delivered onto the top of the column at a steady flow rate using a rain simulator, and the bottom boundary pressure was maintained at 0 cm by a hanging water column. The sand in the column was equilibrated by flushing the column with two pore volumes (PVs) of a selected NaCl solution (phase 0) before initiating a microbial transport experiment. Then, several PVs of NaBr solution containing *E. coli* D21g at a concentration of $\sim 1.0 \times 10^8$ cells/mL were introduced into the column at a constant rate and IS (phase I), followed by NaCl solution at the same flow rate and IS as in phase I until the effluent microbe concentration returned to a baseline level (phase II). Effluent samples were continuously collected during the transport experiment at selected intervals using a fraction collector, and then analyzed for Br and microbe concentrations.
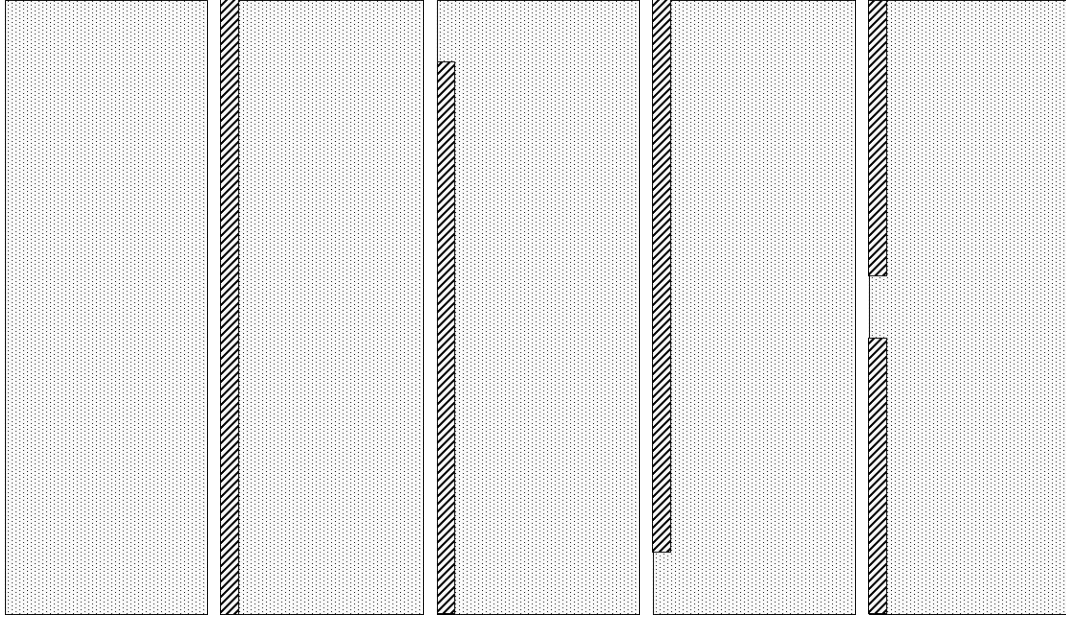
Figure 4.1. Axi-symmetric representation of the five types of lens structures (column center is on the left hand side) studied in this research: Type 0 – homogeneous fine sand column with no lens, Type I - one lens through the whole column, Type II - one lens opened to the bottom boundary, Type III - one lens opened to the top boundary, and Type IV - a discontinuous lens opened to both boundaries (diagonal pattern represents coarse sand and point pattern represents fine sand).

4.3 Numerical Modeling

Dual-permeability models describe preferential flow using one equation for flow in the matrix and one for flow in the fracture system, with the two flow regions coupled by a water transfer term:

$$\frac{\partial \theta_f}{\partial t} = \frac{\partial}{\partial z}(K_f \frac{\partial h_f}{\partial z} - K_f) - \frac{\Gamma_w}{w_f} \qquad \text{[1a]}$$

$$\frac{\partial \theta_m}{\partial t} = \frac{\partial}{\partial z}(K_m \frac{\partial h_m}{\partial z} - K_m) - \frac{\Gamma_w}{1 - w_f} \qquad \text{[1b]}$$

where the subscript "f" defines a property of the fracture system, the subscript "m" represents the matrix, θ [−] is the water content, h is the pressure head [L, L denotes the units of length], K denotes the saturated hydraulic conductivity [LT^{-1}, T denotes the units of time], w_f is the fraction of total soil occupied by the fracture system ($0 < w_f < 1$), and Γ_w is the water transfer term (T^{-1}). Γ_w is assumed to be proportional to the pressure head difference between matrix and fracture system, h_f-h_m. Thus, under saturated steady-state conditions, Γ_w equals to 0.

Modified convection-dispersion equations were used to describe transport and deposition of microorganisms in both the fracture and matrix regions:

$$\frac{\partial\left(\theta_f C_f\right)}{\partial t} = -\frac{\partial J_f}{\partial z} - E_f - \frac{\Gamma_s}{w_f} \qquad [2a]$$

$$\frac{\partial\left(\theta_m C_m\right)}{\partial t} = -\frac{\partial J_m}{\partial z} - E_m - \frac{\Gamma_s}{1-w_f} \qquad [2b]$$

where C [N$_c$L^{-3}; N$_c$ denotes the number of microbes] is the microbe concentration in the aqueous phase, J [N$_c$L^{-2}T^{-1}] is the microbe flux (sum of the advective and dispersive fluxes), the mass transfer rate between the fracture and matrix regions Γ_s is given as

$$\Gamma_s = k_{fm}(1-w_f)\theta_m(C_f - C_m) + \Gamma_w C* \qquad [3]$$

where k_{fm} is a first-order diffusive mass transfer coefficient (T^{-1}), C^* is equal to C_m for Γ_w > 0 and C_f for Γ_w <0, and E is the mass transfer function from the aqueous phase to/from solid-water interface as:

$$E = \frac{\partial\left(\rho S\right)}{\partial t} = \theta \psi k_{att} C - \rho k_{det} S \qquad [4]$$

where S [$N_c M^{-1}$; M denotes units of mass of soil] is the microbe concentration on the solid phase, k_{det} [T^{-1}] is the microbe detachment rate coefficient, k_{att} [T^{-1}] is the microbe attachment rate coefficient, and ρ [ML^{-3}] is the bulk density. The parameter ψ [-] accounts for time and concentration dependent blocking using a Langmuirian approach as [*Adamczyk et al.*, 1994]:

$$\psi = 1 - \frac{S}{S_{max}} \qquad [5]$$

where S_{max} [$N_c M^{-1}$] is the maximum solid phase concentration of microbes.

The simulations were carried out with the HYDRUS-1D code [*Šimůnek et al.*, 2008]. A third-type boundary condition was employed at the column inlet and a zero concentration gradient was used at the outlet for these simulations. Some of the model parameters were experimentally determined in our previous studies [*Wang et al.*, 2013a, b], while other parameters (e.g. K_f and k_{fm}) were determined using a nonlinear least squares optimization routine in HYDRUS-1D.

4.4 Results and Discussion

Results from transport experiments of *E. coli* D21g in columns with preferential flow paths of different lengths and configurations at different ionic strengths (IS) [*Wang et al.*, 2013a, b] were used to investigate the relationship between the geometry properties of preferential path and parameters of dual-permeability model. Breakthrough data of bromide was first used to characterize parameters for water flow before looking into the transport of *E. coli* D21g.

4.4.1 Transport of Bromide

The transport of bromide is depended on following parameters during saturated steady-state conditions: saturated hydraulic conductivities of the matrix (K_m) and the fracture (K_f), saturated water content of the matrix (θ_m) and the fracture (θ_f), dispersivities of the matrix (λ_m) and the macropore (λ_f), the ratio of the volumes of the macropore domain and the total column system (w_f), and the mass transfer rate at the interface between matrix and macropores (k_{fm}).

The saturated hydraulic conductivity of the matrix, K_m, is considered as a constant value based on the value in the homogeneous column for all the cases. However, due to the variation caused by packing, K_m was determined by the arrival time of the brominde pulse from the matrix for each column experiment [*Wang et al.*, 2013a]. We set the dispersivities of the matrix and the macropore as the values obtained from homogeneous column experiments of fine sand and coarse sand, respectively [*Wang et al.*, 2013a]. The porosities of both matrix and macropore were set as the measured values in homogeneous column experiments. w_f was calculated based on the volume of macropore and the total volume of column with type I lens configuration, and the same value was set for all other lenses with different lengths and configurations. The values of these parameters are listed in Table 4.1.

Table 4.1. Model parameters obtained from previous studies and optimized saturated conductivities of the fracture, K_f, and mass transfer coefficients for bromide, k_{fm}, and their 95% confidence intervals.

Lens Configuration	Lens Length (cm)	K_m (cm/min)	θ_m	θ_f	λ_m (cm)	λ_f (cm)	w_f	K_f (cm/min)	k_{fm} (min^{-1})
Type I	20	0.31	0.36	0.36	0.10	0.55	0.00746	10.9±0.5	$(1.40\pm0.7)*10^{-4}$
Type II	19	0.32	0.36	0.36	0.10	0.55	0.00746	8.3±0.7	$(1.37\pm1.2)*10^{-4}$
Type II	18	0.30	0.36	0.36	0.10	0.55	0.00746	7.8±0.7	$(2.35\pm1.0)*10^{-4}$
Type II	16	0.32	0.36	0.36	0.10	0.55	0.00746	6.2±0.7	$(2.82\pm1.5)*10^{-4}$
Type II	10	0.34	0.36	0.36	0.10	0.55	0.00746	4.0±0.7	$(5.91\pm3.1)*10^{-4}$
Type III	19	0.32	0.36	0.36	0.10	0.55	0.00746	9.7±0.9	$(1.60\pm1.0)*10^{-4}$
Type III	16	0.32	0.36	0.36	0.10	0.55	0.00746	6.7±1.1	$(2.86\pm2.0)*10^{-4}$
Type IV	19	0.32	0.36	0.36	0.10	0.55	0.00746	8.1±0.8	$(5.80\pm1.7)*10^{-4}$
Type IV	18	0.32	0.36	0.36	0.10	0.55	0.00746	7.1±0.8	$(5.40\pm2.1)*10^{-4}$
Type IV	16	0.32	0.36	0.36	0.10	0.55	0.00746	4.2±0.7	$(5.27\pm2.3)*10^{-4}$

Since K_m and w_f were set as constants, K_f was the main parameter, which determined the relative concentration of bromide of the first pulse during preferential transport. As the relative contribution of the preferential transport decreased and arrival time of the preferential transport was delayed when the length of lens decreased, K_f was expected to decrease as well. Table 4.1 shows that K_f decreased as the length of lens decreased for all three types of lens configurations. K_f of type IV lens configuration was smaller than that of type II and type III when the length was the same. This was consistent with the observation that type IV lens configuration had later arrival and less amount of preferential transport compared to type II and type III lens configurations.

Larger dispersion was reported for type IV lens configuration compared to type II and type III configurations [*Wang et al.*, 2013b], which indicated greater mixing at the interface between the matrix and the fracture domains. The greater mixing at the interface for type IV lens configuration was reflected by the larger mass transfer coefficient in dual-permeability model as shown in Table 4.1. The mass transfer coefficient for type IV configuration was almost independent of the length of lens. However, the mass transfer coefficient increased with a decrease in the length for type II and type III lens configurations.

Figure 4.2 shows examples of observed BTCs of bromide and corresponding simulations with parameters in Table 4.1.
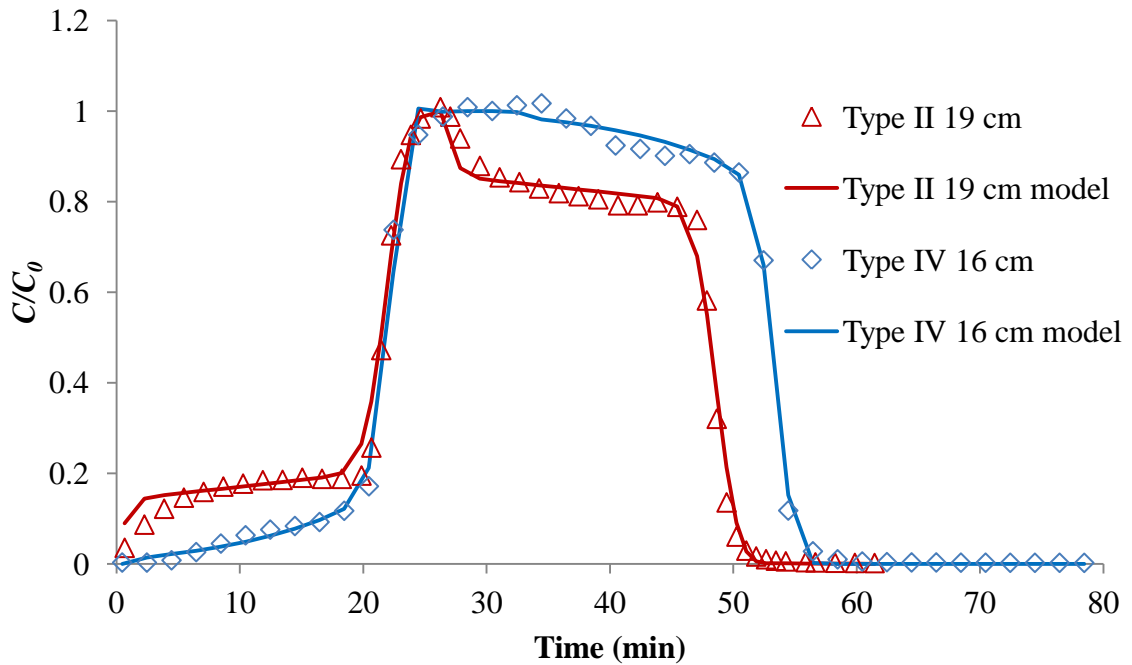
Figure 4.2. Observed and simulated BTCs of bromide from columns of Type II 19 cm and Type IV 16 cm.

4.4.2 Transport of *E. coli* D21g

After obtaining the information required to describe water flow and transport of conservative tracer during the first step, transport of *E. coli* D21g should be well quantified with the retention parameters of *E. coli* D21g (microbe attachment rate coefficient, k_{att}; microbe detachment rate coefficient, k_{det}; maximum solid phase concentration of microbes, S_{max}) obtained from homogeneous experiments under the same conditions by *Wang et al.* [2013a] (Table 4.2). However, forward simulations based on these parameters had relatively poor agreement with most of the experiment results.

Table 4.2. Retention parameters for the matrix used in simulations (k_{det} for the matrix and k_{att}, S_{max}, and k_{det} for the macropore were set as 0), and optimized saturated water content of the fracture (θ_f) and matrix (θ_m), the ratio of saturated conductivities optimized from *E. coli* D21g to that optimized from bromide for the fracture and matrix (θ_m/θ^*_m and θ_f/θ^*_f, respectively), and mass transfer coefficients, k_{fm}, for *E. coli* D21g at 1 and 20 mM, and their 95% confidence intervals.

Lens Configuration	Lens Length (cm)	IS (mM)	k_{att}	S_{max}	θ_m	θ_m/θ^*_m	θ_f	θ_f/θ^*_f	k_{fm} (min^{-1})
Type II	19	1	0.0004	0.01	0.327±0.002	0.91	0.313±0.03	0.87	(1.97±1.2)*10^{-4}
Type III	19	1	0.0004	0.01	.333±0.003	0.93	0.265±0.02	0.74	(2.98±1.1)*10^{-4}
Type IV	19	1	0.0004	0.01	.339±0.003	0.94	0.263±0.02	0.73	(5.80±1.6)*10^{-4}
Type I	20	20	0.2	3.5	NA	NA	NA	NA	(4.40±0.38)*10^{-4}
Type II	19	20	0.2	3.5	NA	NA	NA	NA	(5.27±0.62)*10^{-4}
Type II	18	20	0.2	3.5	NA	NA	NA	NA	(1.28±0.15)*10^{-3}
Type II	16	20	0.2	3.5	NA	NA	NA	NA	(2.31±0.89)*10^{-3}

Type IV	19	20	0.2	3.5	NA	NA	NA	NA	$(6.39\pm0.58)*10^{-4}$
Type IV	18	20	0.2	3.5	NA	NA	NA	NA	$(2.96\pm0.61)*10^{-3}$
Type IV	16	20	0.2	3.5	NA	NA	NA	NA	NA[a]

[a] Not available due to the extremely low concentration in collected effluent

At low IS (1 mM), when there was very small retention of *E. coli* D21g in both matrix and lens, forward simulations had later arrival time for transport in the matrix and lower concentration for transport in preferential path. This phenomenon was explained as size exclusion by *Wang et al.* [2013b]. Thus, while using the retention parameters obtained from homogeneous experiments (Table 4.2), saturated water content of the fracture (θ_f) and matrix (θ_m) were optimized to account for size exclusion for the transport data of *E. coli* D21g at low IS, and the mass transfer coefficient k_{fm} was also optimized (Table 4.2). Smaller θ_m and θ_f were obtained from *E. coli* D21g data compared to that from bromide data as small pores were excluded for *E. coli* D21g, which resulted in earlier arrival time. This finding is consistent with the assumption that size exclusion may increase the transport velocity of *E. coli* D21g by constraining cells to faster flow domains and larger pore networks than bromide [*Wang et al.*, 2013b]. The mass transfer coefficients of *E. coli* D21g at low IS were quite close to that of bromide for the same lens configuration. Figure 4.3 shows an example of observed BTCs of *E. coli* D21g at 1 mM and simulations with parameters in Table 4.1 and 4.2.

At high IS (20 mM), forward simulations tended to have higher concentrations for the breakthrough from preferential path. The mass transfer coefficient k_{fm} were optimized to better describe the transport of *E. coli* D21g at high IS with the retention parameters obtained from homogeneous experiments (Table 4.2). The mass transfer coefficients for *E. coli* D21g at high IS were significantly greater than that for bromide of the same lens configuration and length. Similar to the trend of bromide, the mass transfer coefficient increased with a decrease in length, and Type IV lens configuration had greater transfer

rate than Type II and Type III lens configurations of the same length. Examples of observed BTCs of *E. coli* D21g at 20 mM and simulations with parameters in Table 4.1 and 4.2 are given in Figure 4.4.
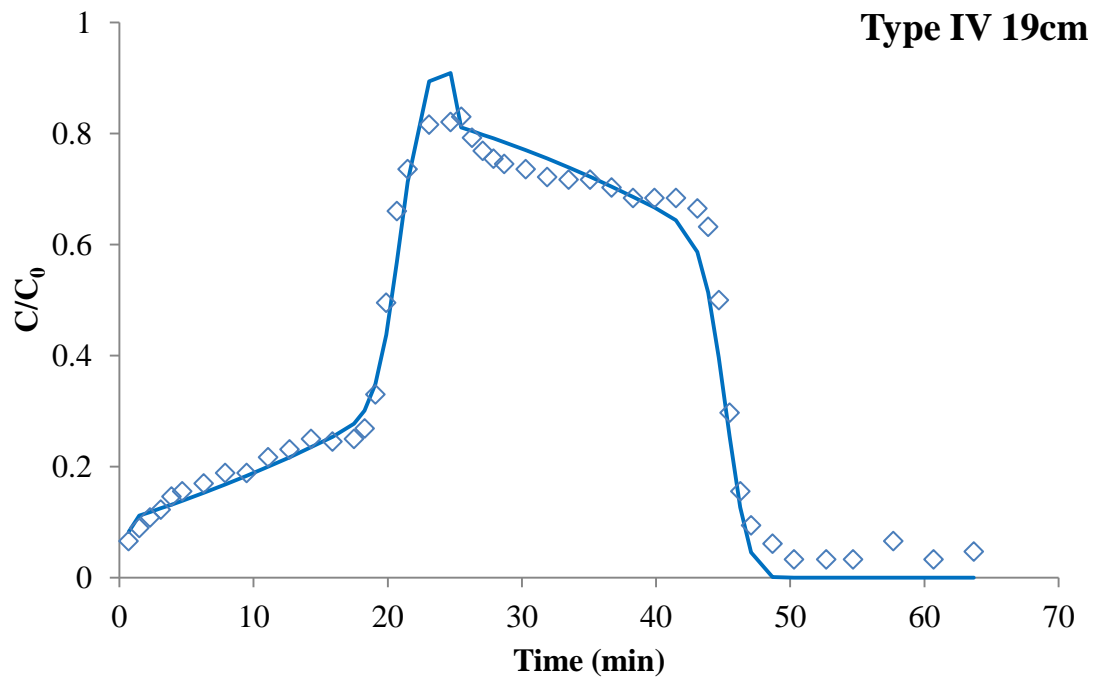

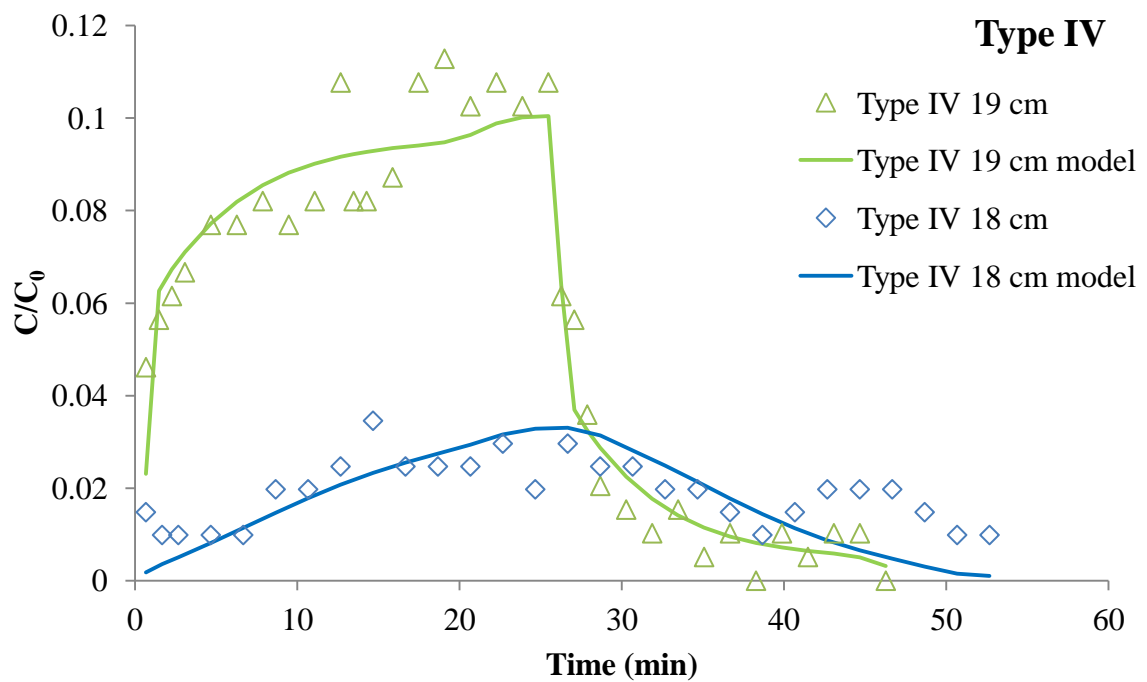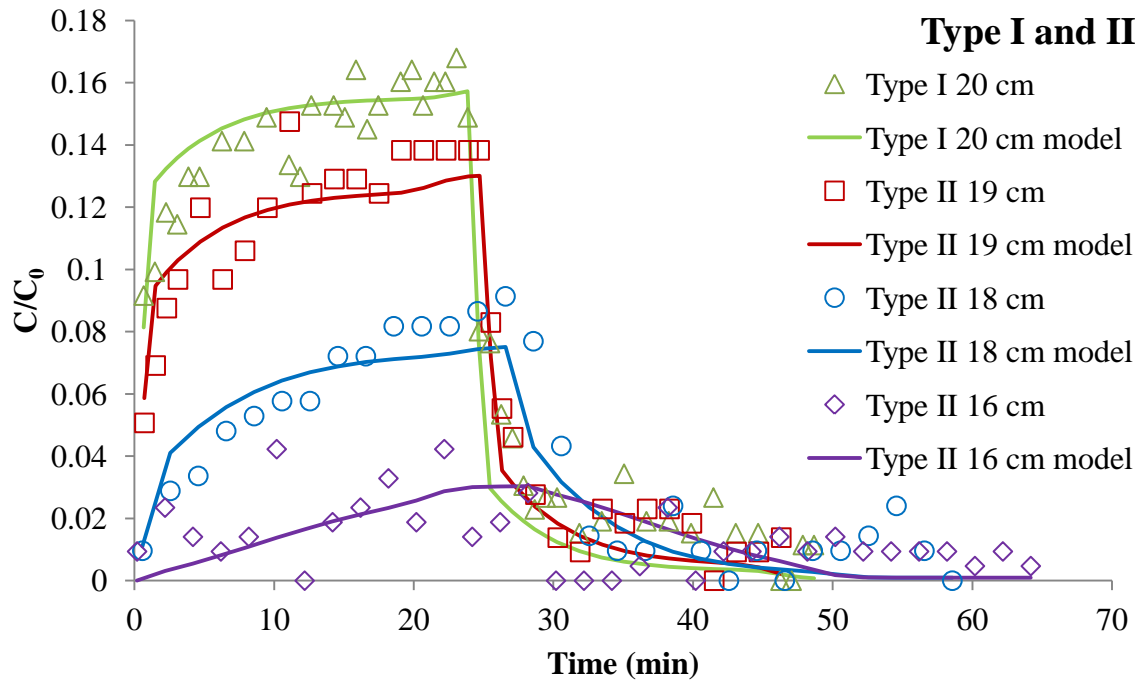**Figure 4.3.** Observed and simulated BTCs of *E. coli* D21g at IS=1 mM from column of Type IV 19 cm.

Figure 4.4. Observed and simulated BTCs of *E. coli* D21g at IS=20 mM.

4.5 Upscaling Approach

4.5.1 Virtual Field

In order to investigate the ability of the dual-permeability model to simulate the transport of *E. coli* D21g at larger scales, we generated virtual fields with a distribution of preferential pathways. The virtual fields consisted of independent "stream tubes" that were run in parallel (e.g., no interaction between the stream tubes). Transport within each individual stream tube was consistent with the results of a particular column experiment with selected macropore length and configuration, and solution ionic strength (Figs. 4.3 and 4.4; Table 4.2). The virtual field was comprised of selected amounts of each column type. Table 4.3 shows some examples of virtual field with their fractions, f_i, of each column unit and the estimated parameters. The fractions of all column units were randomly allocated with the same probability to cover a wide range of possible situations.

Simulations were carried out for each column unit with IS equaled to 1 and 20 mM and the same boundary conditions as for the laboratory experiments. The duration of the bacterial input suspension was 24 minutes to be consistent with the laboratory experiments. The model parameters for each column unit were given in Tables 4.1 and 4.2. The saturated hydraulic conductivity of the macropore domain was set equal to that of the course sand matrix in the homogeneous column (Type 0), so there is no preferential flow path in this unit. The mean solute concentration at the bottom boundary for an entire virtual field is given by the ensemble average of the local concentrations in all stream tubes as described by following equation:

$$C*(\mathrm{t}) = \sum_{i=1}^{n} f_i q_i C_i(t) \tag{6}$$

where $C^*(t)$ is the combined effluent concentration of the virtual field at time t; f_i is the fraction of unit i; q_i is the flow rate of unit i; and $C_i(t)$ is the effluent concentration of unit i at time t.

After obtaining the BTC of a virtual field with Equation 6, we estimated a new set of model parameters for the virtual field. Only K_f^* and k_{fm}^* were fitted to the field BTC as all other parameters were the same for all units. Figure 4.5 shows the ensemble and simulated BTCs of the virtual fields listed in Table 4.3 at 1 and 20 mM. At 1 mM, the ensemble BTCs were very similar to the typical BTC from laboratory experiment as shown in Figure 4.3, and differences between different virtual fields were very small. Similar to what has been observed in transport experiments conducted at IS=20 mM in Figure 4.4, early breakthrough from the preferential path was observed while no significant breakthrough came from the matrix. The amount of breakthrough from the preferential path was positively correlated with the fractions of units with long lenses (Type I, Type II 19 cm, and Type IV 19 cm) as these units could transport more cells than others.

Table 4.3. Examples of virtual fields with their fractions (f_i) for each unit, estimated model parameters, and R^2.

|		IS=20 mM				IS=1 mM		
		Field 1	Field 2	Field 3	Field 4	Field 5	Field 6	Field 7	Field 8
f_i	Type 0	.24	.22	.18	.08	.32	.17	.17	.21
	Type I	.20	.05	.07	.16	.13	.25	.21	.21
	Type II 19 cm	.15	.07	.13	.15	.12	.02	.05	.07
	Type II 18 cm	.22	.14	.17	.19	.26	.22	.07	.22
	Type II 16 cm	.07	.18	.18	.22	.06	.05	.08	.03
	Type IV 19 cm	.08	.11	.12	.07	.02	.01	.22	.02
	Type IV 18 cm	.04	.23	.15	.13	.09	.28	.20	.24
K^*_f (cm/min)		8.7±0.3	7.0±0.5	7.5±0.5	7.9±0.6	5.8±0.2	7.1±0.1	7.1±0.1	7.4±0.6
k^*_{fm} (min^{-1})		$(7.8\pm0.8)*10^{-4}$	$(10.4\pm1.6)*10^{-4}$	$(9.5\pm1.2)*10^{-4}$	$(9.0\pm1.5)*10^{-4}$	$(1.6\pm0.1)*10^{-4}$	$(2.4\pm0.2)*10^{-4}$	$(2.9\pm0.2)*10^{-4}$	$(2.6\pm0.9)*10^{-4}$
R^2		.997	.989	.991	.990	.999	1.000	1.000	.999
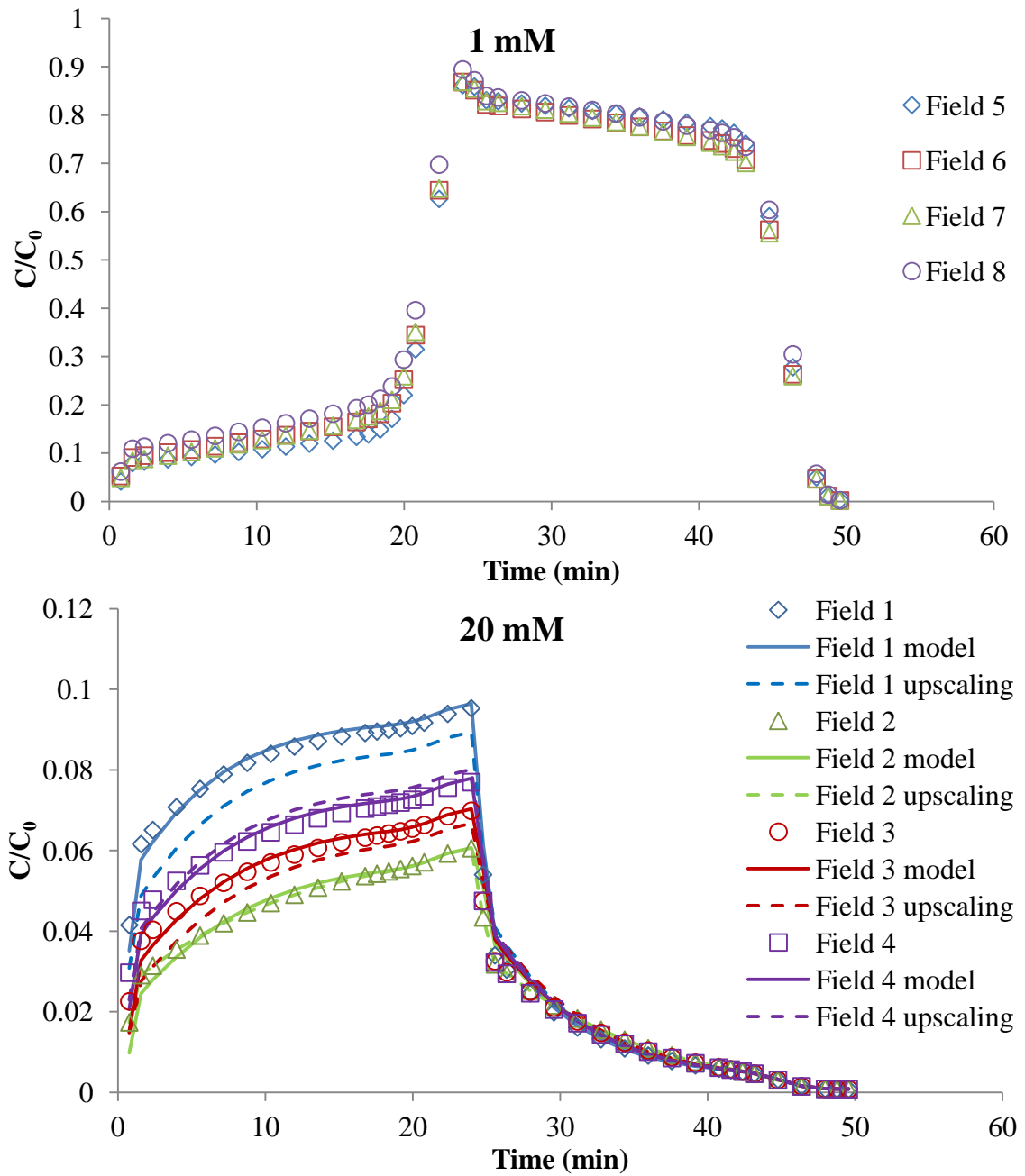
Figure 4.5. BTCs of *E. coli* D21g at 1 mM and 20 mM from virtual fields (calculated using eq. [6] and simulations with inversely estimated (model) and upscaled (upscaling; using eqs. [8] and [10]) model parameters. Upper figure does not show model simulations as they virtually mimic virtual field data.

4.5.2 Parameter Upscaling

The field scale values of K_f^* and k_{fm}^* were obtained in the previous section. In this section we investigate ways to predict these parameters from properties of individual stream tubes. As the properties of the matrix were the same for all column units, they were the same for the virtual field. Several methods were investigated to predict the upscaled parameters K_f^* and k_{fm}^* for the virtual fields as follows:

$$K_f^* = \frac{\sum_{i=1}^{n} f_i K_{f,i}}{\sum_{i=1}^{n} f_i} \qquad\qquad [7]$$

$$K_f^* = \frac{\sum_{i=1}^{n} f_i K_{f,i}^2}{\sum_{i=1}^{n} f_i K_{f,i}} \qquad\qquad [8]$$

$$k_{fm}^* = \frac{\sum_{i=1}^{n} f_i k_{fm,i}}{\sum_{i=1}^{n} f_i} \qquad\qquad [9]$$

$$k_{fm}^* = \frac{\sum_{i=1}^{n} f_i}{\sum_{i=1}^{n} \frac{f_i}{k_{fm,i}}} \qquad\qquad [10]$$

Equations [7] and [9] assume that an upscale parameter can be determined as a simple linear combination of local parameters. Equations [8] and [10] represent a nonlinear relationship between field and column scale parameters that were developed by trial and error. Table 4.4 lists the upscaled model parameters obtained from Equation [7]-[10] for the virtual fields listed in Table 4.3. The simulated BTCs with Equation [8] for

K_f^* and Equation [10] for k_{fm}^* matched the BTCs of the virtual fields the best (R^2>0.98), and proved that the upscaled model parameters can be used to predict the transport of microorganism in virtual fields. However, the studied cases were still very limited compared to the possible situations in the field. For instance, if the duration of the microorganism applications is very short and the arrival times from different local preferential flow pathways vary a lot, the ensemble field BTCs could show multiple peaks. On the other hand, the dual-permeability model with one set of parameters can only predict one possible peak for the preferential flow and one for the matrix flow. In this case, stochastic models may perform better than the dual-permeability model.

Table 4.4. Upscaling model parameters obtained by different methods.

		Field 1	Field 2	Field 3	Field 4
K_f^* (cm/min)	Equation 7	6.5	5.9	6.3	7.3
	Equation 8	8.8	7.7	7.9	8.3
k_{fm}^* (min^{-1})	Equation 9	$7.8*10^{-4}$	$14.0*10^{-4}$	$12.5*10^{-4}$	$13.3*10^{-4}$
	Equation 10	$9.3*10^{-4}$	$14.6*10^{-4}$	$11.7*10^{-4}$	$9.6*10^{-4}$

4.6. Conclusions

Dual-permeability models were able to describe the transport of bromide, and *E. coli* D21g at both high and low IS conditions when optimized parameters were used. However, forward simulation of *E. coli* D21g based on information from transport experiments with *E. coli* D21g in homogeneous columns and from transport experiments

with bromide in columns with preferential flow could not describe some features of transport of *E. coli* D21g at both high and low IS.

Inverse estimation indicated strong correlations between the parameters of the dual-permeability model (e.g., hydraulic conductivity of the fracture, mass transfer coefficient) and the configuration and length of the preferential path. In general, 1) hydraulic conductivity of the fracture decreased with a decrease in lens length; 2) mass transfer coefficient increased with a decrease in lens length, and Type IV lens configuration produced greater mass transfer rate; 3) *E. coli* D21g had similar mass transfer coefficient as bromide at low IS, but the mass transfer coefficient was much greater for *E. coli* D21g at high IS compared to a low IS and that of bromide.

The estimated model parameters can well describe the BTCs of virtual fields composed of various preferential flow paths, and the upscaling method when upscaled parameters are estimated from local column parameters using Equations [8] and [10] proved to be accurate to predict the transport of *E. coli* D21g in virtual fields. We hypothesize that this upscaling approach may also work in real situations.

4.7 References:

Abu-Ashour, J., D. M. Joy, H. Lee, H. R. Whiteley, and S. Zelin (1994), Transport of microorganisms through soil, *Water Air Soil Pollut.*, 75(1-2), 141-158

Adamczyk, Z., B. Siwek, M. Zembala, and P. Belouschek (1994), Kinetics of localized adsorption of colloid particles, *Adv Colloid Interfac*, 48(0), 151-280. doi:10.1016/0001-8686(94)80008-1.

Allaire-Leung, S. E., S. C. Gupta, and J. F. Moncrief (2000a), Water and solute movement in soil as influenced by macropore characteristics - 1. Macropore continuity, *J. Contam. Hydrol.*, 41(3-4), 283-301.

Allaire, S. E., S. C. Gupta, J. Nieber, and J. F. Moncrief (2002b), Role of macropore continuity and tortuosity on solute transport in soils: 1. Effects of initial and boundary conditions, *J. Contam. Hydrol.*, *58*(3-4), 299-321.

Anderson, S., H. Wang, R. Peyton, and C. Gantzer (2003), Estimation of porosity and hydraulic conductivity from x-ray CT-measured solute breakthrough, *Geological Society, London, Special Publications*, *215*(1), 135-149.

Andreu, L., F. Moreno, N. Jarvis, and G. Vachaud (1994), Application of the model MACRO to water movement and salt leaching in drained and irrigated marsh soils, Marismas, Spain, *Agr. Water Manage*, *25*(1), 71-88.

Bales, R. C., C. P. Gerba, G. H. Grondin, and S. L. Jensen (1989), Bacteriophage transport in sandy soil and fractured tuff, *Appl. Environ. Microbiol.*, *55*(8), 2061-2067.

Beven, K., and P. Germann (1982), Macropores and water flow in soils, *Water Resour. Res.*, *18*(5), 1311-1325.

Bradford, S. A., and H. Kim (2010), Implications of Cation Exchange on Clay Release and Colloid-Facilitated Transport in Porous Media, *J Environ Qual*, 39(6), 2040-2046. doi:10.2134/Jeq2010.0156.

Bradford, S. A., J. Šimůnek, M. Bettahar, M. Th. van Genuchten, and S. R. Yates. (2006). Significance of straining in colloid deposition: Evidence and implications. *Water Resour. Res.* 42, W12S15, doi:10.1029/2005WR004791.

Castiglione, P., B. P. Mohanty, P. J. Shouse, J. Šimůnek, M. T. van Genuchten, and A. Santini (2003), Lateral Water Diffusion in an Artificial Macroporous System: Modeling and Experimental Evidence, *Vadose Zone J.*, *2*(2), 212-221.

Cey, E. E., D. L. Rudolph, and J. Passmore (2009), Influence of macroporosity on preferential solute and colloid transport in unsaturated field soils, *J. Contam. Hydrol.*, *107*(1-2), 45-57.

Chen, G. X., and S. L. Walker (2007), Role of solution chemistry and ion valence on the adhesion kinetics of groundwater and marine bacteria, *Langmuir*, 23(13), 7162-7169.

Dagan, G. (1984), Solute transport in heterogeneous porous formations, *Journal of Fluid Mechanics*, *145*, 151-177.

Dagan, G. (1993), Higher-order correction of effective conductivity of heterogeneousformations of lognormal conductivity distribution, *Transp. Porous Media*, 12, 279–290.

Dong, H. L., T. C. Onstott, M. F. Deflaun, M. E. Fuller, T. D. Scheibe, S. H. Streger, R. K. Rothmel, and B. J. Mailloux (2002), Relative dominance of physical versus chemical effects on the transport of adhesion-deficient bacteria in intact cores from South Oyster, Virginia, *Environ. Sci. Technol.*, *36*(5), 891-900.

Flury, M., H. Fluhler, W. A. Jury, and J. Leuenberger (1994), Susceptibility of Soils to Preferential Flow of Water - a Field-Study, *Water Resour. Res.*, *30*(7), 1945-1954.

Freyberg, D. L. (1986), A natural gradient experiment on solute transport in a sand aquifer: 2. Spatial moments and the advection and dispersion of nonreactive tracers, *Water Resour. Res.*, *22*(13), 2031-2046.

Gelhar, L. W., and C. L. Axness (1983), Three-dimensional stochastic analysis of macrodispersion in aquifers, *Water Resour. Res.*, *19*(1), 161-180.

Greco, R. (2002), Preferential flow in macroporous swelling soil with internal catchment: model development and applications, *J. Hydrol.*, *269*(3), 150-168.

Gwo, J., P. Jardine, G. Wilson, and G. Yeh (1995), A multiple-pore-region concept to modeling mass transfer in subsurface media, *J. Hydrol.*, *164*(1), 217-237.

Gwo, J., P. Jardine, G. Wilson, and G. Yeh (1996), Using a multiregion model to study the effects of advective and diffusive mass transfer on local physical nonequilibrium and solute mobility in a structured soil, *Water Resour. Res.*, *32*(3), 561-570.

Hendry, M. J., J. R. Lawrence, and P. Maloszewski (1999), Effects of velocity on the transport of two bacteria through saturated sand, *Ground Water*, *37*(1), 103-112.

Jarvis, N., P. E. Jansson, P. Dik, and I. Messing (1991), Modelling water and solute transport in macroporous soil. I. Model description and sensitivity analysis, *J. Soil Sci.*, *42*(1), 59-70.

Jiang, S., L. P. Pang, G. D. Buchan, J. Šimůnek, M. J. Noonan, and M. E. Close (2010), Modeling water flow and bacterial transport in undisturbed lysimeters under irrigations of dairy shed effluent and water using HYDRUS-1D, *Water Res.*, *44*(4), 1050-1061.

Jury, W. A., and K. Roth (1990), *Transfer functions and solute movement through soil: theory and applications*, Birkh äuser Verlag AG.

Kabala, Z., and G. Sposito (1991), A stochastic model of reactive solute transport with time-varying velocity in a heterogeneous aquifer, *Water Resour. Res.*, *27*(3), 341-350.

Kohler, A., K. Abbaspour, M. Fritsch, M. T. Van Genuchten, and R. Schulin (2001), Simulating unsaturated flow and transport in a macroporous soil to tile drains subject to an entrance head: Model development and preliminary evaluation, *J. Hydrol.*, *254*(1), 67-81.

K öhne, J. M., S. K öhne, and J. Šimůnek (2009a), A review of model applications for structured soils: b) Pesticide transport, *J. Contam. Hydrol.*, *104*(1-4), 36-60.

K öhne, J. M., S. K öhne, and J. Šimůnek (2009b), A review of model applications for structured soils: a) Water flow and tracer transport, *J. Contam. Hydrol.*, *104*(1-4), 4-35.

Kung, K.-J., M. Hanke, C. Helling, E. Kladivko, T. Gish, T. Steenhuis, and D. Jaynes (2005), Quantifying pore-size spectrum of macropore-type preferential pathways, *Soil Sci. Soc. Am. J.*, *69*(4), 1196-1208.

Larsson, M., and N. Jarvis (1999a), Evaluation of a dual-porosity model to predict field-scale solute transport in a macroporous soil, *J. Hydrol.*, *215*(1), 153-171.

Larsson, M. H., and N. J. Jarvis (1999b), A dual-porosity model to quantify macropore flow effects on nitrate leaching, *J. Environ. Qual.*, *28*(4), 1298-1307.

Leij, F. J., and S. A. Bradford (2009), Combined physical and chemical nonequilibrium transport model: Analytical solution, moments, and application to colloids, *J. Contam. Hydrol.*, *110*(3-4), 87-99.

Madsen, E. L., and M. Alexander (1982), Transport of Rhizobium and Pseudomonas through Soil1, *Soil Sci. Soc. Am. J.*, *46*(3), 557-560.

Mccaulou, D. R., R. C. Bales, and R. G. Arnold (1995), Effect of Temperature-Controlled Motility on Transport of Bacteria and Microspheres through Saturated Sediment, *Water Resour. Res.*, *31*(2), 271-280.

Mills, A. L., J. S. Herman, G. M. Hornberger, and T. H. Dejesus (1994), Effect of Solution Ionic-Strength and Iron Coatings on Mineral Grains on the Sorption of Bacterial-Cells to Quartz Sand, *Appl. Environ. Microbiol.*, *60*(9), 3300-3306.

Monga, O., F. Ndeye Ngom, and J. François Delerue (2007), Representing geometric structures in 3D tomography soil images: Application to pore-space modeling, *Comput. Geosci.*, *33*(9), 1140-1161.

Russo, D. (1991), Stochastic analysis of simulated vadose zone solute transport in a vertical cross section of heterogeneous soil during nonsteady water flow, *Water Resour. Res.*, *27*(3), 267-283.

Šimůnek, J., N.J. Jarvis, M.T. van Genuchten and A. Gardenas. (2003), Review and comparison of models for describing non-equilibrium and preferential flow and transport in the vadose zone. *J. Hydrol.*, 272: 14-35.

Singh, P., and R. S. Kanwar (1991), Preferential Solute Transport through Macropores in Large Undisturbed Saturated Soil Columns, *J. Environ. Qual.*, *20*(1), 295-300.

Sposito, G., and D. Barry (1987), On the Dagan model of solute transport in groundwater: Foundational aspects, *Water Resour. Res.*, *23*(10), 1867-1875.

Unc, A., and M. J. Goss (2003), Movement of faecal bacteria through the vadose zone, *Water Air Soil Poll.*, *149*(1-4), 327-337.

Wang, Y., S. A. Bradford, and J. Šimůnek (2013a), Transport and fate of microorganisms in soils with preferential flow under different solution chemistry conditions, *Water Resour. Res.*, *49*(5), 2424-2436.

Wang, Y., S. A. Bradford, and J. Šimůnek (2013b), Physical and Chemical Factors Influencing the Transport and Fate of *E. coli* D21g in Soils with Preferential Flow, *Vadose Zone J.*, Under Review

Wollum, A., and D. Cassel (1978), Transport of microorganisms in sand columns, *Soil Sci. Soc. Am. J.*, *42*(1), 72-76.

Yee, N., J. B. Fein, and C. J. Daughney (2000), Experimental study of the pH, ionic strength, and reversibility behavior of bacteria-mineral adsorption, *Geochim. Cosmochim. Acta*, 64(4), 609-617.

Chapter 5

Summary and Conclusions

The overall goal of this doctoral work was to investigate the influence of physical and chemical factors on microorganism transport in soils with preferential flow and to improve and refine mathematical models for microorganism transport under preferential flow condition. To reach the goal, two microorganisms − *E. coli* D21g and φX174 − were selected. The transport of microorganisms was examined over a range of IS in columns with systematically selected lens configuration and length. The release of attached cells was examined by introducing transients in solution chemistry. Numerical models in 2D and 1D were applied to simulate transport of microorganisms for various physical and chemical situations.

Chapter 2 highlights the importance of solution chemistry on the transport of microorganisms in the preferential flow systems. Retention of *E. coli* D21g and φX174 was enhanced as the solution IS increased in both homogeneous and heterogeneous sand columns as DLVO calculations indicate that the depth of the secondary minimum increased and that the height of the energy barrier deceased with an increase in IS. *E. coli* D21g was mainly reversibly retained in the sand as a result of interactions in a secondary minima, whereas φX174 was largely irreversible retained as a result of primary minima interactions. The relative amount of preferential transport of microbes through the lens increased with IS. This indicates that preferential transport of microbes became more important under conditions of higher overall retention. Cell RPs demonstrated significant amounts of mass transfer at the interface between the lens and matrix. Cell release with a reduction in solution IS exhibited multi-peaked breakthrough in the preferential flow systems.

As discussed in Chapter 3, the transport and release of *E. coli* D21g was highly affected by the length and configuration of lens. A decrease in the lens length produced later arrival times and lower effluent concentrations through the preferential pathway and this effect became more pronounced for *E. coli* D21g at a high IS because of increased cell retention in the matrix. The Type IV (lens is discontinuous in the center) lens configuration produced a larger dispersivity and later arrival time in the preferential path than Type II (lens is open at the bottom) and III (lens is open at the top) configurations, and it also yielded less transport of *E. coli* D21g at high IS due to enhanced mixing of the flow through the preferential path and matrix compared to the other two configurations. Size exclusion not only increased the travel speed of *E. coli* D21g in both the matrix and preferential path, but also increased the relative amount of *E. coli* D21g that was transported in the preferential path in comparison to tracer. Numerical simulations of *E. coli* D21g under both constant and transient solution chemistry conditions had very high agreement with the experiment data. However, the model wasn't capable of simulating some of the subtle differences in transport between the various lens configurations.

Chapter 4 sets up correlations between geometry information of preferential flow path with parameters in 1D preferential flow model. In dual-permeability model, hydraulic conductivity of the fracture decreased with a decrease in lens length, and the mass transfer coefficient increased as the length of lens decreased and Type IV lens configuration produced greater mass transfer rate. The estimated model parameters can well describe the BTCs of virtual fields composed of various preferential flow paths, and the upscaling method when upscaled parameters are estimated from local column

parameters using adequate equations proved to be accurate to predict the transport of *E. coli* D21g in virtual fields. We hypothesize that this upscaling approach may also work in real situations.

The findings from this dissertation suggest the following critical insights: first, the solution chemistry can strongly affect the transport of microorganisms in preferential systems; second, preferential transport of microorganisms is important, especially when the retention of microorganisms is strong in the matrix; third, the length and configuration of preferential pathway is an important factor for preferential transport of microorganisms; and forth, the retained microorganisms on solid phase can be released back into liquid phase during transients in solution chemistry. However, future work is still requisite for the prediction of microorganism transport at field scale, especially, an efficient method to obtain model parameters for numerical simulations.